Novel Insights into Titin's Mobility and Function

Derived from a Knockin Mouse Model

Inaugural-Dissertation

to obtain the academic degree

Doctor rerum naturalium (Dr. rer. nat.)

submitted to the Department of Biology, Chemistry, and Pharmacy

of Freie Universität Berlin

by

Katharina da Silva Lopes (née Rost)

from Lauchhammer (Germany)

2011

I completed my doctorate studies from February 01, 2008 to July 29, 2011 under the supervision of Prof. Dr. M. Gotthardt at the Max-Delbrück-Center for Molecular Medicine, Berlin-Buch.

1st Reviewer: Prof. Dr. Rupert Mutzel

2nd Reviewer: Prof. Dr. Michael Gotthardt

Date of defense: October 27, 2011

Acknowledgement

First of all I would like to thank my supervisor Prof. Dr. M. Gotthardt for the opportunity to work on an exciting project over the last 3.5 years. I am very grateful for the resources he offered, his encouragement, and the freedom he gave me to explore research.

I thank Prof. Dr. R. Mutzel of the Freie Universität Berlin for his interest in my doctorate studies and the supervision at the university.

I am grateful to all the current and former members of the Gotthardt lab for their kindness and helpfulness. I really enjoyed working in this group. I especially want to thank Beate Golbrich-Hannig and Carolin Gärtner for expert technical assistance. I'm very thankful to Dr. Nora Bergmann for all the thoughtful advices, her kindness, and the critical reading of my thesis. Additionally, I thank Dr. Ulrike Lisewski, Dr. Michael Radke, and Christopher Polack for their time to read my thesis to refine my work. Dr. Uta Wrackmeyer and Franziska Rudolph I want to thank for inspirations as well as thoughtful and enthusiastic discussions. I'm grateful to our exchange student Lily Yu for her help and support of my project in the summer of 2010.

Special thanks go to Dr. Anje Sporbert and Dr. Zoltan Cseresnyes from the "Microscope Core Facility" of the MDC for the excellent technical support. They were always very helpful when I had technical problems and we spent endless hours and nights to fix the microscope. I want to acknowledge Dr. Bettina Purfürst from the "Electron Microscopy Core Facility" for performing the EM analysis and Martin Taube from the "*In Vivo* Mouse Phenotyping Platform" for the measurement of the body composition.

I'm very grateful to my family and friends for their cheerful support and enthusiasm. I especially thank Janna Krüger for her helpfulness and our creative discussions.

My parents Gerhard and Karin Rost as well as my brother Sebastian Rost deserve special thanks for their support throughout my studies. Without their love, understanding, and encouragement I would never have come so far.

Finally, I want to thank my husband Tiago da Silva Lopes for his generous patience, encouragement, and endless faith in me and my work.

Table of contents

1 Abstract

The giant muscle protein titin (up to 3.7 MDa) is a scaffolding protein that extends from the Z-disc to the M-band of the sarcomere and forms a continuous filament system along the myofiber. During muscle development, titin has been proposed to act as a molecular blueprint to enable sarcomere assembly. In mature muscle, titin acts as an adjustable molecular spring that provides elasticity and stability to the sarcomere. Titin's tight integration into the myofilament and its interaction with multiple structural, regulatory, and contractile proteins has suggested that it is a static protein in the sarcomere. Here we provide evidence that sarcomeric titin may be more dynamic than previously anticipated. To investigate its role in sarcomere assembly and disassembly we used the titin-eGFP knockin mouse, where the fluorescent protein eGFP is attached to titin's C-terminus flanking the M-band region of the sarcomere. This model provides the first tool to investigate the expression and localization of titin in striated muscle in real time. In non-muscle cells titin is expressed at low levels so that the fluorescent signal is under the detection limit of current fluorescent microscopes. We studied titin's mobility using FRAP (fluorescence recovery after photobleaching) and found that calcium is the main determinant of titin dynamics. This effect is independent from calcium-induced contraction and could reflect changes in the affinity of titin to actin. Titin dynamics was independent from protein biosynthesis, but depended on protein degradation. We determined that movement of titin molecules and not myofibril rearrangement was the main mechanism for fluorescent recovery. Neither domain composition nor developmental stage led to changes in titin's mobility, which was equally efficient along and across the myofiber. These results suggest a model where the largely unrestricted movement of titin within and between sarcomeres largely depends on calcium. Our findings have implications for skeletal muscle and cardiac disease, as the stability and remodeling of the myofilament determine its ability to regenerate and adapt to a changing environment.

2 Zusammenfassung

Das Muskelprotein Titin ist außergewöhnlich groß (bis zu 3,7 MDa) und erstreckt sich von der Z-Scheibe bis zur M-Bande des Sarkomeres und bildet dabei ein kontinuierliches Filamentsystem entlang der Myofibrille. Während der Entwicklung der Muskelfibrillen fungiert Titin als Gerüstsystem und ermöglicht den Aufbau der Sarkomere. Titin enthält elastische Domänen, welche die mechanischen Eigenschaften des Myofilaments bestimmen. Als Gerüstprotein ist Titin fest in das Sarkomer integriert und interagiert mit unterschiedlichen strukturellen, regulatorischen und kontraktilen Proteinen. Entgegen der vorherrschenden Meinung, dass Titin stabil im Sarkomer fixiert ist, zeigen unsere Studien eine unerwartete Mobilität für ein Protein seiner Größe. Zur funktionellen Untersuchung von Titin beim Auf- und Abbau von Sarkomeren haben wir die Titin-eGFP Knockin-Maus verwendet, bei der Titins C-Terminus im Bereich der M-Bande durch das Fluoreszenzprotein eGFP markiert ist. Das Mausmodell ermöglichte es uns die Expression und Lokalisation von Titin im quergestreiften Muskel in Echtzeit zu untersuchen. Aufgrund der geringen Expression von Titin in Nichtmuskelzellen konnte ein Fluoreszenzsignal mit der aktuell verfügbaren Mikroskopietechnik nicht detektiert werden. Die Untersuchung der Mobilität von Titin im Sarkomer erfolgte mittels FRAP (Fluorescence Recovery after Photobleaching) und zeigte, dass diese insbesondere durch Kalzium beeinflusst wird. Der Kalzium-Effekt war unabhängig von der Kontraktion und könnte damit auf einer veränderten Affinität von Titin zu Aktin beruhen. Die Dynamik von Titin war abhängig vom Proteinabbau, aber nicht von der Proteinbiosynthese. Insgesamt spielt die Verschiebung von Myofibrillen im Vergleich zur Bewegung von Titin-Molekülen nur eine untergeordnete Rolle bei der Wiederherstellung des Fluoreszenzsignals. Weder die Domänenstruktur noch der Entwicklungsstand führten zu Veränderungen in der Mobilität. Unsere Ergebnisse weisen darauf hin, dass die weitgehend uneingeschränkte Bewegung von Titin-Molekülen innerhalb und zwischen Sarkomeren hauptsächlich durch Kalzium beeinflusst wird. Unsere Untersuchungen sind insbesondere für Skelettmuskel- und Herzmuskelerkrankungen relevant, da Umbauprozesse und Stabilität des Myofilaments die Möglichkeit zur Regeneration und Anpassung an veränderte Umweltbedingungen bestimmen.

3 Introduction

3.1 Structure and function of muscle

The muscle is a specialized tissue that generates force in order to produce movement or perform essential organ functions. The mechanism of contraction is similar in every muscle cell, but different functions require the adaptation in the structural composition of the muscle. Muscle tissue is divided into striated and smooth muscle. The latter is not under conscious control and mainly located in the walls of hollow organs such as the gastrointestinal tract, uterus, urinary bladder, and blood vessels. Striated muscle tissue is subdivided into skeletal (controlled voluntary) and cardiac muscle (involuntary). Skeletal muscle is composed of muscle fibers (myofibers) arranged into muscle bundles. The myofiber is a single multinucleated muscle cell, which arises from the fusion of multiple precursor cells (myoblasts). Myofibrils, mitochondria, nuclei, and the sarcoplasmic reticulum (SR) are located within the myofiber. Myofibrils contain the basic contractile elements, the sarcomeres. Cardiac muscle cells are similar to skeletal muscle cells in structure and function. In contrast to skeletal muscle, cardiac cells are branched, mononuclear, and single cells are connected by intercalated discs, protein complexes important for the transmission of the contractile force from one cell to the adjacent cell.

3.1.1 Muscle contraction

Already in 1954 the sliding filament theory was described (Huxley and Hanson, 1954; Huxley and Niedergerke, 1954). Huxley and colleagues observed that under contraction the I-band region of the sarcomere (mainly actin filaments) shortened while the A-band length (mainly myosin filaments) was constant. The sliding of actin along myosin shortens the sarcomere and consequently the muscle (Huxley and Hanson, 1954; Huxley and Niedergerke, 1954). The interaction of actin and myosin filaments is the actual mechanism of contraction (Hynes et al., 1987; Huxley, 2000). The muscle myosin is a hexameric protein, composed of two heavy chains (MHC; ~220 kDa) and four light chains (MLC; ~20 kDa). The functional regions of the protein are the rod and the head. The C-termini of both MHCs form the coiled-coil rod and the portion of the rod which connects the myosin head with the thick filament core is referred to as subfragment S2. The head domain (S1) contains the actin binding site

and is formed by the association of the two MLCs and the N-terminus of the MHC (Rayment et al., 1993). The actin filament is made up of two α-helices where tropomyosin (TPM) and the troponin (Tn) complex bind and control the myosin-actin cycling (Weber and Murray, 1973).

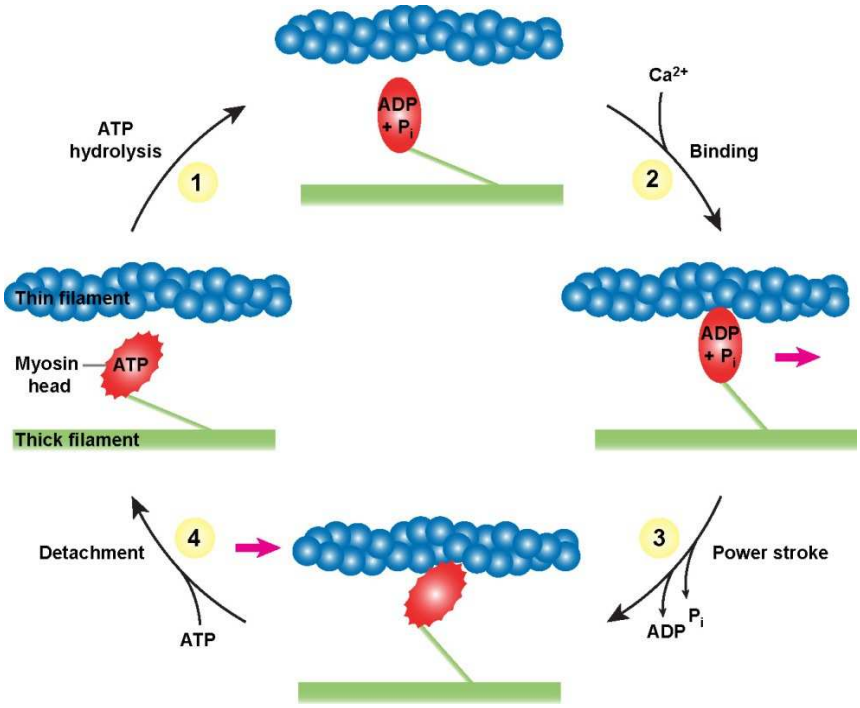

Figure 1. The basic mechanism of muscle contraction. (1) The hydrolysis of ATP provides the energy for contraction and leads to changes in the myosin head conformation. (2) Increase in the intracellular calcium concentration and binding to troponin C releases the myosin binding site on actin. Binding of actin and the myosin head separates the phosphate. (3) The position of the myosin head changes towards the M-band when ADP is released and the energy from the ATPase reaction is used for the actin sliding along the myosin filament (power stroke). (4) Binding of ATP leads to the detachment of myosin from the active site of actin. The new cycle starts with the cleavage of ATP. Modified from Karlson et al., 1994.

The contraction cycle includes four basic stages and is regulated by the calcium concentration (Figure 1). The depolarization of the muscle membrane results in the opening of the ryanodine receptors (RyR) of the sarcoplasmic reticulum and the calcium release increases the calcium concentration in the sarcoplasm. Calcium ions bind to the calcium-binding domain of troponin (TnC). Consequently TnI (inhibitory subunit) and TnT (TPM-binding subunit) change their conformation and pull TPM away from the active site on the actin molecule in order to permit cross-bridge formation between myosin and actin. In the resting state the myosin heads point away from the M-band of the sarcomere. The hydrolysis of ATP

to ADP and P_i produces energy to change the conformation of the myosin head and allows the myosin-actin interaction. After cross-bridging ADP + P_i are released when the myosin head pivots toward the M-band and pulls actin in the same direction. The power stroke shortens the sarcomere and since all sarcomeres perform the same action the entire muscle contracts. The binding of ATP to the myosin head breaks the link between myosin and the active site of actin and allows the formation of another cross-bridge.

3.1.2 Myofibrillogenesis

Myofibrillogenesis is a complex process and involves the arrangement of different proteins into filaments, the binding and interaction of additional proteins, and finally the alignment and assembly into the highly ordered structure of the sarcomere. Different models of myofibril formation have been described and according to the three-step premyofibril model (Figure 2) mature myofibrils are formed through two intermediate structures: the premyofibril and the nascent myofibril (Rhee et al., 1994; Dabiri et al., 1997; Sanger et al., 2000). The premyofibril is characterized by the appearance of Z-bodies and non-muscle myosin IIB (Rhee et al., 1994). They form near the plasma membrane of the developing myocyte and are composed of sarcomeric α-actinin associated with actin filaments (Kelly, 1969; Dlugosz et al., 1984; Rhee et al., 1994). The premyofibril forms minisarcomeres where the Z-bodies define the boundaries of the sarcomere and actin filaments bind Tn, TPM, and interact with non-muscle myosin IIB. The actin filaments from adjacent Z-bodies overlap, but striation develops only at the stage of nascent myofibrils (Siebrands et al., 2004). In the early stage of myofibril formation non-muscle myosin IIB appears to be important for the alignment of the thin filaments, but subsequently it is replaced by muscle myosin II filaments during the transformation into mature myofibrils (Du et al., 2003; Sanger et al., 2004; Wang et al., 2005b). The nascent myofibril is formed when the Z-bodies align laterally and additionally, titin becomes localized in the Z-bodies (Schultheiss et al., 1990; Rhee et al., 1994; Dabiri et al., 1997; Turnacioglu et al., 1997). At this stage, muscle myosin II filaments begin to align along the nascent myofibril an event guide by titin (Wang and Wright, 1988; Whiting et al., 1989; Rhee et al., 1994). Finally, the aligned Z-bodies fuse to form the solid Z-discs (Dabiri et al., 1997). During this process the Z-bodies move further apart (from 1 µm in nascent myofibrils to 2 µm in mature myofibrils) and thus, titin is stretched and the elongation of the titin protein makes binding sites available for other sarcomeric proteins (van der Loop et al., 1996). The mature myofibril is composed of thin filaments anchored at the Z-disc and thick

filaments aligned in the A-band. The proposed role for titin during myofibril assembly is to act as a template and molecular ruler. This is based on titin's early appearance in myofibrillogenesis, the association with α-actinin, myosin, and actin filaments, and its unique domain structure that contains various binding sites for sarcomeric proteins (McElhinny et al., 2000).

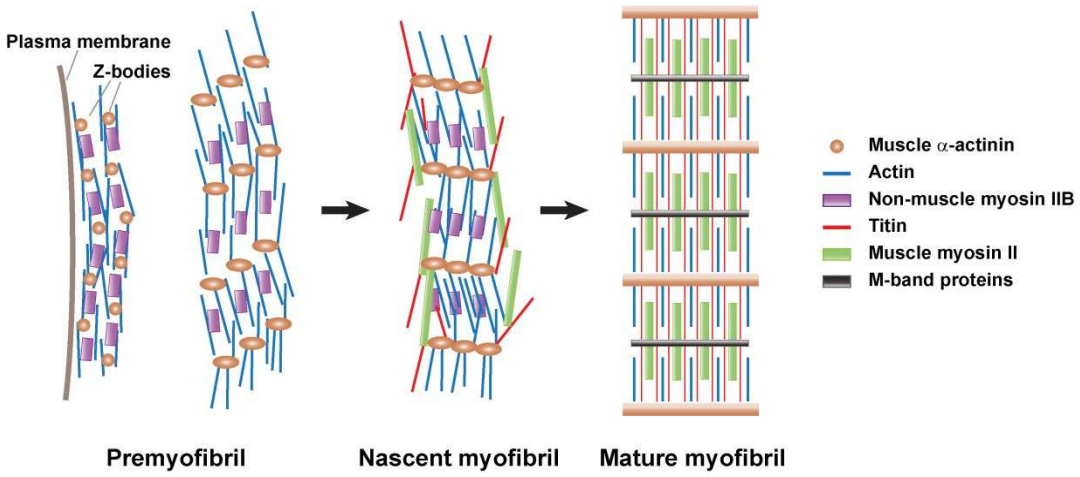

Figure 2. The premyofibril model of myofibrillogenesis. Formation of myofibrils starts with the assembly of muscle α-actinin enriched Z-bodies, actin, and non-muscle myosin IIB into premyofibrils, which consist of minisarcomeres. Nascent myofibrils develop when Z-bodies align laterally and titin and muscle myosin II are added. During the transition of nascent into mature myofibrils, non-muscle myosin IIB is replaced by muscle myosin II. The aligned Z-bodies fuse and form the solid, linear Z-disc and at the same time titin stretches, which enables the binding of other sarcomeric proteins. Modified from Du et al., 2003.

3.1.3 The sarcomere

The sarcomeres, the basic contractile units of the myofilament, are arranged in series and characterized by the defined organization and alignment of specialized proteins (Figure 3). The main components of the myofilament are the thin-, thick-, titin-, and nebulin filaments. When observed by light microcopy the sarcomere appears as periodic light and dark bands. The lateral border of the sarcomere is defined by dark lines, termed the Z-disc. Adjacent sarcomeres align in parallel and their Z-discs are connected by intermediate filament proteins. The light band surrounding the Z-disc is called the I-band and is isotropic in polarized light. The thin filament system is integrated into the Z-disc and extends to the middle of the sarcomere. Along the thin filaments actin is associated with nebulin, tropomodulin, TPM, and the Tn complex (Drabikowski and Nowak, 1973; Wegner, 1979; Wang and Wright, 1988; Weber et al., 1994). Actin polymerization and depolymerization are regulated by the capping proteins tropomodulin and CapZ, which cover the pointed and barbed ends of the actin filament, respectively (Caldwell et al., 1989; Weber et al., 1994). The contractile force is produced by the interaction of the thin filaments with the thick filaments at the A-band region (anisotropic in polarized light) of the sarcomere. The myosin binding protein-C (MyBP-C) associates with the thick filament system at the A-band and may function as a thin-thick-filament linking protein (Bennett et al., 1986). Myosin represents the main component of the thick filament system and extends from the A-band to the M-band, where it is cross-linked in the center of the sarcomere. Titin forms the third filament system and spans the half-sarcomere (~1 μm), thereby interacting with thin and thick filaments (Furst et al., 1988). A major component of the Z-disc is α-actinin, which is able to cross-link actin and titin from adjacent sarcomeres (Maruyama and Ebashi, 1965; Sorimachi et al., 1997). At the M-band region of the sarcomere the interaction of titin and myosin is mediated by myomesin and M-protein (van der Ven et al., 1996; Obermann et al., 1997). In skeletal muscle the fourth filament system is built up by nebulin, a giant protein of 600-900 kDa, which spans the length of the thin filaments and may act as a molecular ruler by determining the growth of the actin filaments (McElhinny et al., 2003).

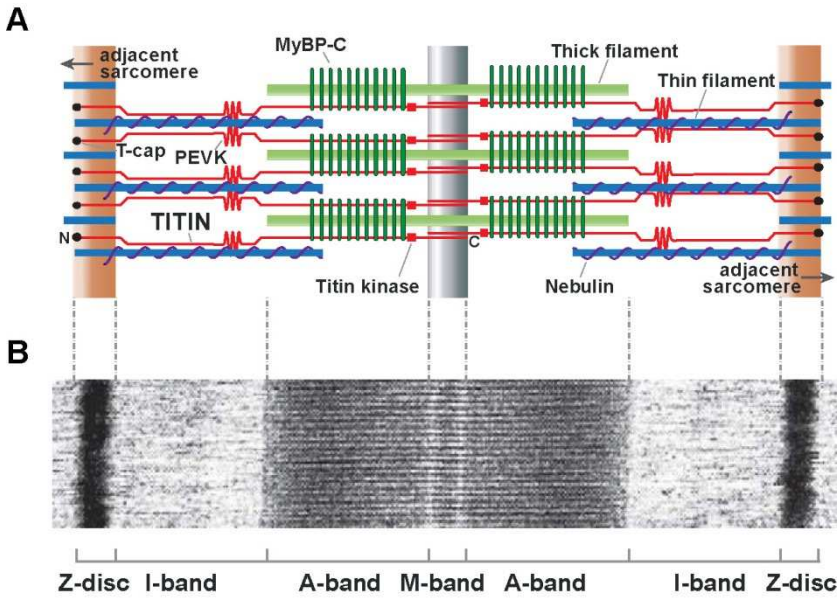

Figure 3. The sarcomeric structure. (A) Schematic layout of the sarcomere including the four filament systems: thin filaments (blue), thick filaments (light green), titin (red), and nebulin (purple). Titin spans the half-sarcomere and integrates with its N-terminus into the Z-disc and with its C-terminus into the M-band. The interaction of titin with the thick filament at the A-band is mediated by the myosin binding protein-C (MyBP-C, dark green). Titin contains elastic elements at the I-band (PEVK domain) and a kinase domain (red square) near the M-band. T-cap (black circle) integrates titin into the Z-disc. Modified from Gregorio et al., 1999. (B) Electron micrograph of a skeletal muscle section shows the lateral boundary of the sarcomere in dark lines (Z-disc) surrounded by the isotropic I-band. The A-band (anisotropic) appears as a dark band and encloses the M-band in the middle of the sarcomere. Modified from Agarkova and Perriard, 2005.

3.2 Muscle titin

In 1977 researchers uncovered the elastic protein connectin in skeletal and cardiac muscle (Maruyama et al., 1977). Shortly after the giant protein titin (~3-3.7 MDa) was purified from striated muscle myofibrils (Wang et al., 1979). Later investigations of the electrophoretic mobility of the two proteins made clear that connectin and titin are the same protein (Maruyama et al., 1981).

Titin forms a continuous filament system along the myofibril. The N-terminal part of titin is anchored in the Z-disc, where molecules from adjacent sarcomeres overlap. The protein extends from the I-band to the A-band and integrates with its C-terminus into the M-band, where molecules from both half-sarcomeres overlap (Furst et al., 1988; Wang et al., 1991; Labeit et al., 1997). Approximately 90% of titin's mass consist of repeating immunoglobulin (Ig) and fibronectin-III (FN-III) domains, so-called super repeats (Figure 4) (Labeit et al., 1990; Gautel et al., 1996). The super repeats provide several binding sites for various sarcomeric proteins. The remaining 10% of the titin molecule mass contain 17 unique

sequences (e.g. PEVK domain, kinase domain), located between the Ig and FN-III domains (Sebestyen et al., 1996; Greaser et al., 2000). The first 90 kDa of titin lie in the Z-disc and are composed of nine Ig elements (Z1-Z9) and up to seven repeating sequence motifs (Z-repeats), which are differentially expressed depending on the muscle (Gautel et al., 1996; Gregorio et al., 1998). Approximately 100 nm away from the center of the Z-disc starts the I-band part of titin, which is mechanically active and undergoes alternative splicing depending on the isoform (Linke et al., 1999). I-band titin is extensible through four spring-like elements and produces passive tension during the stretch of the sarcomere. The spring elements include tandem Ig modules of variable length and the PEVK motifs (enriched in proline (P), glutamic acid (E), valine (V), and lysine (K) residues). Skeletal titin isoforms contain the N2A region and cardiac titin additionally the N2B element (Linke et al., 1999; Greaser et al., 2000; Granzier and Labeit, 2006). When stretch of the sarcomere is initiated, the tandem Ig segments extend by straightening of linker sequences and subsequently the PEVK and N2B elements extend to produce passive tension and resting force (Watanabe et al., 2002). Titin's A-band part (~2 MDa) consists of Ig and FN-III motifs, which make ~70% of the A-band titin (Labeit et al., 1992; Tskhovrebova and Trinick, 2004). The FN-III repeats are exclusively found in the A-band region of titin whereas the Ig domains are present in all parts of the molecule (Linke et al., 1996). A-band titin is tightly associated with the thick filament system and during the contraction and relaxation of the sarcomere it is largely inextensible and does not change position in respect to the M-band, suggesting that the A-band region of titin may regulate the length of the thick filament (Whiting et al., 1989). Titin's C-terminus (~200 kDa) is anchored in the M-band and consists of six exons (MEx1-MEx6) (Kolmerer et al., 1996). M-band titin includes ten Ig motifs (M1-M10) and seven specific interdomains (is1-is7) of variable length (Gautel et al., 1993). Additionally, a catalytically active serine/threonine kinase is encoded in titin's MEx1. It contains a catalytic domain that binds ATP and the substrate as well as a regulatory domain that is able to inhibit the ATP binding (Labeit et al., 1992; Gautel et al., 1995).

3.2.1 Titin isoforms

Titin is encoded by a single gene and different isoforms with a distinct spring composition are generated by alternative splicing (Figure 4). In human and mouse the gene is located on the long arm of chromosome 2 (Muller-Seitz et al., 1993; Rossi et al., 1994; Pelin et al., 1997). The human titin gene contains 363 exons, which encode for 38,138 amino acids with a predicted size of ~4.2 MDa (Bang et al., 2001).

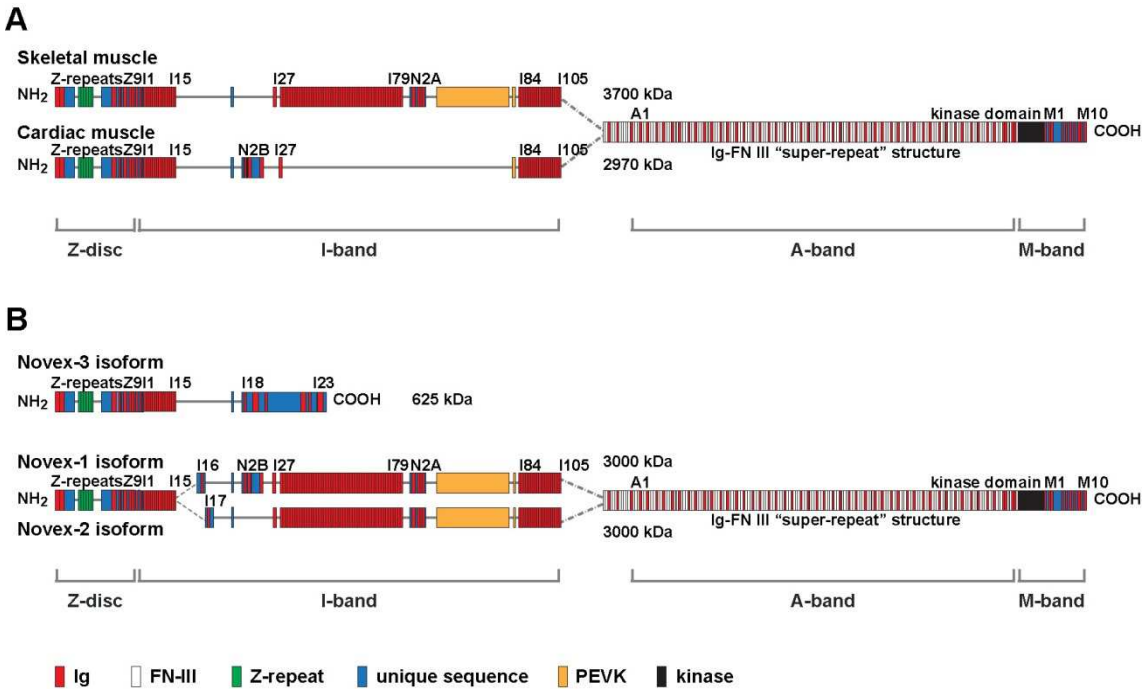

Figure 4. The domain compositions of titin's isoforms. Titin isoforms contain immunoglobulin (Ig, red) and fibronectin-III (FN-III, white) domains, Z-repeats (green), unique sequences (blue), PEVK elements (yellow), and a kinase domain (black). (A) The large N2A titin isoform with a size of 3700 kDa is expressed in skeletal muscle. The major isoform of the adult heart is the 2970 kDa N2B titin. Embryonic and neonatal cardiac tissue expresses the larger N2BA isoform, which contains the N2B and the N2A element (not shown). (B) Three unique I-band splice variants, termed novex 1-3, are expressed in cardiac and skeletal muscle. The short 625 kDa novex-3 titin does not reach the A-band region of the sarcomere and provides an alternative C-terminus. Modified from Bang et al., 2001.

Titin's Z-disc region contains Z-repeats (45-amino acid repeat motifs) that provide binding sites for α-actinin (Sorimachi et al., 1997). The number of Z-repeats varies as a result of alternative splicing and determines the thickness and the mechanical strength of the Z-disc in different muscle tissues (Gautel et al., 1996). The spring elements of I-band titin are differentially expressed in order to facilitate functional and structural properties of the

particular muscle (Freiburg et al., 2000). In the heart three classes of titin isoforms are known: N2B, N2BA, and fetal N2BA titin, which contain differentially expressed tandem-Ig, PEVK, and N2B elements (Freiburg et al., 2000). The splicing of exon 49/50 to exon 219 leads to the relatively small cardiac N2B titin isoform with a size of ~3 MDa (Freiburg et al., 2000). The N2B sequence is encoded in exon 49 and only present in cardiac titin isoforms (Freiburg et al., 2000; Bang et al., 2001). The cardiac N2BA titin contains in addition to the N2B element the exons 102-109 which code for the N2A element (Cazorla et al., 2000; Freiburg et al., 2000). The N2BA titin is larger in size (~3.3-3.5 MDa) due to the long PEVK element and the variable number of Ig domains (Bang et al., 2001). The third cardiac isoform includes the large embryonic/neonatal titin with additional tandem-Ig and PEVK domains and a molecular weight of ~3.6-3.8 MDa (Lahmers et al., 2004; Opitz et al., 2004). After birth the dominant embryonic N2BA titin is rapidly replaced by the shorter and stiffer N2B isoform in the heart and the ration of N2BA:N2B determines the stiffness of the sarcomere (Lahmers et al., 2004; Opitz et al., 2004; Greaser et al., 2005). The characteristic isoform of skeletal muscle is N2A titin which ranges in size from ~3.3 up to 3.7 MDa, with the largest form in the soleus muscle (Freiburg et al., 2000; Prado et al., 2005). The N2A titin is expressed as a single isoform with exception of quadriceps and tibialis cranialis where two N2A titin isoforms are detectable (Ottenheijm et al., 2009). Additionally, three unique isoforms of I-band titin, so-called novex 1-3, are expressed in heart and skeletal muscle (Figure 4B) (Bang et al., 2001). In the heart the novex-1/N2B and novex-2/N2B titin are co-expressed with N2B and N2BA titin (Cazorla et al., 2000; Freiburg et al., 2000; Bang et al., 2001). Novex-3, with a molecular weight of ~700 kDa, is integrated into the Z-disc and provides an alternative C-terminus. It spans from Z1-Z2 to the novex-3 exon in the I-band and does not extend to the A-band of the sarcomere (Bang et al., 2001). Novex-3 titin has also been described in *Xenopus laevis*, where *Xtn3* is developmentally expressed in cardiac and skeletal muscle (Brown et al., 2006). The expression of a variable number of extensible elements of I-band titin modulates the extension of titin and therefore the elasticity of the myofilament (Freiburg et al., 2000). In contrast, the A-band and M-band parts of titin are constitutively expressed and only titin's MEx5 undergoes alternative splicing (Kolmerer et al., 1996).

3.2.2 Titin binding proteins

Titin's unique domain structure provides several binding sites for structural, regulatory, and contractile proteins. The interaction of titin with sarcomeric proteins makes it an essential component of the myofilament with signaling, scaffolding, and elastic functions.

3.2.2.1 Binding partners of Z-disc titin

The Ig domains Z1 and Z2 at the extreme N-terminal part of titin bind T-cap (titin-cap; also known as telethonin), a small 19 kDa protein which is expressed in cardiac and skeletal muscle and localizes at the periphery of the Z-disc (Valle et al., 1997; Gregorio et al., 1998; Mues et al., 1998). T-cap binds two titin molecules, positioned in the same sarcomere, in an antiparallel orientation suggesting that T-cap promotes the integration of titin into the Z-disc (Gregorio et al., 1998; Zou et al., 2006). Additionally, titin's Ig domains Z1 and Z2 interact with the SR transmembrane protein small ankyrin 1 (sAnk1) that is concentrated at the Z-disc and M-band (Zhou et al., 1997; Kontrogianni-Konstantopoulos and Bloch, 2003). sAnk1 and T-cap can simultaneously bind to titin, forming a complex that mediates the organization between the Z-disc and the surrounding SR (Kontrogianni-Konstantopoulos and Bloch, 2003). Another binding partner of titin is α-actinin, which is important in the assembly and maintenance of the Z-disc and cross-links titin with the thin filament system. Titin provides three distinct binding sites for α-actinin. The C-terminus of α-actinin is able to bind to titin's Z-repeats 1-7 (Ohtsuka et al., 1997b; Sorimachi et al., 1997; Young et al., 1998). Depending on the muscle the number of the Z-repeats varies, resulting in a variable number of α-actinin-dependent cross-links between the thin and the third filament system (Peckham et al., 1997; Sorimachi et al., 1997; Young et al., 1998). Another binding site for α-actinin lies distal of titin's Z-repeats and the third binding site is located in an interdomain sequence of Z-disc titin (Young et al., 1998; Labeit et al., 2006). The interdomain sequence has also been shown to interact with filamin C and this interaction may coordinate the connection between membranes and myofibrils during early myofibrillogenesis (van der Ven et al., 2000). In addition, titin's Z-disc region binds to the giant muscle proteins obscurin (~720-900 kDa) and nebulin (500-800 kDa) (Bang et al., 2001; Young et al., 2001; Labeit et al., 2006). The titin-obscurin association may be functionally significant for signal transduction, whereas the titin-nebulin interaction has been suggested to specify the width of the Z-disc in skeletal muscle (Young et al., 2001; Witt et al., 2006). The interaction of Z-disc titin with sarcomeric and

membrane-associated proteins indicates the importance in assembly, stability, and maintenance of the sarcomere.

3.2.2.2 Binding partners of I-band titin

I-band titin contains several binding sites for proteins related to contraction, metabolism, and regulation of gene expression. Titin overlaps with the thin filament system at the I-band region of the sarcomere and provides two binding sites for sarcomeric actin. The first interaction site is located at the Z-disc/I-band junction and suggested to anchor the I-band region of the titin molecule in the sarcomere (Linke et al., 1997). Secondly, the actin filaments bind to titin's PEVK domain, an interaction that may regulate the generation of the passive force and is controlled by the calcium-binding protein S100A1 (Linke et al., 1998; Yamasaki et al., 2001). Additionally, the stiffness of the PEVK region can be increased by direct binding of calcium to the PEVK domain (Labeit et al., 2003). Recently it has been shown that the actin-binding protein TPM is able to bind directly to I-band titin at regions known to contain the actin-binding sites. This suggests that TPM and actin sequentially arrange with I-band titin (Raynaud et al., 2004). Furthermore, nebulin is able to interact with the PEVK region in skeletal muscle and their interaction mediates the proper integration of nebulin into the I-band (Ma and Wang, 2002). The cardiac-specific N2B element binds the small heat shock protein (Hsp) αB-crystallin that increases the stability of titin under stress (Bullard et al., 2004). The heart-specific four and a half LIM domain protein DRAL/FHL2 is another target of the N2B domain and FHL2 recruits metabolic enzymes in situations where the sarcomere requires high energy (Lange et al., 2002). Another four and a half LIM domain protein, FHL1, binds to titin's N2B region and is important in the general mechanism of pathological hypertrophy by initiating titin's response to biochemical stress (Sheikh et al., 2008). The stiffness of cardiac titin can be regulated by the protein kinase A (PKA)-mediated phosphorylation of the N2B domain in response to β-adrenergic signaling (Yamasaki et al., 2002). In skeletal muscle the non-lysosomal calcium-dependent cysteine protease calpain-3 (alias p94) binds to the Ig domains of titin's N2A region. This interaction regulates the activity of calpain-3 by inhibition of proteolytic autoactivation of the protease (Sorimachi et al., 1995). Calpain-3 plays a significant role in the protein quality control by regulating the degradation of sarcomeric proteins such as MyBP-C, TPM, nebulin, titin, TnT, and TnI (Huang and Forsberg, 1998). Moreover, the N2A region of titin interacts with the three muscle-ankyrin-repeat proteins (MARPs): the cardiac ankyrin repeat protein (CARP), the

diabetes-related ankyrin repeat protein (DARP), and the ankrd2 (Miller et al., 2003b). MARPs not only bind to titin, but also respond to stretch and regulate transcription and may therefore link stretch-induced signaling pathways and muscle gene expression (Miller et al., 2003b).

3.2.2.3 Binding partners of A-band titin

The A-band region of titin is composed of multiple Ig and FN-III domains that arrange in super-repeats and provide regular spaced binding sites for the thick filament system. Two major interaction partners have been identified, myosin and MyBP-C (Furst et al., 1992; Wang et al., 1992; Houmeida et al., 1995). MyBP-C's binding to the MHC of myosin is important for the assembly and stability of the sarcomere. Additionally, MyBP-C is involved in the regulation of the contraction by controlling the formation and cycling of cross-bridges (Oakley et al., 2007). The proper assembly of the MyBP-C is regulated by myosin and by the interaction of MyBP-C with titin's Ig-FN III-super-repeats (Furst et al., 1992; Freiburg and Gautel, 1996). MHC mainly binds to titin's FN-III motifs and integrates titin into the thick filament system, where it may act as a protein-ruler for the assembly, organization, and length determination of myosin (Houmeida et al., 1995). The muscle-specific RING finger protein (MuRF)-1 is an E3-ubiquitine ligase that binds various muscle proteins including TnT, TnI, MLC, T-cap, and nebulin, and in addition, interacts with titin's A-band domains A168-170, located adjacent to the titin kinase domain (Centner et al., 2001; Witt et al., 2005). MuRF-1 controls the proteasome-dependent protein degradation. Moreover, the association with A-band titin plays an important role in the assembly and maintenance of the thick filament and the M-band, since overexpression led to disruption of the sarcomeric structure at the M-band region (McElhinny et al., 2002). MuRF-1 is located in the nucleus and binds transcription factors, suggesting an essential role in the regulation of cardiac hypertrophy (Gregorio et al., 2005; Willis et al., 2007). Another target of titin's A-band motifs A164-169 is MuRF-2 (Centner et al., 2001). MuRF-2 can bind to MuRF-1 and several muscle proteins and is crucial for the maintenance of the M-band structure (McElhinny et al., 2004; Witt et al., 2005). The binding of titin to the signaling proteins MuRF has been suggested to link the contractile system with mechanisms that regulate protein synthesis and degradation (Tskhovrebova and Trinick, 2003).

3.2.2.4 Binding partners of M-band titin

Titin's Ig domain M4 binds the M-band protein myomesin in a phosphorylation-dependent manner (Obermann et al., 1996, 1997). Myomesin provides a binding site for the MHC and cross-bridges titin with the thick filament system at the M-band region (Nave et al., 1989; Obermann et al., 1996). Similar to myomesin, the M-protein interacts with myosin and titin. M-protein acts as an elastic cross-linker in postnatal cardiac and fast-twitch myofibrils (Obermann et al., 1996; Vinkemeier et al., 1993). As demonstrated for the I-band portion of titin the Ig domains M3-M4 of M-band titin bind DRAL/FHL2 (Lange et al., 2002). Furthermore, the protease calpain-3 targets I-band and M-band titin (MEx5), thus binding sites vary with the muscle type and the developmental stage (Sorimachi et al., 1995). Calpain-3 links to protein quality control mechanisms in skeletal muscle (Sorimachi et al., 1995, 1996; Kinbara et al., 1997). Furthermore, titin's Ig domain M10 interacts with obscurin and the association promotes the stability of the sarcomeric M-band region (Fukuzawa et al., 2008). Another link to sarcomere organization and stability is provided by titin's interaction with the tumor suppressor protein Bin1 (bridging integrator protein 1), which assembles mature sarcomeres and thus coordinates the differentiation of skeletal muscle cells (Fernando et al., 2009).

M-band titin (exon 358 alias MEx1) contains a catalytically active serine/threonine (Ser/Thr)-kinase domain homologous to the myosin light-chain kinase (MLCK) (Labeit et al., 1992). The titin kinase is composed of a catalytic domain that binds ATP and the substrate as well as a regulatory domain that contains the autoinhibitory domain and a binding site for calcium/calmodulin (Gautel et al., 1995). Activation of the kinase occurs by phosphorylation of a tyrosine residue (Y170) and binding of calcium/calmodulin to the regulatory domain, which results in the release of the ATP-binding site (Mayans et al., 1998). It has been proposed that the titin kinase phosphorylates the Z-disc protein T-cap in differentiating myocytes and therefore plays an important role in sarcomere assembly (Mayans et al., 1998). The zinc-finger protein nbr1 (neighbor of Brca1 gene) and the nbr1-related zinc finger protein p62 (sequestosom 1) have been identified as ligands of the titin kinase (Lange et al., 2005). P62 is a multivalent scaffolding platform that controls the ubiquitin proteasome-mediate degradation and interacts with various kinase pathways (Geetha and Wooten, 2002; Seibenhener et al., 2004). In response to mechanical stimuli titin changes its confirmation and enables the interaction of the kinase domain with the scaffolding protein nbr1, which recruits p62 to the sarcomere. Subsequently, MuRF-2 interacts with p62 and the complex translocates

to the nucleus. In the nucleus the complex suppresses the transcriptional activity of the serum response factor (SRF) and consequently suppresses hypertrophic signals (Lange et al., 2005). SRF has a prominent role in the normal development and growth of the heart and the titin-MuRF-2 signaling pathway may be crucial for normal cardiac response to mechanical stress (Lange et al., 2005; Li et al., 2005; Linke, 2008).

3.3 Non-muscle titin

In cardiac and skeletal muscle titin interacts with the thick and thin filaments. Besides muscle cells, non-muscle cells arrange actin and myosin into cellular structures. Non-muscle titin isoforms have been found to interact with these systems, but their role is only poorly understood.

3.3.1 Cellular and nuclear isoforms of titin

Cellular titin localizes in stress fibers and interacts with non-muscle myosin II filaments, but not with muscle myosin (Eilertsen et al., 1994). Non-muscle myosin II filaments align to form highly ordered structures. The alignment depends on titin indicating that cellular titin is important for the assembly and maintenance of non-muscle myosin filaments in the cytoskeleton (Eilertsen et al., 1994). This finding is supported by observations that cellular titin also interacts with the actin binding protein α-actinin and stabilizes the actin-myosin II cytoskeletal structures *in vivo* (Eilertsen et al., 1997). Cellular titin of stress fibers shows structural similarities to titin in muscle cells, including Z-repeats that interact with α-actinin, sequences matching the region of titin at the Z/I-junction, I-band Ig domains, arrays of the PEVK domain, and a kinase domain (Cavnar et al., 2007). The presence of elastic elements may suggest a role of cellular titin in the generation of passive tension, since stress fibers stretch and contract similar to the myofilament (Peterson et al., 2004; Cavnar et al., 2007). Furthermore, cellular titin is present in human blood platelets and co-assembles with non-muscle myosin filaments *in vitro* to form different structural organizations (Keller et al., 2000). A titin-like protein has also been identified in erythrocytes, where it may be present on the cytoplasmic surface of the erythrocyte membrane, but a function is still unknown (Maruyama et al., 1977).

Moreover, titin has been identified as a chromosomal component in human cells and *Drosophila melanogasta* embryos (D-titin) (Machado et al., 1998). D-titin shares structural domains with the vertebrate titin, including Ig and PEVK domains, but not FN-III elements or the kinase domain (Machado and Andrew, 2000). D-titin is essential for chromosome condensation and chromosome segregation during mitosis, since mutations in D-titin lead to chromosomal defects (Machado and Andrew, 2000). D-titin provides elastic properties to the spindle matrix and interacts with actin, myosin, and the *Drosophila* matrix proteins skeletor, megator, and chromator (Fabian et al., 2007). Additional evidence for an important role of non-muscle titin was provided in *Caenorhabditis elegans*, where nuclear titin contributes to the nuclear organization during the interphase by binding of lamins, intermediate filament proteins essential for the structure of the nucleus (Goldman et al., 2002; Zastrow et al., 2006).

3.3.2 Titin in the brush border of the small intestine

The small intestine is a part of the gastrointestinal tract, where the ingested macromolecules are broken down into amino acids, fatty acids, and carbohydrates, and absorbed together with water, electrolytes, and vitamins. The small intestine is divided into three parts: duodenum, jejunum, and ileum. The duodenum is the predominant site of digestion and absorption. Furthermore, the duodenum plays an essential role in iron metabolism and the processes of iron uptake (Latunde-Dada et al., 2002). The jejunum is the place where the digestion of the chyme is completed and nutrients are absorbed into the blood stream. The ileum is separated from the colon by the ileocaecal valve and mainly responsible for the absorption of vitamin B12 (Gräsbeck, 1997; Seetharam and Yammani, 2003). Furthermore, bile salts and the non-absorbed nutrients are absorbed by the ileum.

All parts of the small intestine display a similar histological structure that can be divided into four distinct layers. The outer layer is the serosa, which is composed of an epithelial layer and connective tissue. The muscularis externa, an outer longitudinal and an inner circular smooth muscle layer, follows the serosa. The submucosa is composed of connective tissue and located between the muscle layer and the mucosa. The innermost layer of the small intestine is the mucosa, which is involved in nutrient digestion, absorption, and secretion. To increase the absorption efficiency the surface area of the mucosa is covered with valves of Kerckring, which project into the lumen of the intestine. The luminal surface is further extended by intestinal villi along the valves of Kerckring. The villus itself is composed of small intestinal

epithelial cells (enterocytes) with a tightly packed microvilli surface (brush border), the major amplification of the absorption area (Figure 5). The brush border on the apical surface of the enterocytes is the primary site for food breakdown and absorption (Mooseker, 1985).

The microvillus core and the terminal web are the two functional and structural parts of the brush border (Figure 5). About 20 uniformly polarized actin filaments reach from the microvillus core into the terminal web (Mooseker and Tilney, 1975; Drenckhahn and Dermietzel, 1988). The organization and stability of the actin bundles are provided by the cross-linking proteins villin, fimbrin, and espin (Bretscher and Weber, 1979, 1980; Bartles et al., 1998). The actin bundles are attached to the plasma membrane via the actin-based motor protein myosin-1a that is capable to bind calmodulin light chains and interacts directly with membranes (Mooseker and Cheney, 1995). The part of the microvillus core that extends to the terminal web is termed the core rootlet and includes the cross-linking proteins and in addition tropomyosin, but lacks myosin-1a (Drenckhahn and Gröschel-Stewart, 1980; Mooseker, 1985). Tropomyosin regulates the interaction of actin and myosin and is able to block the binding of actin and myosin-1a (Mooseker et al., 1984; Collins et al., 1991). The terminal web is composed of myosin II and spectrin, which form cross-links between two neighboring actin bundles (Bretscher and Weber, 1978; Mooseker et al., 1978; Hirokawa et al., 1982, 1983). Cellular titin may connect the microvilli in the terminal web similar to myosin II and stabilize the ends of the actin bundles reaching into the cell (Eilertsen and Keller, 1992). Cellular titin isolated from intestinal brush borders is ~900 nm long and co-assembles with brush border myosin to form highly ordered myosin filaments (Eilertsen and Keller, 1992; Eilertsen et al., 1994). Furthermore, cellular titin is distinctly located in the terminal web and absent from the microvillus core, suggesting that cellular titin contributes to the cross-linking of the actin bundles, the organization of the terminal web, and mediates the interaction of myosin with the cytoskeleton (Eilertsen and Keller, 1992).

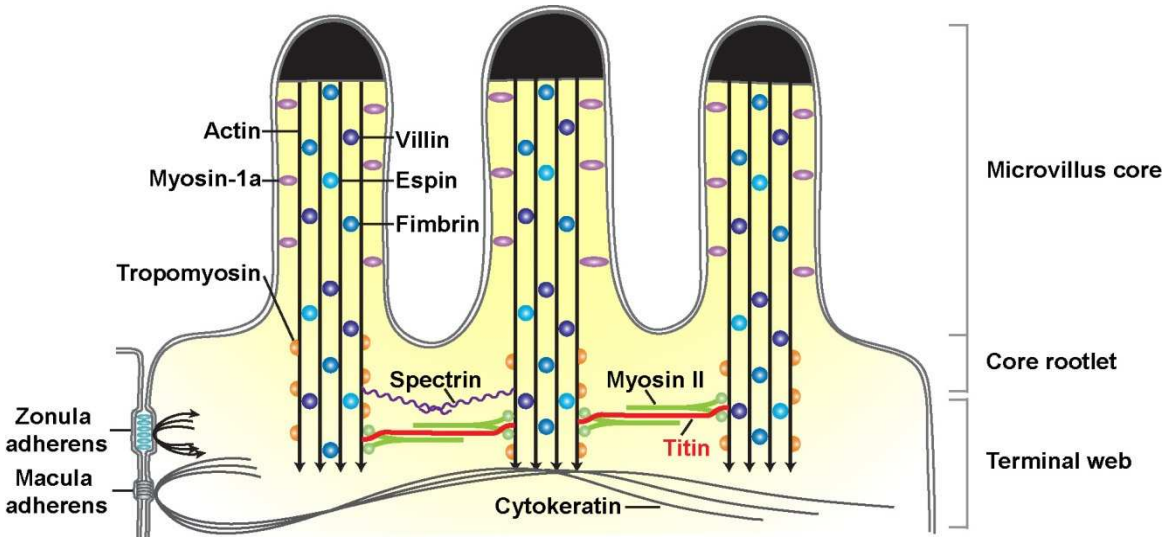

Figure 5. Model for the functional organization of cellular titin in the intestinal brush border. Microvilli at the apical surface of the enterocytes form the brush border, where parallel oriented actin bundles extend from the microvillus core into the terminal web. Actin filaments are cross-linked by villin, fimbrin, and espin, and connected to the plasma membrane via the motor protein myosin-1a. The core rootlet includes tropomyosin and the actin bundles with the cross-linking proteins villin, fimbrin, and espin, but not myosin-1a. Within the terminal web the adjacent microvilli are connected by spectrin and myosin II, which associates with cellular titin. The zonula adherens is the lateral border of the terminal web and includes microfilaments from the terminal web, actin, myosin, and tropomyosin. Cytokeratin filaments organize and stabilize the terminal web by association with the macula adherens. Modified from Mooseker, 1983.

The lateral border of the terminal web is the zonula adherens, a specialized membrane region of the brush border, where microfilaments located in the terminal web terminate (Mooseker et al., 1984; Drenckhahn and Dermietzel, 1988). Within the zonula adherens actin filaments encircle the terminal web and associate with myosin filaments, thus forming a circular stress fiber that can produce force and may regulate the transport of substances between adjacent cells (Drenckhahn and Dermietzel, 1988; Keller et al., 2000). The contractions may fan out the microvilli and therefore increase the contact of the nutrients to the luminal surface between the microvilli, which enhances absorption (Mooseker et al., 1984). Additionally, the zonula adherens includes filamin and tropomyosin, but spectrin and cellular titin are absent from this area (Bretscher and Weber, 1978; Mooseker et al., 1984; Eilertsen and Keller, 1992). Finally, cytokeratin filaments at the basal region of the terminal web associate with the macula adherens. This region below the zonula adherens displays an architectural element of the brush border that is involved in its organization and stabilization (Franke et al., 1981; Mooseker et al., 1984).

3.4 Clinical relevance

Mutations in human titin have been identified in the Z-disc, I-band, A-band, and M-band region and lead to inherited cardiac myopathies and/or skeletal muscle dystrophies. Titin mutations in the Z-disc, N2B element, A-band, or the MEx1 alter the binding affinity for T-cap, α-actinin, and FHL2 and were identified in patients with dilated cardiomyopathy (DCM) (Itoh-Satoh et al., 2002; Gerull et al., 2002; Matsumoto et al., 2005; Gerull et al., 2006). DCM is characterized by the enlargement of the heart and systolic dysfunction, which can result in heart failure (Richardson et al., 1996). Additionally, in patients with hypertrophic cardiomyopathy (HCM) a mutation in Z-disc titin was reported, which increased the binding affinity for α-actinin (Satoh et al., 1999). Furthermore, titin mutations have been identified in patients with tibial muscular dystrophy (TMD), an autosomal dominant late-onset distal myopathy that is characterized by the weakness and atrophy mainly of the tibialis anterior muscle (Hackman et al., 2002; Van den Bergh et al., 2003; Hackman et al., 2008). In this disease titin mutations are found in the M-band region (mainly MEx6 and MEx5) of the protein, which reduce the binding for the protease calpain-3 and therefore influence the mechanisms that control protein quality (Hackman et al., 2002, 2008). Moreover, mutations in titin's MEx1 and MEx3 disrupt the M-band complex and lead to a truncated protein in heart and skeletal muscle (Carmignac et al., 2007). Titin is also affected in the diseased heart. For example, in the failing heart the ratio of titin/MHC is reduced and a structural altered form of titin may contribute to the impaired contraction of the heart (Morano et al., 1994). Furthermore, in DCM and the ischemic heart the expression of N2BA titin is increased by reduced expression of the stiffer N2B titin. Consequently the shift of titin isoforms results in a depression of titin-based myofibrillar stiffness and negatively influences the contraction of the heart (Neagoe et al., 2002; Makarenko et al., 2004).

Titin acts as a molecular blueprint during sarcomere formation and as a molecular spring to produce passive tension when the muscle contracts and relaxes (Granzier and Labeit, 2006; Trinick, 1996). Additionally, titin may have a role as stress-sensor by regulating signaling pathways in response to stretch (Linke, 2008). Consequently, impaired protein-protein interaction caused by mutations can result in cardiomyopathy or muscle dystrophy.

3.5 Aim of the study

The sarcomere is the contractile unit of striated muscle and generates force through the interaction of the thin and thick filaments. Although the myofilament appears as a highly ordered framework, sarcomeric proteins are not fixed to their site of interaction, but in a dynamic equilibration and constantly move between the myofilament (bound) and an unbound pool (Wang et al., 2005a). The mobility of sarcomeric proteins has important implications for muscle assembly, organization, structure, and maintenance. The giant muscle protein titin runs from the Z-disc to the M-band and forms a myofibrillar backbone of the sarcomere (Furst et al., 1988). Due to its functions in the muscle cell and its enormous size, titin has been thought to be a static protein that, when incorporated into the sarcomere, stays bound and interacts with other proteins of the myofilament. Here we addressed the question to what extent titin is mobile in myocytes. Evidence that titin may be in a dynamic exchange came from FRAP analysis of other sarcomeric proteins, where fluorescence recovered within minutes to hours and was distinguished from *de novo* synthesis, which occurred in the order of days (Zak et al., 1977; Isaacs et al., 1989). Aim of the study was to test the hypothesis if titin is capable to move within the sarcomere, similar to actin and myosin. The size of the protein makes it extremely difficult to study the holoprotein *in vitro* and *in vivo*. Therefore we used the knockin mouse model available in our laboratory, where titin's C-terminus is labeled with the green fluorescent protein eGFP. Initially the model had to be validated. This includes the analysis of expression and proper localization of titin-eGFP in the sarcomere and the exclusion of any phenotypic defects that would interfere with the visualization of titin-eGFP in the healthy striated muscle. To directly test the proposed mobility of titin-eGFP, we performed FRAP experiments on embryonic cardiomyocytes and evaluated the impact of protein synthesis and degradation, calcium, contraction, developmental stage, and titin isoform expression. In addition to the kinetic properties of titin, another important question concerning sarcomere assembly and disassembly was addressed. Using the titin knockin mouse we investigated the dynamic remodeling of the sarcomere. To understand how muscle cells work and how myofilaments assemble, it is important to understand the structure and function of a single sarcomere, and more precisely the structure and the function of titin.

Initially titin was identified in cardiac and skeletal muscle, but based on subsequent studies cellular and nuclear titin isoforms have been identified (Eilertsen and Keller, 1992; Machado and Andrew, 2000). To test whether titin is expressed in non-muscle cells, we used the titin-eGFP knockin mouse. The role of non-muscle titin in the organization and maintenance of the

architecture of the brush border in the small intestine was assessed using a gut specific titin knockout mouse. These animals can help elucidate if titin preforms basic cellular functions independent from its role in sarcomere assembly, structure, and biomechanics.

4 Material and methods

4.1 Material

4.1.1 Chemicals and kits

Chemicals were purchased from GE Healthcare, Invitrogen, Roth, or Sigma-Aldrich if not stated otherwise.

Table 1. Kits.

Kit	Manufacturer
Supersignal West Femto Chemiluminescent Substrate	Pierce Chemical Co.
peqGOLD TriFast™	peqlab
qPCR MasterMix Plus	Eurogentec
RNeasy Micro Kit	QIAGEN
RNeasy Mini Kit	QIAGEN
ThermoScript™ RT-PCR System	Invitrogen
Trichrome Stain (Masson) Kit (HT15-1KT)	Sigma-Aldrich

4.1.2 Enzymes

Table 2. Enzymes.

Enzyme	Manufacturer
DNase I	QIAGEN
Proteinase K	Roche
Taq DNA polymerase	Invitrogen

4.1.3 Oligonucleotides

Table 3. Primers for genotyping.

Primer	Sequence
Cre800-for	5'-GCTGCCACGACCAAGTGACAGCAATG-3'
Cre1200-rev	5'-GTAGTTATTCGGATCATCAGCTACAC-3'
eGFP-for	5'-GTCCTGCTGGAGTTCGTGAC-3'
eGFP-rev	5'-AGATGAACTTCAGGGTCAGCTTG-3'

Table 3 continued

Primer	Sequence
eGFP SAK-for	5’-GCCCTTGTAAGACTTTCCAGAAT-3’
Flp-for	5’-GTCACTGCAGTTTAAATACAAGACG-3’
FRT-rev	5’-CAGGTCAAGTATGAAAGGATTGC-3’
MEx6Sai-for	5’-AGAACAACAAGGAAGATTCCACA-3’
MG-FLP1-for	5’-GTCACTGCAGTTTAAATACAAGACG-3’
MG-FLP2-rev	5’-GTTGCGCTAAAGAAGTATATGTGCC-3’
MRZE2 5’-for	5’-ACTTTGATTCCCTATCTTCCTGG-3’
MRZE2 3’-rev	5’-GGGGATACATCCTATAATCAGCC-3’
NbfdsRed-for	5’-CAGCATCATGGTAAAGGCCATCAA-3’
NbrdsRed-rev	5’-CATTCAAATGTTGCCATGGTGTCC-3’
NBfP1Ex2-for	5’-CACTGGCTTACAGACAGGAAAA-3’
NBrP2Ex2-rev	5’-CATTAAAGGGCAGGCTCTGA-3’
SAK-rev	5’-TCTCAACCCACTGAGGCATA-3’

For: forward; rev: reverse.

Table 4. Primers and probes for quantitative real-time PCR (qRT-PCR).

Primer and probe	Sequence
18S RNA-for	5’-CGCCGCTAGAGGTGAAATTC-3’
18S RNA-rev	5’-TGGGCAAATGCTTTCGCTC-3’
18S RNA-probe	6-FAM-TGGACCGGCGCAAGACGGAC-TAMRA
N2B-for	5’-GCAAAGCCTCCAATGAGTATGG-3’
N2B-rev	5’-AGGAAGTAATTTACGAACTTTCTTTTCAG-3’
N2B-probe	6-FAM-TGCACAGCCACACTAACTGTGACAGTGC-TAMRA
N2BA-for	5’-ACAGTGGGAAAGCAAAGACATC-3’
N2BA-rev	5’-AGGTGGCCCAGAGCTACTTC-3’
N2BA-probe	6-FAM-GAAAGAGCTGCCCCTGTGATCA-TAMRA
MEx3-4-for	5’-CCCCTGAAATTGAGTGGTTTAAA-3’
MEx3-4-rev	5’-TTCTGGAGCGACTCACACTGA-3’
MEx3-4-probe	6-FAM-AACCTTCCAATTTCCATTTCTTCA-TAMRA
ZEx1-2-for	5’-CGATGGCCGCGCTAGA-3’
ZEx1-2-rev	5’-CTCAGGGAGTATCGTCCACTGTT-3’
ZEx1-2-probe	6-FAM-TGATGATCCCCGCCGTGACTAAAGC-TAMRA

For: forward; rev: reverse; 6-FAM: 6-carboxyfluorescein; TAMRA: 6-carboxytetramethylrhodamine.

4.1.4 Antibodies

Table 5. Primary antibodies used for immunofluorescence (IF) and Western blotting (WB).

Antibody	Species	Dilution IF	Dilution WB	Manufacturer
α-actinin EA-53 (sarcomeric)	mouse	1:200	-	Sigma-Aldrich
eGFP	rabbit	1:1000	-	Abcam
Titin M8/M9	rabbit	1:200	1:500	Prof. Dr. S. Labeit
Titin Z1/Z2	rabbit	1:50	1:1000	Prof. Dr. S. Labeit
Villin	goat	1:50	-	Santa Cruz

Table 6. Secondary antibodies and fluorescent-labeled reagents used for immuno-fluorescence (IF) and Western blotting (WB).

Antibody	Species	Dilution IF	Dilution WB	Manufacturer
Anti-goat biotin conjugated	donkey	1:500	-	Jackson
Anti-mouse biotin conjugated	goat	1:500	-	Jackson
Anti-rabbit biotin conjugated	goat	1:500	-	Jackson
Anti-rabbit IgG HRP conjugated	goat	-	1:2500	Sigma-Aldrich
Alexa Fluor 488 phalloidin	-	1:20	-	Invitrogen
Alexa Fluor 647 streptavidin	-	1:1000	-	Invitrogen

Jackson: Jackson ImmunoResearch.

4.2 Methods

4.2.1 Molecular biological methods

4.2.1.1 HotSHOT genomic DNA preparation from mouse tail

For genotyping, short fragments of genomic DNA were isolated from mouse tail using the HotSHOT method (Truett et al., 2000). The mouse tail snip (1-2 mm) was incubated in 75 µl alkaline lysis buffer (see below) at 95ºC and 300 rpm for 30 min and subsequently placed on ice. After cooling, 75 µl of neutralization buffer was added and the DNA was directly used for PCR analysis (4.2.1.4).

Alkaline lysis buffer
25 mM NaOH, 0.2 mM EDTA pH 8.0

Neutralization buffer
40 mM Tris-HCl

4.2.1.2 Preparation of genomic DNA from mouse small intestine

Mouse small intestine (0.5 cm) or isolated enterocytes (4.2.2.4) were digested in 700 µl tail buffer supplemented with 25 µl proteinase K (10 mg/ml) at 52ºC and 700 rpm overnight. The proteinase K was inactivated at 95ºC for 10 min. To separate DNA from proteins 700 µl of phenol/chloroform/isoamyl alcohol (25/24/1) was added and the solution was centrifuged for 5 min at 13,000 rpm. The upper phase was transferred into a new tube and 1250 µl of 99% ethanol was added. The DNA was precipitated at -20ºC for 30 min. Subsequently, the samples were centrifuged at 4ºC and 13,000 rpm for 30 min. The pellet was washed with 70% ethanol, air-dried for 10 min, and resuspended in 100 µl Tris-EDTA (TE) buffer. For PCR analysis, 20-50 ng/µl of genomic DNA was used (4.2.1.4).

Tail buffer
20 mM Tris-base pH 8.0, 5 mM EDTA pH 8.0, 0.2% SDS, 400 mM NaCl

TE buffer
10 mM Tris-HCl, 1 mM EDTA, pH 8.0

4.2.1.3 Determination of nucleic acid concentration

The DNA and RNA concentrations were determined at 260 nm using the NanoDrop ND-1000 spectrophotometer (Thermo scientific) following the manufacturer's instructions.

4.2.1.4 Polymerase chain reaction for mouse genotyping

The polymerase chain reaction (PCR) was performed in a PTC-225 Thermo Cycler (MJ Research) with *Taq* DNA polymerase buffer from Invitek and dNTPs from Invitrogen. One µl of HotSHOT (4.2.1.1) or 20-50 ng/µl of genomic DNA (4.2.1.2) served as template for PCR reactions. Primers and expected sizes of the PCR products are listed in Table 3 and Table 7.

Table 7. Primers for genotyping and sizes of PCR products.

Mouse model	PCR name	Analysis	Forward primer	Reverse primer	Product size
TiMEx6-eGFP	eGFP	Genotype	MEx6Sai-for	SAK-rev	562 bp WT
				eGFP-rev	326 bp KI
TiMEx6-eGFP	T	Integration	eGFP-SAK-for	eGFP-rev	1480 bp
TiMEx6-eGFP	Flp	Flp	MG-FLP1-for	MG-FLP2-rev	400 bp
TiMEx6-eGFP	RECf	Recombination	EGFP-for	FRT-rev	500 bp
TiEx28-dsRed	dsRed	Genotype	NBfdsRed-for	NBrdsRed-rev	282 bp WT
					369 bp KI
TiEx2-Vc	Ex2-RECf	Genotype	NBfP1Ex2-for	NBrP2Ex2-rev	256 bp WT
					540 bp RECf
TiEx2-Vc	Cre	Cre	Cre800-for	Cre1200-rev	480 bp
TiEx2-Vc	Ex2-REC	Recombination	MRZE2 5'-for	MRZE2 3'-rev	500 bp

Vc: villin-Cre; WT: wild-type; KI: knockin; REC: deleted allele; RECf: floxed allele; T: targeted allele; Flp: flippase recombination enzyme; Cre: causes recombination; for: forward; rev: reverse.

The genotyping PCR (eGFP-PCR) of TiMEx6-eGFP knockin mice was used to detect the wild-type and knockin allele and was carried out as displayed in Table 8.

Table 8. Genotyping PCR of TiMEx6-eGFP animals.

eGFP PCR	**PCR cycle conditions**		
	Step	**Temperature**	**Time**
1 x *Taq* DNA polymerase buffer	1. Initial denaturation	94ºC	3 min
10% DMSO	2. Denaturation	94ºC	15 s
0.4 µM primer mix	3. Annealing	58ºC	15 s
0.2 mM dNTP	4. Elongation	68ºC	35 s
1.5 mM $MgCl_2$	5. Final elongation	68ºC	8 min
0.025 U/µl *Taq* DNA polymerase	6. Storage	4ºC	∞
	Repeat steps 2-4: 35 x		

The flippase recombination enzyme (Flp) gene or the Cre recombinase (Cre) gene of TiEx2-villin mice was detected using the PCR protocol described in Table 9 with 3 mM of $MgCl_2$ and an annealing temperature of 55ºC. The same protocol was used for the genotyping of TiEx28-dsRed mice, but with 1.5 mM $MgCl_2$ and an annealing temperature of 57°C. The genotyping PCR of TiEx2-villin Cre (Ex2-RECf-PCR) was carried out with 2 mM $MgCl_2$ and an annealing temperature of 58ºC.

Table 9. Genotyping PCR of TiEx28-dsRed and TiEx2-villin Cre mice and detection of the Flp and Cre gene.

dsRed, Ex2-RECf, Flp, Cre PCR	**PCR conditions**		
	Step	**Temperature**	**Time**
1 x *Taq* DNA polymerase buffer	1. Initial denaturation	94ºC	2 min
0.4 µM primer mix	2. Denaturation	94ºC	15 s
0.2 mM dNTP	3. Annealing	55, 57 or 58ºC	15 s
1.5, 2 or 3 mM $MgCl_2$	4. Elongation	72ºC	45 s
0.03 U/µl *Taq* DNA polymerase	5. Final elongation	72ºC	8 min
	6. Storage	4ºC	∞
	Repeat steps 2-4: 35 x		

The proper integration of the eGFP construct into the titin locus (T-PCR, targeted allele) and recombination (RECf-PCR, floxed allele) after Flp introduction was confirmed by PCR (Table 10). T-PCR and RECf-PCR were carried out with an annealing temperature of 60ºC

and 57ºC, respectively. Recombination by villin-Cre in TiEx2-villin Cre mice was confirmed by PCR using an annealing temperature of 58ºC (Ex2-REC-PCR).

Table 10. PCR of TiMEx6-eGFP and TiEx2-villin Cre mice to detect recombination and integration.

T, RECf, Ex2-REC PCR	PCR conditions		
	Step	**Temperature**	**Time**
1 x Gitschier buffer	1. Initial denaturation	93ºC	3 min
10% DMSO	2. Initial annealing	57, 58, or 60°C	5 min
0.4 µM primer mix	3. Initial elongation	65ºC	5 min
0.5 mM dNTP	4. Denaturation	93ºC	30 s
0.08 mg/ml BSA	5. Annealing	57, 58, or 60°C	1 min
0.025 U/µl *Taq* DNA polymerase	6. Elongation	65ºC	1 min
	7. Final elongation	65°C	10 min
	8. Storage	4ºC	∞
	Repeat steps 4-6: 40 x		

The PCR products were analyzed by DNA agarose gel electrophoresis (4.2.1.5).

10 x Gitschier buffer

166 mM $(NH_4)_2SO_4$, 670 mM Tris-HCl pH 8.8, 67 mM $MgCl_2$, 50 mM β-mercaptoethanol, 67 mM EDTA pH 8.0

4.2.1.5 DNA agarose gel electrophoresis

Agarose gel electrophoresis was used to separate and analyze DNA fragments amplified by PCR (4.2.1.4). The UltraPure™ agarose powder (Invitrogen) was mixed with 0.5 x Tris-acetate EDTA (TAE) electrophoresis buffer and heated until completely melted. To visualize DNA after electrophoresis, ethidium bromide was added (final concentration 0.5 µg/ml) and the solution was poured into a casting tray. Gels were placed into an electrophoresis chamber (Cosmo Bio Co, Mupid-21) and covered with 0.5 x TAE buffer. The DNA samples were mixed with 3 µl loading buffer and loaded onto the gel. DNA fragments were separated at 100 V for 20 min. To visualize the DNA fragments, the gel was placed on an ultraviolet

transilluminator (Gel Doc 2000; Bio Rad). The 1 Kb DNA ladder (Invitrogen) was used to determine DNA fragment size.

0.5 x TAE buffer

20 mM Tris-base, 0.05% acetic acid, 0.5 mM EDTA pH 8.0

Loading buffer

0.5% orange G, 50% glycerol, 25 mM EDTA pH 8.0

4.2.1.6 Preparation of RNA from mouse tissue and cells

Total RNA was isolated from heart, skeletal muscle, and small intestine of adult TiMEx6-eGFP wild-type, heterozygous, and homozygous mice. Alternatively, primary embryonic cardiomyocytes (4.2.2.1) and neonatal cardiomyocytes (4.2.2.3) cultures were used for RNA extraction. Snap frozen tissue was homogenized twice for 2 min at a frequency of 30/s using the TissueLyser II (QIAGEN). Total RNA was prepared using the peqGOLD TriFast^{TM} kit according to the manufacturer's instructions. The RNA was dissolved in RNase-free water and the concentration was determined (4.2.1.3). A maximum of 100 µg was used for DNase digestion followed by RNA cleanup (4.2.1.7).

4.2.1.7 RNA cleanup

Isolated RNA from tissues or cells (4.2.1.6) was incubated with DNase I to digest contaminating DNA using the RNase-Free DNase Set following the manufacturer's protocol. A maximum of 100 µg RNA was purified using the RNeasy Mini Kit or a maximum of 45 µg RNA was purified using the RNeasy Micro Kit according to the manufacturer's instructions. RNA was eluted in RNase-free water and the final concentration was measured using the NanoDrop (4.2.1.3). The quality of purified RNA was assessed by formaldehyde gel electrophoresis (4.2.1.8).

4.2.1.8 Formaldehyde gel electrophoresis

Formaldehyde (FA) gel electrophoresis was used to assess the quality of the purified RNA (4.2.1.7). According to the handbook of the RNeasy Mini Kit a 1.2% agarose FA gel with 1 x

FA gel buffer and 0.5 µg/ml ethidium bromide was prepared. Four volumes of RNA solution were mixed with one volume of 5 x RNA loading buffer. The samples were incubated at 65°C for 5 min, chilled on ice, and loaded onto the FA gel. The gel was run in 1 x FA buffer at 100 V for 20 min. To visualize the RNA, the gel was placed on an ultraviolet transilluminator (Gel Doc 2000; Bio Rad).

10 x FA gel buffer

200 mM MOPS, 50 mM sodium acetate, 10 mM EDTA, pH 7.0

5 x RNA loading buffer

0.16% saturated aqueous bromphenol blue solution, 4 mM EDTA pH 8.0, 2.7% FA, 20% glycerol, 31% formamide, 40% 10 x FA gel buffer, add RNase-free H_2O

4.2.1.9 cDNA synthesis

The ThermoScript™ RT-PCR System was used to generate complementary DNA (cDNA) from RNA used as template. The reverse transcription (RT) PCR was performed with 3 µg of high quality intact RNA (4.2.1.7). The two-step protocol is outlined below.

50 ng/µl random primer	1 µl
3 µg RNA	x µl
10 mM dNTP Mix	2 µl
DEPC-H_2O	add 12 µl

RNA and primer were denatured by incubation at 65°C for 5 min and cooled down on ice. The following master mix was added to the samples.

5 x cDNA synthesis buffer	4 µl
0.1 M DTT	1 µl
40 U/µl RNaseOUT™	1 µl
DEPC-H_2O	1 µl
15 U/µl ThermoScript™ reverse transcriptase	1 µl

The samples were incubated at 25°C for 10 min, followed by 50 min at 50°C. The reaction was terminated by incubation at 85°C for 5 min. The RT-PCR was carried out in a PTC-225 Thermo Cycler (MJ Research). cDNA was used for quantitative real-time PCR (4.2.1.10).

4.2.1.10 Quantitative real-time PCR

Gene expression was analyzed by quantitative real-time PCR (qRT-PCR) using the TaqMan probe based chemistry (Applied Biosystems). The fluorophore labeled probe enabled the detection of a specific PCR product as it accumulated during qRT-PCR cycles. The amplification reaction was performed with a Sequence Detection System (7900 HT; Applied Biosystems). The reaction mix was prepared according to the manufacturer's instructions with adaptation to a reaction volume of 10 µl and is shown below.

qPCR MasterMix Plus (Eurogentec)	1 x
Forward primer	900 nM
Reverse primer	900 nM
Probe	250 nM
cDNA	25 ng

Reaction volume: 10 µl

Used primer and probe sets are listed in Table 4. Thermal cycling conditions were as follows:

1. UNG incubation	50°C	2 min
2. *Taq* activation, UNG inactivation	95°C	10 min
3. Denaturation	95°C	10 s
4. Elongation	60°C	1 min

Repeat steps 3-4: 50 x

Data was collected and analyzed with the Sequence Detection System 2.3 software (Applied Biosystems). The comparative CT Method ($\Delta\Delta C_T$ Method) was used as described in the User Bulletin 2: ABI PRISM 7700 Sequence Detection System. The data was normalized to 18S RNA and controls were set as 1.

4.2.2 Cell biological methods

4.2.2.1 Preparation of embryonic cardiomyocytes

Homozygous TiMEx6-eGFP or TiEx28-dsRed animals were set up for timed matings (4.2.5.1). Hearts were dissected from 13.5 days old embryos (E13.5) and digested in a 0.05% trypsin/EDTA solution (Invitrogen) for 2-4 h at 4°C followed by incubation at 37°C for 15 min. The samples were centrifuged at 800 x g for 3 min and the pellets were resuspended in Dulbecco's modified Eagle medium (DMEM; Cambrex) supplemented with 10% fetal

bovine serum (FBS), 1% penicillin-streptomycin, and 1% non-essential amino acids. Embryonic cardiomyocytes (ECM) were dissociated by gentle pipetting and plated onto 0.1% gelatin-coated plastic dishes (ibidi). Cultures were maintained at 37°C and 5% CO_2 until transfer for FRAP experiments (4.2.2.6).

4.2.2.2 Myoseverin treatment

Primary cardiomyocytes (4.2.2.1) were kept in culture for 3 days before treatment. Cells were incubated in DMEM (10% FBS, 1% penicillin-streptomycin, 1% non-essential amino acids) supplemented with 20 µM myoseverin at 37°C and 5% CO_2. Cells without treatment or incubated in DMSO were used as controls. Cardiomyocytes were fixed and co-stained with α-actinin after 2, 6, 12, 18, 24, and 48 h of treatment (4.2.2.5). In washout experiments, the cells were incubated in myoseverin for 12 h. After washing 4 times with serum-free DMEM, cells were maintained in DMEM (supplemented with 10% FBS, 1% penicillin-streptomycin, 1% non-essential amino acids) for up to 6 h. Sarcomere structure was analyzed using immunofluorescence staining (4.2.2.5). Live cell imaging was performed using a ZEISS LSM 510 NLO microscope and a Plan-Apochromat 63x/1.4 oil DIC M27 objective (Carl Zeiss, Inc.). Figures were assembled using Adobe Photoshop and Adobe Illustrator CS5.

4.2.2.3 Preparation of neonatal cardiomyocytes

The neonatal cardiomyocyte (NCM) culture was prepared from homozygous TiMEx6-eGFP mice. Whole neonatal hearts (postnatal day 2, P2) were harvested, pooled, and immediately transferred into phosphate buffered saline (PBS). The tissue was minced into small pieces and washed with PBS. After pre-trypsinization with 2.5 ml of 0.25% trypsin/EDTA for 3 min at 34°C and 800 rpm, the trypsin solution was replaced and the tissue was incubated for 10 min at 37°C and 800 rpm. The supernatant containing the dispersed cells was collected. The digestion was stopped with 1.25 ml cold FBS and the cell suspension was centrifuged at 1000 rpm for 8 min. The pellet was resuspended in 750 µl DMEM and 750 µl FBS and stored on ice. The digestion step was repeated three times. The fractions from each digestion were pooled and centrifuged at 1000 rpm for 10 min. The pellet was resuspended in DMEM supplemented with 10% FBS, 1% penicillin-streptomycin, and 1% non-essential amino acids. Non-cardiomyocytes were removed by pre-plating for 2 h. Cardiomyocytes were plated onto

0.1% gelatin-coated plastic dishes (ibidi) and cultures were maintained at 37°C and 5% CO_2 until transfer for FRAP experiments (4.2.2.6).

PBS

137 mM NaCl, 2.7 mM KCl, 4.3 mM Na_2HPO_4 x 2 H_2O, 1.4 mM KH_2PO_4, pH 7.4

4.2.2.4 Isolation of primary enterocytes

For isolation of primary enterocytes, we collected fragments of small intestine of TiEx2-villin Cre control, heterozygous, and knockout animals. Luminal contents were emptied and tissue was washed with ice-cold PBS. Intestine was several times rinsed with PBS, longitudinally cut, and subsequently cut into smaller pieces. Intestinal fragments were incubated in 5 ml Cell Recovery Solution (BD Bioscience) for 1 h at 4°C. The tissue was washed with PBS for 5 min at 4°C on an orbital shaker. An additional 5 ml of PBS was added and the fragments were taped gently into the solution. The villi started to dissociate from the intestinal fragments and the PBS/villi suspension was collected. The villi collection was repeated 4 to 5 times, the fractions were pooled, and centrifuged for 3 min at 1000 rpm and 4°C. The pellet was washed with PBS. Isolated primary enterocytes were used for preparation of genomic DNA (4.2.1.2) or total RNA (4.2.1.6).

4.2.2.5 Immunofluorescence staining of cells

Embryonic cardiomyocytes from homozygous TiMEx6-eGFP mice (4.2.2.1) were plated on 0.1% gelatin coated coverslips in a 24-well plate. After 3 days in culture or treatment with myoseverin (4.2.2.2), cells were fixed with 4% paraformaldehyde (PFA) for 10 min at room temperature. Afterwards, coverslips were washed 4 x 5 min with PBS. To ensure free access of the antibody to its antigen, cells were blocked and permeabilized in blocking solution for 1 h at room temperature. Cardiomyocytes were incubated with primary antibodies at 4°C overnight followed by the incubation with a biotin-conjugated antibody at room temperature for 1 h. Unbound antibodies were removed by washing 5 times with PBS between the incubation steps. Cells were incubated with a fluorescent-labeled reagent for 1 h at room temperature. Used primary and secondary antibodies and fluorescent-labeled reagents are listed in Table 5 and Table 6. Cells were washed 5 times with PBS. The coverslips were removed from the well and rinsed with dH_2O to remove excess PBS. Coverslips were placed

in Fluorescent Mounting Medium (Dako) on a glass microscope slide and dried overnight. Fluorescence images were acquired using a confocal scanning laser microscope (LSM 510 with software 3.2 SP2; Carl Zeiss, Inc.) with a Plan-Apochromat 63x/1.4 oil Ph3 or 100x/1.4 oil DIC objective (Carl Zeiss, Inc.). Figures were assembled using Adobe Photoshop and Adobe Illustrator CS5.

PFA

4% paraformaldehyde in PBS, pH 7.5

Blocking solution

10% serum, 0.3% Triton X-100, 0.2% BSA in PBS

4.2.2.6 Fluorescence recovery after photobleaching

A Zeiss LSM 510 Meta and a ZEISS LSM 510 NLO laser scanning confocal microscope were used for fluorescence recovery after photobleaching (FRAP) experiments with homozygous TiMEx6-eGFP, TiEx28-dsRed, or double heterozygous TiEx28-dsRed/TiMEx6-eGFP primary cardiomyocytes (4.2.2.1 and 4.2.2.3). For photobleaching analysis cells were kept at 37°C and 5% CO_2 using an Okolab CO_2 Microscope Cage Incubation system (Okolab) or a CO_2-Module S with TempModul S and Heating Unit XL S (ZEISS). The excitation wavelength and emission filters to image eGFP were 488 nm/band-pass 500-550 nm. To image dsRed, the excitation wavelength and emission filter were 488/543 nm/long-pass 560 nm. Image processing was performed using Zeiss LSM 510 Image Browser version 4.2 or ZEISS Zen 2008 software. For FRAP experiments, a Plan-Apochromat 63x/1.4 oil Ph3 or Plan-Apochromat 63x/1.4 oil DIC M27 objective was used and the confocal pinhole was set to 1.5 µm. Data represent 3-4 individual experiments (n=3-4) with 4-10 cells per experiment. For every cell, 1 or 2 different regions of interest (ROI) were chosen for bleaching squares of 1, 3, or 8 sarcomere lengths and areas of 1 sarcomere length x 3 or 8 sarcomere lengths along or across the myofibril. Images were taken before and immediately after bleaching and every hour over a 14 h time period. Photobleaching was done with 100% intensity of the 488 nm laser for 60 iterations. The fluorescence recovery was measured using the LSM Image Examiner (ZEISS) or Fiji ImageJ. Data was normalized and FRAP curves were generated from raw data as described (Al Tanoury et al., 2010). A region outside of the cell was selected and the background intensity ($I_{base}(t)$) was subtracted from the intensity of the bleached area ($I_{frap}(t)$) and the whole cell ($I_{whole}(t)$) at each time point. The intensities were

normalized by rescaling to the pre-bleach intensities in the corresponding regions ($I_{frap\text{-}pre}$, and $I_{whole\ pre}$). The resulting equation for the normalized FRAP curve is:

$$I_{frap-norm}(t) = \frac{I_{frap}(t) - I_{base}(t)}{I_{whole}(t) - I_{base}(t)} \times \frac{I_{whole-pre}}{I_{frap-pre}} \quad (1)$$

To obtain the exchange half-life ($t_{1/2}$) data was displayed as normalized fluorescence intensity versus time using GraphPad Prism 5.0. The model of one phase association was applied to fit the data:

$$y(t) = \left(y_0 + M_f\right) \times \left(1 - e^{(1-K \times x)}\right) \quad (2)$$

The fluorescence intensity at time zero after bleaching is defined as y_0. K is the rate constant. The exchange half-life ($t_{1/2}$) is computed as followed:

$$t_{1/2} = \frac{\ln(2)}{K} \quad (3)$$

M_f is the mobile fraction and is calculated with the following equation:

$$M_f = \frac{F_{end} - F_{post}}{F_{pre} - F_{post}} \quad (4)$$

F_{end} is the fluorescence intensity when the recovery has reached the plateau level. F_{pre} is defined as the fluorescence intensity before and F_{post} after photobleaching. FRAP data is displayed as mean of 3-4 individual experiments.

4.2.2.7 Cycloheximide, MG132, calcium, and BDM treatment

Cultures of embryonic cardiomyocytes from homozygous TiMEx6-eGFP mice (4.2.2.1) were incubated with 10 µg/ml cycloheximide (CX) 1 h prior and during the FRAP experiment (4.2.2.6) to inhibit protein synthesis. The complementary process, protein degradation, was analyzed using the proteasome inhibitor MG132. Cardiac cells were pretreated with 1 µM MG132 for 6 h and maintained at 37°C until transfer for FRAP experiments. Since MG132 had to be dissolved in DMSO, control cells were incubated in 1.4 mM DMSO 6 h before and during FRAP experiments.

After 3 days in culture, embryonic cardiomyocytes were incubated with 0.9 mM (low, LCa), 1.8 mM (normal, NCa, control), or 2.8 mM (high, HCa) calcium in the culture medium. The treatment was repeated after 2 days and cells were used for FRAP analysis on the fifth day of treatment (4.2.2.6).

Cardiomyocytes were treated with 15 mM 2,3-butanedione monoxime (BDM) to inhibit cell contraction. When cells had stopped beating (after ~15 min), cardiomyocytes were analyzed by FRAP.

4.2.3 Biochemical methods

4.2.3.1 Protein preparation for vertical SDS-agarose gel electrophoresis

Tissue from wild-type, heterozygous, and homozygous adult knockin mice (4.2.5.2) was dissected, snap frozen, and analyzed using vertical SDS-agarose gel electrophoresis (VAGE) (4.2.3.3). Samples were homogenized in liquid nitrogen. The tissue powder was weighted and 20 volumes of VAGE sample buffer were added. The suspension was placed in a Dounce homogenizer (Wheaton) and processed for 5 min. Samples were incubated for 30 min at room temperature followed by centrifugation for 5 min at 13,000 rpm. The supernatant was aliquoted and stored at -80°C. The protein concentration was determined (4.2.3.2) and the samples were analyzed using VAGE (4.2.3.3).

VAGE sample buffer
8 M urea, 2 M thiourea, 3% SDS, 0.03% bromphenol blue, 0.05 M Tris-HCl, 75 mM DTT, pH 6.8

4.2.3.2 Determination of protein concentration

The colorimetric amido black method was used to measure the total protein concentration of samples prepared in VAGE sample buffer (4.2.3.1). The procedure described by Schaffner and Weissmann permitted the removal of interfering substances such as dyes and reducing agents (Schaffner and Weissmann, 1973). A set of protein standards was prepared by diluting bovine serum albumin (BSA) in VAGE sample buffer. The VAGE samples and the protein standards were spotted onto a nitrocellulose membrane (GE Healthcare). The membrane was incubated for 1 min in amido black stain solution. Subsequently the membrane was

transferred into destain solution, which was replaced several times. The protein spots were excised from the membrane and placed in individual tubes to add 800 µl of elution buffer. The stain was eluted by incubation on a shaker for 30 min. The absorbance for each eluate was measured at 630 nm using an Ultraspec 2100 pro spectrophotometer (GE Healthcare). The absorbance of the protein standard was plotted against content of protein and data was fit by linear regression.

Amido black stain solution

45% methanol, 10% acetic acid, 0.1% amido black

Destain solution

90% methanol, 2% acetic acid

Elution buffer

50% ethanol, 0.05 mM EDTA pH 8.0, 25 mM NaOH

4.2.3.3 Vertical SDS-agarose gel electrophoresis

Titin-eGFP from heart, quadriceps, and soleus of wild-type, heterozygous, and homozygous mice (4.2.3.1) was separated using vertical SDS-agarose gel electrophoresis (VAGE) according to Warren et al., 2003. A 1% agarose gel (SeaKem Gold Agarose; Vambrex) was prepared and transferred to the HoeferTM SE 600 Ruby (Amersham Bioscience) electrophoresis unit. The gel was run with 1 x running buffer in the lower chamber and 1 x running buffer supplemented with 10 mM β-mercaptoethanol in the upper chamber at 4°C and 15 mA/gel ~4 h or 3 mA/gel overnight. The titin-eGFP expression was analyzed by Western blotting (4.2.3.4).

5 x Running buffer

250 mM Tris-base, 1.92 M glycerol, 0.5% SDS

Agarose gel solution

1% agarose, 30% glycerol, 1 x running buffer

4.2.3.4 Semi-dry blotting

For Western blot (WB) analysis, VAGE-separated proteins (4.2.3.3) were transferred to a polyvinylidene difluoride (PVDF) membrane (GE healthcare) with the PerfectBlue Semi-Dry Electroblotter SEDEC M (peqlab). The membrane was activated for 10 s in methanol and washed 2 times with dH_2O. Afterwards the membrane was placed in cathode buffer for equilibration. Three Whatman papers (Schleicher & Schuell) were immersed in anode buffer I and placed on the electroblotter followed by 3 Whatman papers soaked in anode buffer II. Membrane and gel were positioned and covered with 6 Whatman papers immersed in cathode buffer. The proteins were transferred at 250 mA for 1.5 h. Transfer was monitored by staining the membrane with Ponceau S Solution for 1 min. The membrane was washed with dH_2O several times to visualize protein transfer and subsequently destained with PBS-Tween 20 (PBS-T). Proteins were analyzed by immunodetection (4.2.3.5).

Anode buffer I

300 mM Tris-base, 0.05% SDS, 10% methanol, pH 10.4

Anode buffer II

25 mM Tris-base, 0.05% SDS, 10% methanol, pH 10.4

Cathode buffer

25 mM Tris-base, 0.05% SDS, 10% methanol, 40 mM caproic acid, 10 mM β-mercaptoethanol, pH 10.4

PBS-T

0.1% Tween 20 in PBS

4.2.3.5 Immunodetection

Proteins separated by VAGE (4.2.3.3) and transferred onto a membrane by Western blotting (4.2.3.4) were analyzed by immunoblotting. The membrane was blocked with superblotto for 1 h at room temperature while shaking. The incubation with the primary antibody (diluted in superblotto) was carried out at 4°C overnight. The membrane was washed 3 times with Tris-buffered saline Tween 20 (TBS-T) followed by the incubation with a HRP-conjugated secondary antibody (diluted in superblotto) for 2 h at room temperature. The primary and secondary antibodies are listed in Table 5 and Table 6. Blots were washed 3 times with TBS-T and developed by chemiluminescence staining using ECL (Supersignal West Femto

Chemiluminescent Substrate; Pierce Chemical Co.). Images were taken using the Stella 8300 imaging system (Raytest) and processed using the Aida Image Analyzer v. 2.24 software (Raytest). Figures were assembled using Adobe Photoshop and Adobe Illustrator CS5.

Superblotto

10 mM Tris-HCl pH 8.0, 150 mM NaCl, 0.1% Tween 20, 0.5% BSA, 2.5% skim milk

TBS-T

50 mM Tris-HCl, 150 mM NaCl, 0.1% Tween 20, pH 7.4

4.2.4 Histological methods

4.2.4.1 Preparation of cryostat sections

Adult cardiac and skeletal muscle tissue from homozygous TiMEx6-eGFP animals and adult small intestine from control and knockout TiEx2-villin Cre animals (4.2.5.2) were fixed in 4% PFA for 6 h at 4ºC followed by equilibration with 30% sucrose/PBS at 4ºC overnight. Tissue was embedded in Tissue Tek (O.C.T. compound; Sakura) and stored at -20ºC. Cryostat sections were prepared using the cryostat HM 560 (Microm) at -25ºC. Tissue was cut longitudinally and 5 µm sections were transferred onto HistoBond glass slides (Marienfeld). The sections were stored at -20ºC until immunofluorescence staining (4.2.4.2).

4.2.4.2 Immunofluorescence staining of cryostat sections

Prior to immunofluorescence staining, cryostat sections (4.2.4.1) were warmed to room temperature and air-dried. Samples were placed in a wet chamber and pretreated with blocking solution (4.2.2.5) for 1 h at room temperature in order to reduce nonspecific bindings. Sections were incubated with the primary antibody (diluted in blocking solution) at 4°C overnight. Consequently, the sections were washed 3 times for 15 min with PBS. The signal was amplified using a biotin-conjugated antibody, which was diluted in PBS and applied for 1 h at room temperature. Sections were washed with PBS followed by incubation with a fluorescent-labeled secondary antibody/reagent for 1 h at room temperature. Primary and secondary antibodies and fluorescent-labeled reagents are specified in Table 5 and Table 6. After washing, the sections were mounted under cover glass with a drop of Fluorescent Mounting Medium (Dako), dried overnight and stored in the dark until

investigated with a Zeiss LSM 510 Meta laser scanning confocal microscope using a Plan-Apochromat 100x/1.4 oil DIC objective (Carl Zeiss, Inc.). Figures were assembled using Adobe Photoshop and Adobe Illustrator CS5.

4.2.4.3 Preparation of paraffin sections

Small intestines from control and knockout TiEx2-villin Cre animals (4.2.5.2) were fixed in 4% PFA at 4ºC overnight. Tissue was placed in embedding cassettes. After shaking in dH_2O for several hours the tissue was dehydrated and coated with paraffin using the Leica TP 1020 automated tissue processor with the following protocol:

70% ethanol	1 x 1 h
90% ethanol	1 x 1 h
96% ethanol	2 x 1 h
100% ethanol	3 x 1 h
Roti®-Histol	3 x 1 h
Paraffin	2 x 1 h

Tissue was embedded in paraffin using the Leica EG 1140 H embedding machine and cooled on a cooling plate (Leica EG 1140 C). Paraffin blocks were sectioned using a microtome HM 355 C (Microm) with cooling. Five µm sections floating on a water bath were transferred on HistoBond glass slides (Marienfeld) and dried on a Raymond A Lamb Drying Hotplate (Thermo Scientific). For histological investigations, the tissue was stained with Masson's trichrome staining (4.2.4.4).

4.2.4.4 Masson's trichrome staining

Paraffin sections (4.2.4.3) were analyzed using Masson's trichrome histology staining (HT15-1KT Kit). Sections were deparaffinized in Roti®-Histol (3 x 5 min) and rehydrated in a descending alcohol series:

100% ethanol	2 x 5 min
96% ethanol	1 x 5 min
80% ethanol	1 x 5 min
70% ethanol	1 x 5 min
50% ethanol	1 x 5 min

Slides were mordanted in Bouin's solution overnight at room temperature. Excess stain was removed in running tap water. Samples were washed in deionized water and stained with working Weigert's iron hematoxylin solution (solution A:B 1:1) for 3 min, which stained nuclei black-blue. After washing in running tap water for 7 min and rinsing in deionized water, tissue was stained in Biebrich Scarlet-Acid Fuchsin solution for 4 min (red stain for cytoplasm and muscle). Sections were washed several times with deionized water and placed in phosphotungstic/phosphomolybdic acid solution for 3 min, to facilitate Aniline Blue staining. Collagen was stained with Aniline Blue solution for 5 min. Slides were rinsed with deionized water and dehydrated in an ascending alcohol series. Samples were mounted using the Roti®-Histokitt and dried overnight at room temperature. Staining was investigated using the Leica DMI 6000 B microscope with a HCX PL APO 63x/1.40-0.60 oil objective (Leica). Images were taken using the LAS 3.4.0 software and figures were assembled using Adobe Photoshop and Adobe Illustrator CS5.

Phosphotungstic/phosphomolybdic acid solution

Phosphotungstic acid solution:phosphomolybdic acid solution: dH_2O (1:1:2)

4.2.4.5 Electron microscopy

Ultrastructural analysis of small intestine from TiEx2-villin Cre control and knockout animals was performed by Dr. B. Purfürst from the "Electron Microscopy (EM) Core Facility" (MDC, Berlin). Tissue was rinsed with PBS and placed in EM fixation solution for 20 min at room temperature followed by incubation at 4°C. After treatment with 1% OsO_4 for 2 h at room temperature, tissue was dehydrated in an ascending alcohol series and propylene oxide. Samples were embedded in Poly/Bed® 812 (Polysciences, Inc.) and ultra-thin sections were cut. The sections were contrasted with uranyl acetate and lead citrate and examined using the ZEISS 910 electron microscope with a CDD camera (Proscan) and iTEM Software (Olympus Soft Imaging Solutions). Figures were assembled using Adobe Photoshop and Adobe Illustrator CS5.

EM fixation solution

2% formaldehyde, 2% glutaraldehyde, 0.1 M phosphate buffer

4.2.5 Animal procedures

Laboratory animals were from own breeding in the animal facility of the MDC, Berlin. Animals were kept in individually ventilated cages (IVC) with a regular 12 h day and night rhythm and free access to food and water. Experiments involving animals were performed following the rules for Animal Welfare of the German Society for Laboratory Animal Science.

TiMEx6-eGFP animals were generated in our group by Dr. A. Pietas and Dr. M. H. Radke (MDC, Berlin) and back-crossed to 129/S6 (Taconic). TiEx28-dsRed mice and titin exon 2 floxed animals (TiEx2) were generated by Dr. N. Bergmann in our group (MDC, Berlin). TiEx2 animals were bred with villin-Cre animals (El Marjou et al., 2004) to generate small intestine specific titin knockout mice (TiEx2-villin Cre).

4.2.5.1 Timed mating

TiMEx6-eGFP or TiEx28-dsRed homozygous females were bred with homozygous males. For the generation of double heterozygous animals, homozygous TiMEx6-eGFP mice were bred with homozygous TiEx28-dsRed. Timed matings were set up in the evening and females were checked daily for a vaginal plug. The morning of plug detection was regarded as embryonic day 0.5 (E0.5). Embryos were harvested at E13.5 and hearts were used for preparation of embryonic cardiomyocytes (4.2.2.1).

4.2.5.2 Harvesting mouse tissue

We determined the body weight of age and gender matched wild-type, heterozygous, and homozygous TiMEx6-eGFP and TiEx2-villin Cre females. Anesthetized animals were sacrificed by cervical dislocation. Hearts were dissected and weighed to calculate heart to body weight ratio. Heart and skeletal muscle were collected and used for the preparation of cryostat sections (4.2.4.1) or were snap frozen in liquid nitrogen and used for RNA isolation (4.2.1.6) or for protein preparation (4.2.3.1). Duodenum, jejunum, and ileum of TiEx2-villin Cre control and knockout animals were dissected, rinsed with PBS and used for paraffin or cryostat sections (4.2.4.3 and 4.2.4.1), EM (4.2.4.5), or isolation of enterocytes (4.2.2.4). In addition, small intestine was snap frozen for isolation of total RNA (4.2.1.6).

4.2.5.3 Body composition analysis

Body composition analysis of TiEx2-villin Cre control and knockout animals was performed by M. Taube from the "*In Vivo* Mouse Phenotyping Platform" of the MDC, Berlin. Two month old TiEx2-villin Cre female mice were analyzed and the measurement was repeated after 6 months. Body fat, free water, and lean mass were measured using the Minispec LF90 II Analyzer (Bruker).

4.2.6 Statistical analysis

We used the GraphPad Prism 5.0 software for statistical analysis. Significant differences between 2 groups were assessed by Student's t-test. Differences between 3 groups were analyzed by one-way ANOVA. Groups affected by two independent variables were assessed by two-way ANOVA. Significance was set at a probability value of 0.05 and all results are expressed as mean ± standard error of the mean (SEM).

5 Results

This study focused on the giant muscle protein titin and its mobility within the sarcomere using the TiMEx6-eGFP knockin mouse model, where the enhanced green fluorescent protein eGFP was integrated into titin's M-band exon 6 at the C-terminus of the protein. Knockin mice were viable and did not show obvious phenotypic defects. We investigated titin dynamics using photobleaching techniques and found that titin's mobility was independent from protein synthesis, but depended on protein degradation. Furthermore, the mobility increased by decreased calcium concentration in the culture medium, an effect independent from contraction. The fluorescence recovery of titin at the Z-disc of the myofilament was analyzed using the TiEx28-dsRed knockin mouse model, where the red fluorescent protein dsRed was integrated near the N-terminus of the protein. Moreover, the TiMEx6-eGFP knockin provided a tool to follow sarcomere disassembly in cardiomyocytes treated with myoseverin and sarcomere reassembly in washout experiments. In addition, the knockin mouse was used to investigate the expressed of cellular titin in the brush border of the small intestine. To assign non-muscle functions of titin, we generated a gut specific titin knockout mouse and found that deletion of cellular titin did not alter the structure of the intestinal brush border.

5.1 The TiMEx6-eGFP knockin mouse

5.1.1 Generation of the TiMEx6-eGFP knockin mouse

Titin's enormous protein size makes it difficult to overexpress or visualize the full length protein in cell culture and *in vivo*. Hence, an eGFP knockin mouse was generated in our group to study the mobility of titin. The green fluorescent protein together with a neomycin (Neo) resistance gene flanked by two flippase recognition target (frt) sites was integrated into titin's M-band exon 6 (MEx6) (Figure 6A). Selected positive embryonic stem (ES) cells were injected into blastocysts. After injection and germline transmission, the integration of eGFP into the titin locus was confirmed by the T-PCR (T; Figure 6B). It has been described that the Neo resistance cassette can influence the phenotype of genetic modified mice (Kaul et al., 2000). To remove the Neo resistance cassette, animals expressing titin-eGFP and Neo were bred with animals expressing the flippase recombination enzyme (Flp) in the germline. Flp recognizes the frt sites and mediates the recombination of the two frt sites as shown in Figure

6A. Flp expression and excision of the Neo resistance cassette were controlled by the Flp- and RECf-PCR (Figure 6B). Homozygous TiMEx6-eGFP animals were back-crossed to 129/S6 (Taconic). Depending on the experiment, animals were bred to obtain hetero- or homozygous offspring and the genotype was confirmed by eGFP-PCR (WT and GFP in Figure 6B).

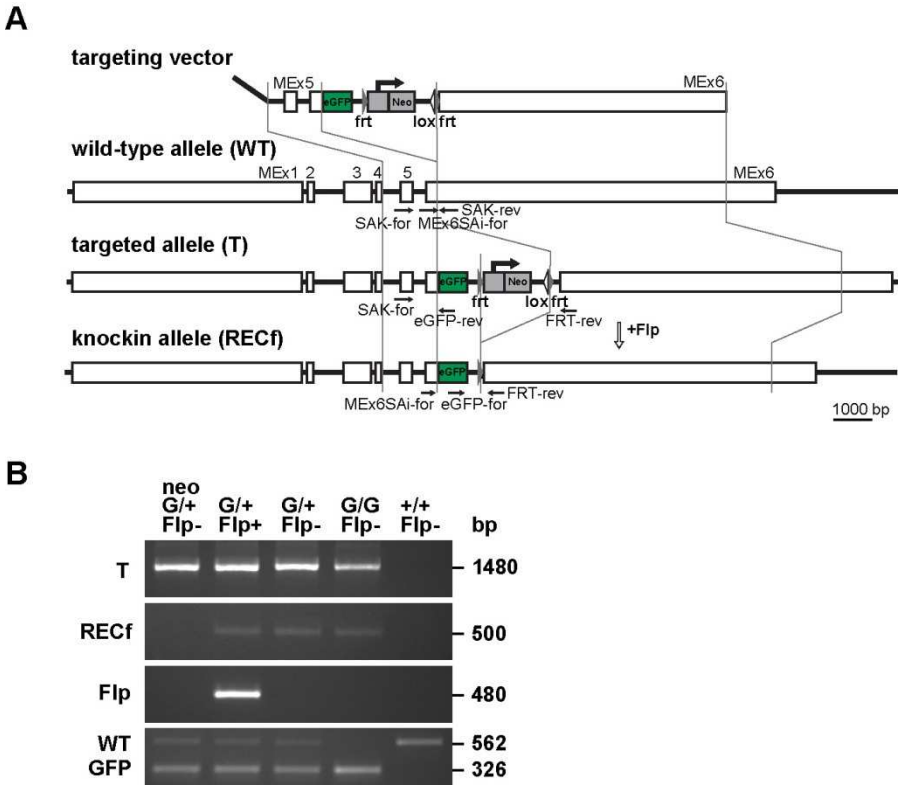

Figure 6. Targeting-strategy and genotyping of the TiMEx6-eGFP knockin mouse. (A) Generation of the TiMEx6-eGFP knockin mouse by integrating the green fluorescent protein eGFP into titin's M-band exon 6 (MEx6). The targeting vector contained the frt flanked neomycin (Neo) resistance cassette. Locations of the genotyping primers are indicated for wild-type (WT), targeted (T), and knockin allele (RECf) (black arrows). Germline expression of the Flp recombinase (open arrow) was used to excise the Neo cassette. (B) PCR based genotyping of wild-type (+/+), heterozygous (G/+), and homozygous (G/G) TiMEx6-eGFP knockin mice using the primers MEx6Sai-for, SAK-rev, and eGFP-rev. Proper integration of the eGFP construct into the titin locus was monitored using the primers SAK-for and eGFP-rev (T). The excision of the Neo cassette (RECf) was confirmed using the primers eGFP-for and FRT-rev after introduction of the Flp transgene (Flp). Bp base pair.

We had to exclude the development of an unexpected phenotype caused by the integration of eGFP into titin's M-band region. Heterozygous and homozygous TiMEx6-eGFP mice were viable and fertile, as confirmed by the presence of the knockin alleles in the homozygous TiMEx6-eGFP animals (G/G Flp-; Figure 6B). Wild-type, heterozygous, and homozygous

TiMEx6-eGFP mice were born at the expected Mendelian ratio. Heterozygous breeding resulted in 29.8% wild-type (n=14), 44.7% heterozygous (n=21), and 25.5% homozygous (n=12) offspring. Moreover, a normal sex ratio was observed with 48.9% males (n=23) and 51.1% females (n=24). The comparison of body weight (BW) and heart weight (HW) of knockin (G/G), heterozygous (G/+), and wild-type (+/+) adult females showed no differences between the genotypes (Figure 7). We determined a body weight of ~24 g, a heart weight of ~112 mg, and a heart weight to body weight ratio (HW/BW) of ~4.6 mg/g for all investigated genotypes (n=6 per group).

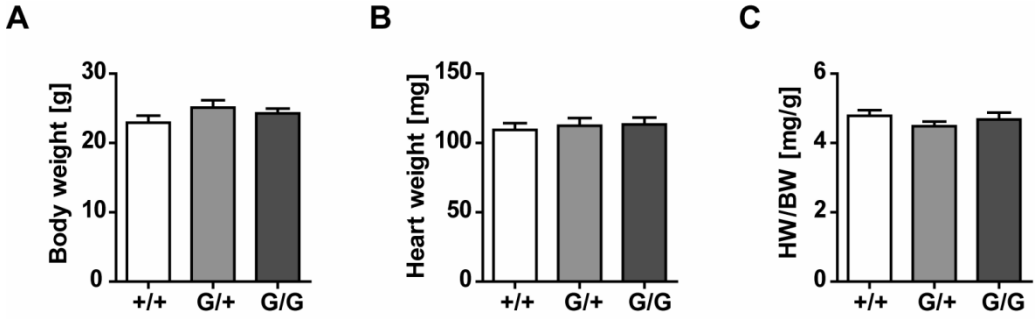

Figure 7. Comparison of heart and body weight from TiMEx6-eGFP knockin mice. (A) Body weight, (B) heart weight, and (C) heart to body weight ratio of female heterozygous (G/+) and homozygous (G/G) TiMEx6-eGFP knockin mice were unchanged compared to wild-type (+/+) (n=6 per group). One-way ANOVA. Error bars indicate SEM.

The TiMEx6-eGFP mice developed normally, showed no obvious behavioral abnormalities, and had a normal life expectancy. To exclude alterations in the protein expression and the sarcomeric structure by the introduction of eGFP, we investigated the expression of titin-eGFP on mRNA and protein level as well as the integration of titin-eGFP into the sarcomere of heart and skeletal muscle.

5.1.2 Expression analysis of titin-eGFP in heart and skeletal muscle

We studied the expression in heart, quadriceps, and soleus of adult male TiMEx6-eGFP wild-type (+/+), heterozygous (G/+), and homozygous (G/G) mice using quantitative real-time PCR (Figure 8).

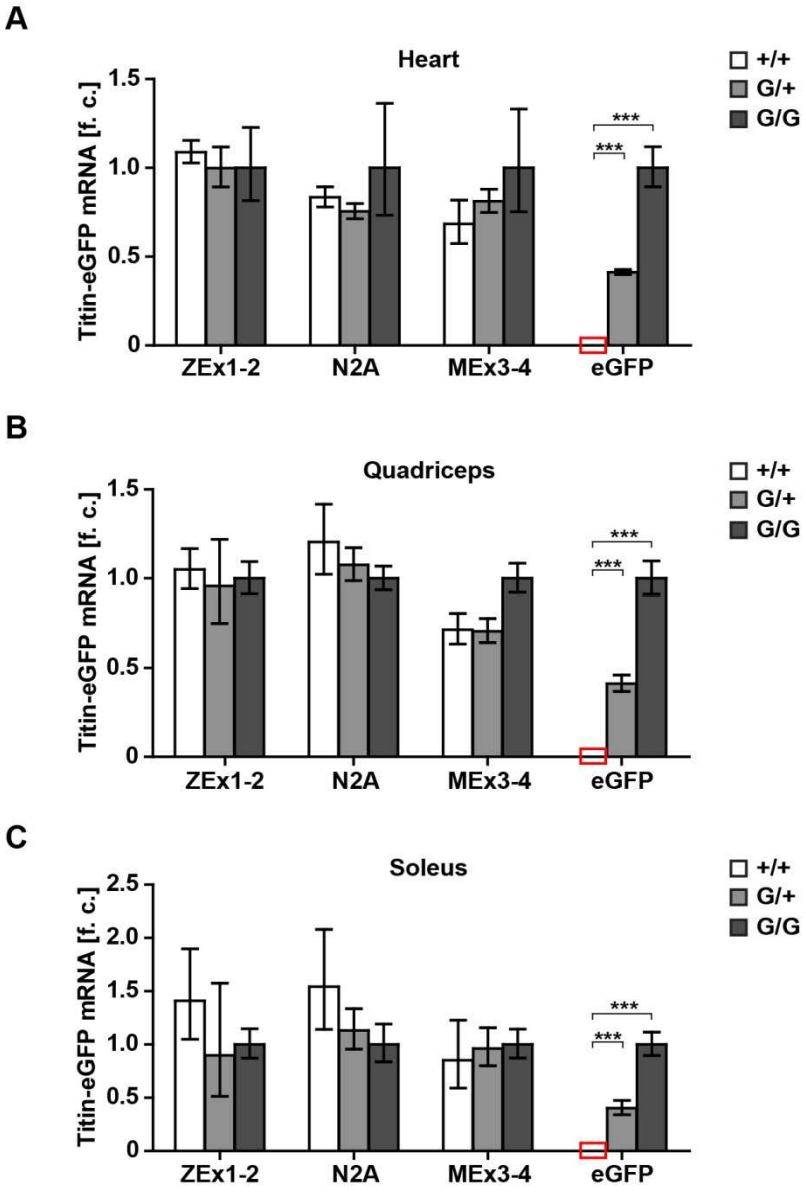

Figure 8. mRNA expression of titin-eGFP in heart and skeletal muscle. The expression of titin-eGFP in (A) heart, (B) quadriceps, and (C) soleus was analyzed using qRT-PCR. As expected, titin-eGFP mRNA levels were intermediate in heterozygotes (G/+) compared with wild-type (+/+) and homozygote animals (G/G). The expression of titin's N-terminus (ZEx1-2), N2A region, and C-terminus (MEx3-4) revealed no difference between the investigated tissues and genotypes. Data was normalized to 18S RNA and titin levels in G/G mice were set as 1 (n=5 per group). Zero values are indicated as an open box. F. c. fold change. Two-way ANOVA ***P<0.001. Error bars indicate SEM.

Titin extends from the Z-disc to the M-band of the sarcomere and eGFP flanks the C-terminus of titin at the M-band region of the myofilament. Analysis of the expression of titin at its Z-disc region (ZEx1-2), A-band region (N2A), and M-band region (MEx3-4) revealed no differences between genotypes. Titin-eGFP expression was verified in heart and skeletal muscle (quadriceps and soleus) of homozygous and heterozygous animals. As expected, heterozygous mice showed an intermediate titin-eGFP mRNA level compared with wild-type and homozygous animals. Wild-type controls did not show an eGFP signal (Figure 8A-C).

We determined the protein level of titin-eGFP in heart, quadriceps, and soleus using vertical SDS-agarose gel electrophoresis and Western blotting (Figure 9). Antibodies directed against titin's N-terminus (Z1/Z2) and titin's C-terminus (M8/M9) showed translation of the full length protein in heterozygous and homozygous muscle, since both ends of the protein are detectable. Furthermore, immunodetection showed equally loaded protein samples.

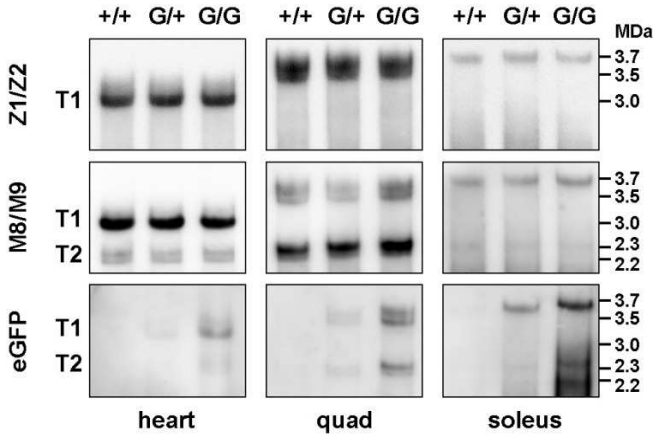

Figure 9. Titin-eGFP protein expression in heart and skeletal muscle. Western blot analysis of heart, quadriceps, and soleus of adult wild-type (+/+), heterozygous (G/+), and homozygous (G/G) TiMEx6-eGFP knockin mice showed the full length titin (T1) and the degradation product (T2). The translation of the full-length protein was confirmed using antibodies against titin's N-terminus (Z1/Z2) and titin's C-terminus (M8/M9). An eGFP antibody detected the eGFP-tagged titin protein in G/+ and G/G, but no signal was obtained in wild-type controls.

Using an antibody against eGFP, we observed expression of titin-eGFP in heterozygous and homozygous animals, but not in wild-types. An intermediate titin-eGFP signal was detected in heterozygous mice compared with wild-type and homozygous animals. The addition of eGFP with a size of 27 kDa did not lead to a visible increase in the size of titin and the full length titin T1 as well as the degradation product T2 could be detected by Western blotting.

In the heart, the shorter titin N2B isoform with a molecular weight of ~3 MDa and the longer N2BA isoform with a molecular weight of 3.2-3.3 MDa could be separated and detected. Additionally, in quadriceps we observed the expression of two titin isoforms: the ~3.5 MDa N2A titin and the second adult N2A titin isoform of lower molecular mass ~3.4 MDa. Soleus expressed the longest titin N2A isoform with a size of ~3.7 MDa (Figure 9).

Titin-eGFP was detected on mRNA (Figure 8) and protein level (Figure 9) in heterozygous and homozygous animals, but not in wild-type controls. We concluded that the integration of eGFP into titin's C-terminus did not alter the expression of mRNA or the translation into protein.

5.1.3 Sarcomeric localization of titin-eGFP

The expression and integration of titin-eGFP into the sarcomere was investigated by confocal imaging of wild-type (+/+), heterozygous (G/+), and knockin (G/G) heart and skeletal muscle (quadriceps and soleus) (Figure 10). No fluorescent signal was detectable in wild-type controls, but a titin-eGFP signal was observed for muscle tissue of heterozygous and homozygous animals. Since heterozygous animals carried one wild-type and one knockin allele, the fluorescent signal intensity was decreased compared with homozygotes. Moreover, the eGFP signal was strong enough without amplification and the fluorescent signal showed a striated pattern with even spacing of the sarcomeres in all hetero- and homozygous muscle tissues investigated (Figure 10).

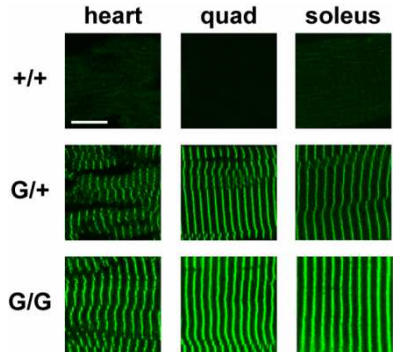

Figure 10. Imaging of titin-eGFP in muscle tissue. Confocal imaging indicated the integration of the titin-eGFP fusion protein into the sarcomere of cardiac and skeletal (quadriceps and soleus) muscle tissue. The fluorescent signal was detectable without amplification in both hetero- (G/+) and homozygote (G/G) muscle and no signal was obtained in wild-type (+/+) samples (n=3 per genotype). Scale bar 10 µm.

We confirmed the proper integration of titin-eGFP into the sarcomere by co-immunofluorescence staining (Figure 11). Cryostat sections of titin-eGFP homozygous heart and skeletal muscle and fixed embryonic cardiomyocytes (ECM) were stained with antibodies against the Z-disc protein α-actinin (Figure 11A). The correct localization of titin's N-terminus into the sarcomere was assessed by staining titin's Z-disc region with an antibody directed against titin's immunoglobulin domains Z1 and Z2 (Z1/Z2). This led to an alternating Z1/Z2-eGFP staining (Figure 11B). The co-localization of eGFP with the M8/M9 epitope was confirmed by staining of titin-eGFP with an antibody that recognized titin's M-band immunoglobulin domains M8 and M9 (M8/M9) (Figure 11C). The fluorescent signal was uniformly distributed over the muscle and the cardiac cells. The sarcomeres displayed equal spacing and the eGFP-tagged protein was properly integrated into the sarcomere, as shown by the anti-Z-disc and anti-M-band antibodies. Overall, the addition of eGFP did not lead to structural changes of the sarcomere or the mislocalization of titin within the myofilament.

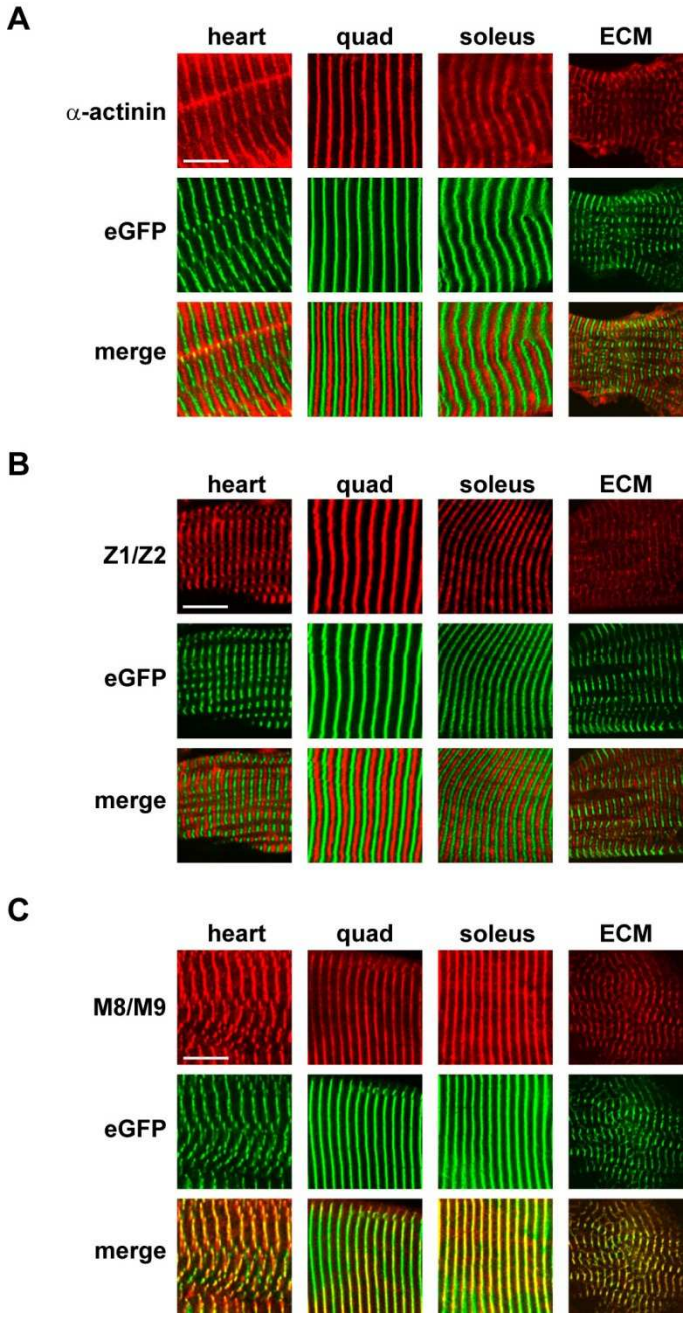

Figure 11. Titin-eGFP expression and localization in the sarcomere. Analysis of cryostat sections from heart, quadriceps, and soleus of homozygous, adult knockin mice and cardiomyocytes from homozygous embryos (ECM). We confirmed proper integration of the titin-eGFP fusion protein into the sarcomere using antibodies directed against (A) the Z-disc protein α-actinin, (B) titin's N-terminus (Z1/Z2), and (C) titin's C-terminus (M8/M9). We detected an alternating α-actinin/eGFP and Z1/Z2-eGFP staining at the Z-disc region. At the M-band region, M8/M9 co-localized with eGFP in all investigated tissues and cells (n=3). Scale bar 10 µm.

The TiMEx6-eGFP knockin mice did not show any phenotypic defects and we confirmed titin-eGFP expression on mRNA and protein level. Furthermore, we showed the proper localization of the tagged protein within the sarcomere. Hence, since the addition of eGFP did

not influence expression or localization of titin, the knockin mouse model was used to study the mobility of the protein.

5.2 Mobility of titin-eGFP

5.2.1 Titin-eGFP mobility is independent from protein synthesis

To investigate the dynamics of titin-eGFP in living cells, we performed confocal microscopy-based FRAP experiments using embryonic cardiomyocytes (ECM) isolated at embryonic day E13.5. The quality of the culture was assessed on the regular and continuous beating after 3 days in culture. To study the kinetics of titin-eGFP and to distinguish protein mobility from protein synthesis, we treated cardiac cells with cycloheximide (CX) (Figure 12), a protein synthesis inhibitor that blocks the translocation step during elongation (Zaal et al., 1999). A region of interest (ROI) was selected and bleached by 100% laser power. Recovery was followed until a steady state was reached. The fluorescence recovery intensities for each ROI were normalized and averaged (Figure 12). We observed that the exchange half-life ($t_{1/2}$) of the fluorescence recovery from CX-treated cells was unchanged compared to control cells (2.1 h vs. 2.6 h, respectively) (Table 11). The time needed to reach half the maximum of the fluorescence recovery is referred to as exchange half-life. The mobile fractions (M_f) from 3-4 experiments were determined from nonlinear regression curves fitted into one-phase association and the fluorescence intensity before bleaching was set as one. M_f represents the percentage of molecules contributing to the fluorescence recovery. 14 h after photobleaching 49% of recovery was reached for control cells and 53% for CX-treated cells (Figure 12C and Table 11). FRAP data suggests that titin-eGFP protein was dynamic and its mobility was independent from *de novo* synthesis, as control and CX-treated cells showed similar kinetics.

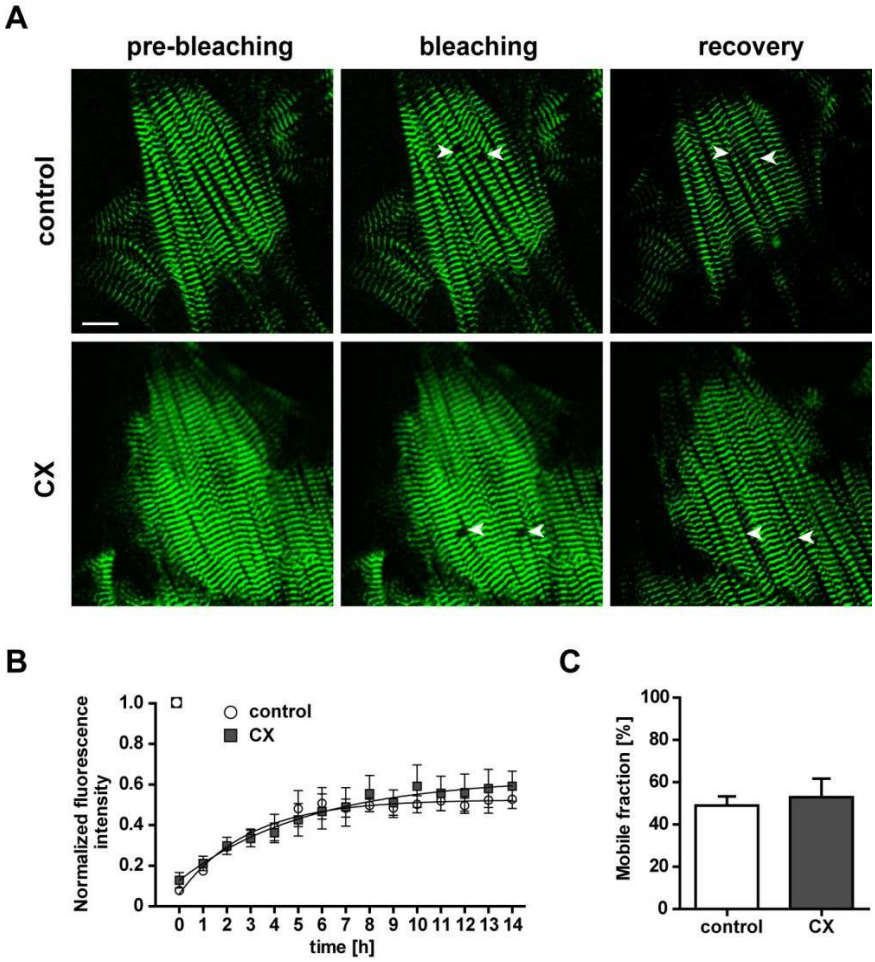

Figure 12. Titin-eGFP dynamics are independent from protein synthesis. Embryonic cardiomyocytes (E13.5) were treated with cycloheximide (CX) to distinguish titin mobility and *de novo* synthesis. Cells were imaged for 14 h after photobleaching to follow recovery. (A) Images of control and CX-treated cells from homozygous TiMEx6-eGFP knockin mice were obtained before and immediately after bleaching (white arrows). Titin-eGFP was homogenously distributed in embryonic cardiomyocytes and its fluorescence significantly recovered after 14 h. Scale bar 10 µm. (B) The normalized fluorescence intensity in the bleached area was plotted as a function of time to compare titin-eGFP protein recovery of control and CX-treated cells. The fluorescence intensity before bleaching was set as 1. Inhibition of protein synthesis did not influence the mobility of titin-eGFP (control n=4, CX n=3). Two-way ANOVA. (C) We observed no difference in the mobile fraction of titin-eGFP between control and CX-treated cardiomyocytes (control n=4, CX n=3). T-test. Error bars indicate SEM.

5.2.2 Inhibition of protein degradation influences titin-eGFP mobility

FRAP analysis of TiMEx6-eGFP cardiomyocytes treated with CX showed that protein synthesis could be excluded as the main basis for titin mobility. Therefore we examined the complementary process protein degradation by exposing cardiac cells to the proteasome inhibitor MG132. The peptidyl aldehyde MG132 inhibits protein degradation by binding reversibly to the β1 subunit within the 26S proteasome (Myung et al., 2001). FRAP analysis of embryonic cardiomyocytes treated for 6 h with MG132 is shown in Figure 13. We

observed that inhibition of protein degradation led to a decrease in titin-eGFP mobility (Figure 13B and C). After 14 h of measurement, the mobile fraction was significantly decreased compared with control cells without treatment (M_f MG132 treatment 22% vs. control 49%). There was a significant increase of the half-fluorescence recovery from 2.1 h in control cells to 7.0 h in MG132-treated cells (Table 11). The addition of MG132 to the medium yielded a slower exchange of bleached titin-eGFP with unbleached proteins and resulted in a decreased mobile fraction with increased half-fluorescence recovery.

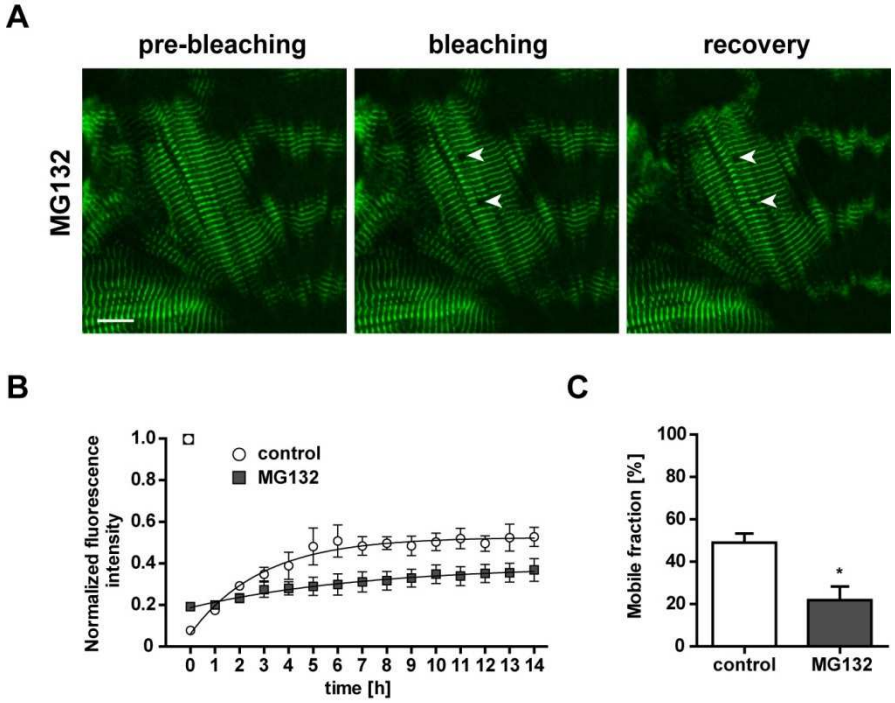

Figure 13. Inhibition of protein degradation resulted in decreased dynamics of titin-eGFP. (A) FRAP analysis (white arrows) of titin-eGFP during inhibition of protein degradation with MG132. Images were taken before, immediately after, and 14 h after photobleaching. Scale bar 10 µm. (B) Graph of the fluorescence recovery kinetics, where the fluorescence intensity before bleaching was set as 1. Titin-eGFP mobility was decreased for cells treated with MG132 compared with control cells (control n=4, MG132 n=3). Two-way ANOVA. (C) The mobile fraction significantly decreased by inhibition of protein degradation (control n=4, MG132 n=3). T-test *P<0.05. Error bars indicate SEM.

The proteasome inhibitor MG132 was dissolved in dimethyl sulfoxide (DMSO). DMSO can cause chemical injury and decreases cell viability (Gomez et al., 1997). To exclude possible negative effects of the solvent on the mobility of titin-eGFP, we treated embryonic cardiomyocytes with DMSO and determined the dynamics of titin-eGFP in DMSO-treated cardiac myocytes using FRAP analysis with a ROI of one sarcomere length (Figure 14).

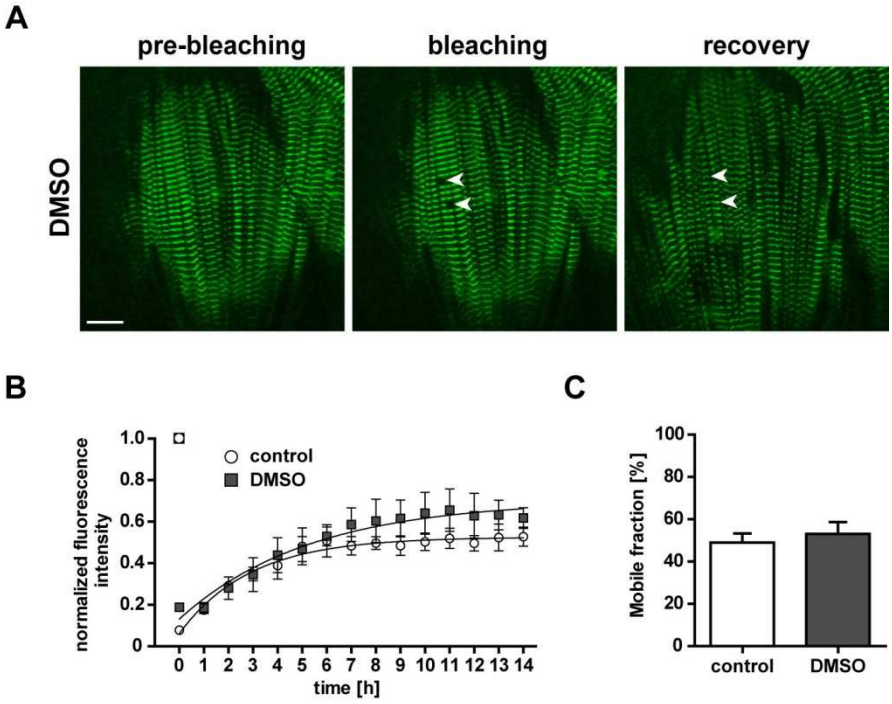

Figure 14. Titin-eGFP mobility in DMSO-treated cardiomyocytes was unchanged. Cardiomyocytes were treated with DMSO to distinguish effects of the proteasome inhibitor MG132 and the solvent DMSO. (A) Images show the fluorescence before, immediately after, and 14 h after photobleaching in embryonic cardiomyocytes treated with DMSO (white arrows). Scale bar 10 µm. (B) Fluorescence recovery curves obtained for control cells and DMSO-treated cells were not different. The fluorescence intensity before bleaching was set as 1 (control n=4, DMSO n=3). Two-way ANOVA. (C) Quantification of the titin-eGFP mobile fractions indicated a level of ~50% in both control and DMSO-treated cardiomyocytes (control n=4, DMSO n=3). T-test. Error bars indicate SEM.

The mobile fraction of DMSO-treated cells did not differ from control cells without treatment (M_f 53% and 49%, respectively) (Figure 14C and Table 11). Similar to control cells, there was a rapid fluorescence recovery of titin-eGFP in DMSO-treated cells. The exchange half-life was not significantly changed compared to control cells (Table 11). Based on these results, it could be excluded that the reduction of the titin-eGFP mobility after MG132 incubation was due to the solvent DMSO.

Table 11. Mobile fractions (M_f) and exchange half-lives ($t_{1/2}$) of titin-eGFP recovery after photobleaching.

Treatment or cell type	M_f [%]	$t_{1/2}$ [h]
Control	49 ± 4	2.1 ± 0.4
CX	53 ± 9	2.6 ± 0.4
MG132	22 ± 6*	7.0 ± 2.4*
DMSO	53 ± 6	4.2 ± 0.4

Control: embryonic cardiomyocytes without treatment; CX: cycloheximide; MG132: proteasome inhibitor (n=13). One-way ANOVA (compared with control) *P<0.05. Data is indicated as mean ± SEM.

Our data demonstrated that the proteasome inhibitor MG132 affects titin-eGFP dynamics, i.e. the exchange of bleached by unbleached titin molecules was significantly reduced. In comparison, the mobility of titin-eGFP of DMSO-treated cells displayed a similar kinetic compared to control cells without any treatment. In addition, we confirmed that DMSO alone did not influence the titin-eGFP mobility in embryonic cardiomyocytes. We concluded that the effect of reduced titin-eGFP dynamics depended on protein degradation.

5.2.3 Titin-eGFP mobility compared with myofibril rearrangement

To address the mechanism underlying the recovery of titin-eGFP after photobleaching, we increased the size of the regions of interest as indicated in Figure 15. Whether structural rearrangements of the myofibrils also contributed to the fluorescence recovery, we analyzed titin's mobility in embryonic cardiomyocytes using FRAP and compared the recovery rates for small (1 x 1 sarcomere length; Figure 12), intermediate (3 x 3 sarcomere lengths), and large (8 x 8 sarcomere lengths) bleached areas (Figure 15). Over the investigated time period there was no drifting of the bleached region within the cell. We only observed minor structural changes or micro-scale rearrangements. Cell shape, spacing of the sarcomeres, and filament direction were conserved during the measurement (Figure 15 and Figure 16). There were no changes in the mobile fractions. Bleaching of a small area led to a fluorescence recovery of 49%. In comparison, 61% of titin-eGFP recovered in intermediate and 52% in large bleached areas (Figure 15C and Table 12). Increasing the size of the bleached region did not influence the pool of titin-eGFP molecules, which were able to move into the bleached area.

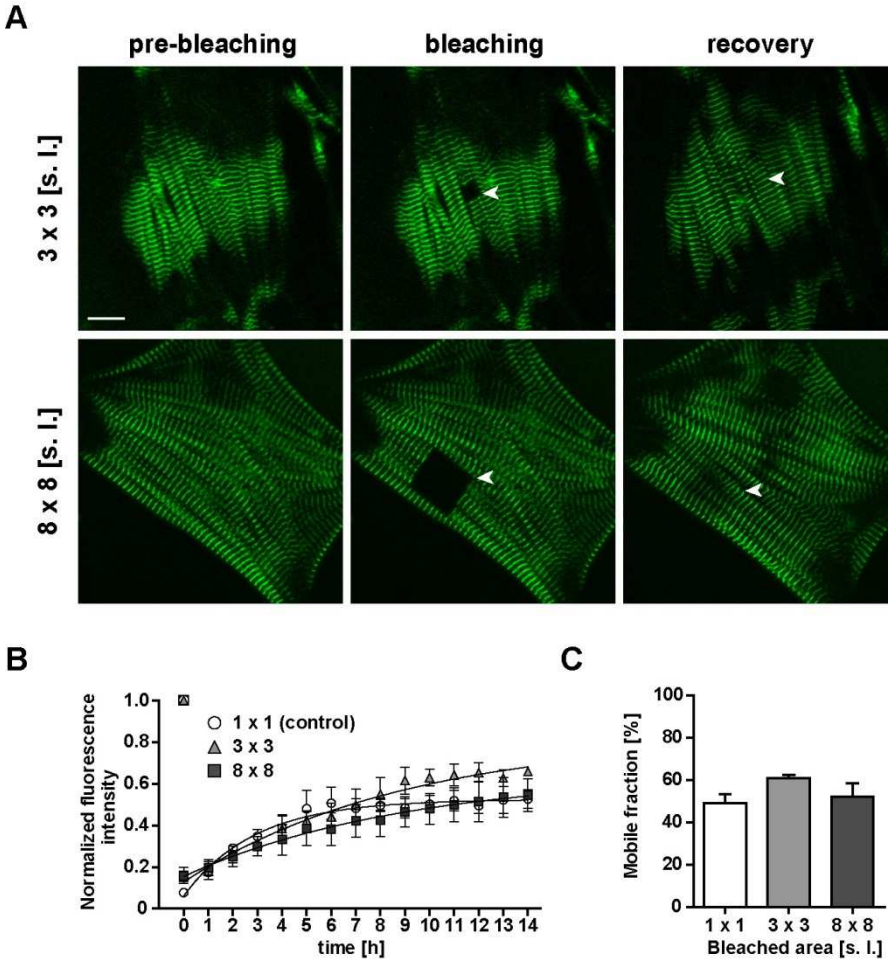

Figure 15. Movement of titin-eGFP vs. myofibril rearrangement. (A) FRAP analysis in areas of 3 x 3 or 8 x 8 sarcomere lengths (white arrows). Images pre-bleaching, immediately post-bleaching, and 14 h post-bleaching are shown. The recovery appeared homogeneous over the bleached region. Scale bar 10 µm. (B) Normalized recovery curves for 1 x 1 sarcomere (control) and areas of 3 x 3 or 8 x 8 sarcomere lengths. The fluorescence intensity before bleaching was set as 1. The increase in the size of the ROI led to a longer recovery time (control n=4, 3 x 3 n=4, 8 x 8 n=3). Two-way ANOVA. (C) The percentage of titin-eGFP moving within the sarcomere (mobile fraction) was independent from the size of the bleached area (control n=4, 3 x 3 n=4, 8 x 8 n=3). S. l. sarcomere length. One-way ANOVA. Error bars indicate SEM.

Analysis of recovery curves revealed that an increase in the photobleached area corresponded with an increase in the exchange half-life. Small bleached regions showed an exchange half-life of 2.1 h and areas of 3 x 3 sarcomere lengths displayed an intermediate half-fluorescence recovery of 6.1 h. In contrast, the exchange half-life significantly increased up to 8.2 h in large bleached areas (Table 12). This indicates that unbleached titin molecules need more time to overcome the distance between the boundary and center of the bleached region.

Table 12. Mobile fractions (M_f) and exchange half-lives ($t_{1/2}$) of titin-eGFP related to the area of bleaching.

Bleached area [s. l.]	M_f [%]	$t_{1/2}$ [h]
1 x 1	49 ± 4	2.1 ± 0.4
3 x 3	61 ± 2	6.1 ± 1.3
8 x 8	52 ± 7	8.2 ± 2.4*

S. l.: sarcomere length (n=11). One-way ANOVA (compared with 1 x 1) *P<0.05. Data is indicated as mean ± SEM.

To gain insight into the dynamics of titin-eGFP, we performed live-cell imaging after photobleaching and investigated the mobility over a time period of 14 h. Figure 16 shows an example of a time-lapse series of the titin-eGFP fluorescence recovery over time. Images were acquired before bleaching (pre-bleaching), immediately after bleaching, and every hour until the recovery reached a steady state. We observed that the shape and the location of the photobleached area were unchanged throughout the experiment. Furthermore, we saw no major micro-scale rearrangements of the myofibrils. The images indicated that recovery rates were slightly faster at the boundaries of the field of measurement. For smaller ROIs, the distance for surrounding fluorophores to move into the bleached area was relatively short. Consequently, increasing the size of the ROI resulted in a longer distance for the unbleached titin-eGFP to travel into the previously bleached area. Therefore the fluorescence recovery was slower towards the center of the ROI. The fluorescent signal gradually recovered over the entire area by movement of unbleached titin-eGFP into the field of measurement and exchange of bleached by unbleached proteins (Figure 16).

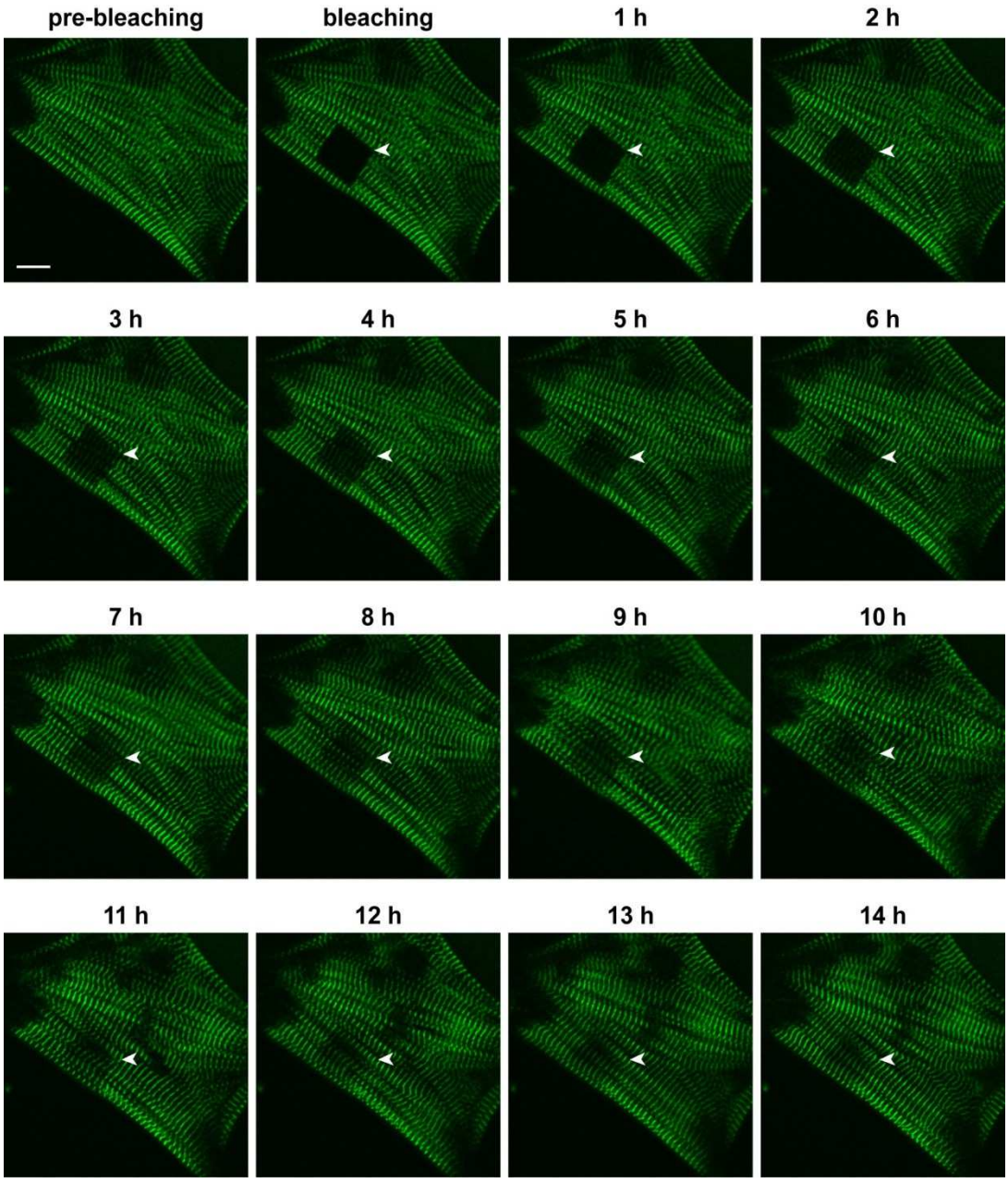

Figure 16. Time-lapse images of the fluorescence recovery of titin-eGFP. To follow the movement of unbleached titin-eGFP into the bleached area, analysis of fluorescence recovery was performed in an area of 8 x 8 sarcomere lengths (white arrow). The sequential images were taken before, immediately after, and every hour over a 14 h time period. Although we did not see any obvious micron-scale rearrangements, we observed that the recovery was slightly faster at the edges of the bleached region, but appeared overall homogenous. Scale bar 10 μm.

Bleaching small, intermediate, and large areas of interest revealed no changes in the mobile fraction of titin-eGFP. However, increasing the size of the ROI produced longer half-fluorescence recovery, since unbleached titin-eGFP needed more time to reach the central area. Only minor dynamic rearrangements were observed during FRAP analysis. We assumed

that the recovery after photobleaching was primarily due to the movement and molecular exchange of individual titin molecules.

5.2.4 Longitudinal vs. lateral movement

With FRAP analysis we examined whether the exchange of bleached by unbleached titin-eGFP molecules occurred within one myofibril and/or between adjacent myofibrils. Thus, we varied the direction of the ROI as indicated in Figure 17. For longitudinal movement of titin-eGFP (white arrows) we assumed that the recovery would be mainly due to diffusion of titin molecules along the myofibrils. Bleaching within one myofibril was used to study lateral titin-eGFP dynamics (open arrows). Recovery would result from diffusion of unbleached titin molecules from adjacent myofibrils. We compared longitudinal and lateral movement of titin-eGFP by bleaching 3 or 8 consecutive sarcomeres (Figure 17A). The recovery curves indicated that longitudinal and lateral movement was equally efficient (Figure 17B and C). The amount of titin molecules able to move into the bleached field of measurement was unchanged between longitudinal and lateral as well as ROIs of 3 and 8 consecutive sarcomeres (Figure 17D, E and Table 13). About 50-60% of titin-eGFP was mobile and contributed to the fluorescence recovery after photobleaching (Figure 17D, E and Table 13). The exchange half-lives were also unchanged between longitudinal and lateral movement, but increased compared with small bleached areas due to increased size of the bleached area (Table 13 compared with Table 12). We assumed that titin-eGFP can move freely in either direction within and between adjacent myofibrils, since we observed no differences in the mobile fraction and half-fluorescence recovery for longitudinal and lateral movement, or bleaching of 3 or 8 consecutive sarcomeres.

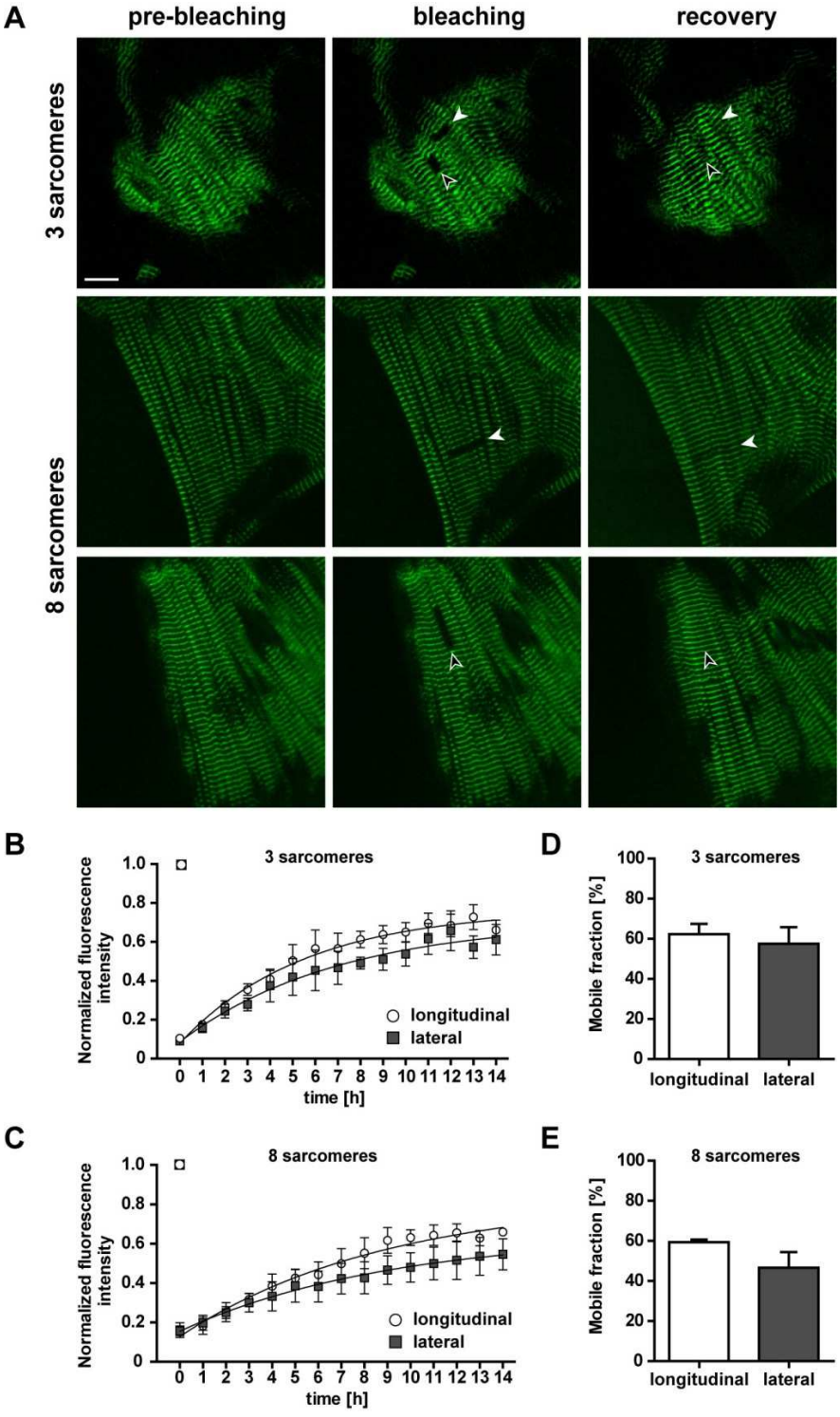

Figure 17. Longitudinal vs. lateral movement of titin-eGFP. (A) Pre-bleaching, bleaching, and recovery images of photobleaching of 3 or 8 consecutive sarcomeres to study longitudinal (white arrows) and lateral (open arrows) mobility of titin-eGFP in embryonic cardiomyocytes. Scale bar 10 µm. (B, C) Relative fluorescence recovery for lateral and longitudinal movement was equally efficient for 3 or 8 sarcomeres. The half-fluorescence recovery increased with the increase of the area of photobleaching. The fluorescence intensity before bleaching was set as 1 (3 sarcomeres n=4, 8 sarcomeres n=3). Two-way ANOVA. (D, E) There was no difference between longitudinal and lateral titin-eGFP mobility. In addition, the mobile fractions were independent from the shape and size of the ROI (3 sarcomeres n=4, 8 sarcomeres n=3). T-test. Error bars indicate SEM.

Table 13. Mobile fractions (M_f) and exchange half-lives ($t_{1/2}$) of titin's longitudinal and lateral movement.

Bleached area [s. l.]	Movement	M_f [%]	$t_{1/2}$ [h]
3	longitudinal	62 ± 5	5.7 ± 1.8
3	lateral	58 ± 8	6.1 ± 2.2
8	longitudinal	59 ± 1	8.5 ± 4.4
8	lateral	47 ± 8	8.1 ± 3.2

S. l.: sarcomere length (n=14). One-way ANOVA (multiple comparison). Data is indicated as mean ± SEM.

We studied the direction in which titin-eGFP is able to move into the bleached area by varying the orientation and the size of the ROI. Hence, we found longitudinal and lateral movement of titin-eGFP equally efficient indicating that titin can freely move in either direction.

5.2.5 Influence of calcium on the titin-eGFP mobility

Calcium is a universal intracellular second messenger and plays an important role in contraction and signaling in cardiac myocytes (Bers, 2008). It has been reported that calcium concentration in the medium can influence the proliferation, morphology, and protein expression in cultured heart cells (Harayama et al., 1998). Here we investigated the impact of calcium on the dynamics of titin-eGFP. We treated embryonic cardiomyocytes with low (LCa; 0.9 mM), normal (NCa; 1.8 mM), or high (HCa; 2.8 mM) calcium concentrations for several days and examined the mobility of titin-eGFP using FRAP analysis (Figure 18). The images taken before, immediately after bleaching, and after 14 h of measurement indicated that recovery occurred only partially in cells treated with high calcium (Figure 18A). FRAP analysis revealed an increase in the mobility at reduced calcium level, but depression under high calcium treatment (Figure 18B). The effect of calcium in the medium on the mobility of titin-eGFP was reflected by changes in the mobile fractions. The mobility was significantly increased under low calcium conditions and significantly decreased under high calcium levels compared with control cells maintained in medium with normal calcium concentration (Figure 18C and Table 14).

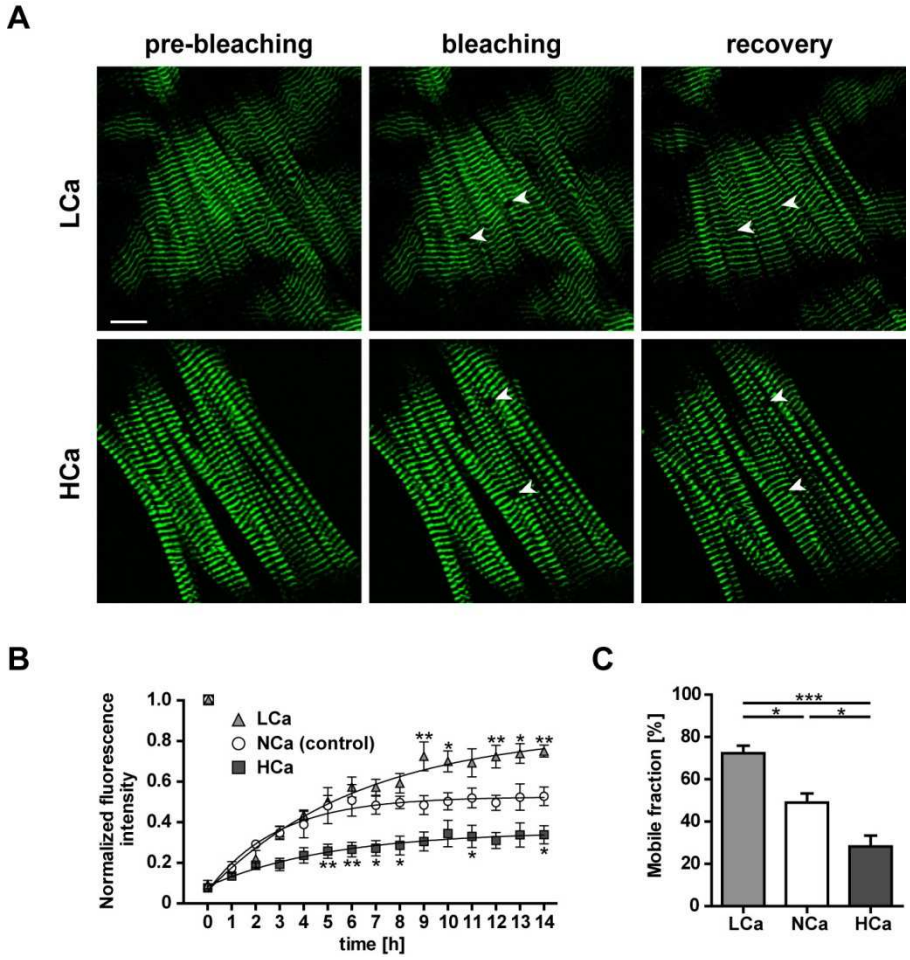

Figure 18. Calcium influence on the mobility of titin-eGFP. (A) FRAP analysis (white arrows indicate ROI) of embryonic cardiomyocytes treated with low (LCa; 0.9 mM) or high (HCa; 2.8 mM) calcium concentrations. Scale bar 10 µm. (B) Cells maintained in low calcium showed a significant increase in titin-eGFP mobility, whereas a high calcium level significantly decreased titin-eGFP mobility compared with control cells (normal calcium, NCa; 1.8 mM). The fluorescence intensity before bleaching was set as 1 (n=4 per group). Two-way ANOVA. (C) Mobile fractions significantly reduced with increased calcium levels (n=4 per group). One-way ANOVA *P<0.05, **P<0.01, ***P<0.001. Error bars indicate SEM.

The half-fluorescence recovery was independent from the calcium concentration in the medium and did not change between low, normal, and high calcium levels (Table 14). Calcium-induced changes in the mobile fraction with unaltered exchange half-lives indicate increased stability of titin in the sarcomere and may not influence titin's movement within the cell.

Table 14. Mobile fractions (M_f) and half-lives ($t_{1/2}$) of calcium-treated titin-eGFP cells.

Treatment	M_f [%]	$t_{1/2}$ [h]
NCa (control)	49 ± 4	2.1 ± 0.4
LCa	72 ± 4**	3.6 ± 0.6
HCa	28 ± 5**	2.9 ± 0.9
BDM	38 ± 1	2.3 ± 0.3
BDM + HCa	24 ± 1**	1.7 ± 0.8

NCa: normal calcium concentration (1.8 mM; control); LCa: low calcium (0.9 mM); HCa: high calcium (2.8 mM); BDM: 2,3-butanedione monoxime (n=18). One-way ANOVA (compared with control) **P<0.01. Data is indicated as mean ± SEM.

Whether the changes in the titin-eGFP dynamics in calcium-treated cardiomyocytes resulted from alterations in the contraction of the cells or calcium signaling, we treated embryonic cardiomyocytes with 2,3-butanedione monoxime (BDM) (Figure 19). BDM was applied to inhibit cell contraction by inhibition of myosin II. BDM is a relatively non-specific myosin inhibitor, but in contrast to the more specific myosin inhibitor blebbistatin, which was reported to be phototoxic when exposed to light with a wavelength of less than 490 nm, BDM treatment was reversible and did not affect cell viability (Kolega, 2004; Skwarek-Maruszewska et al., 2009). We hypothesized that inhibition of contraction by BDM would result in an increased titin-eGFP mobility under normal calcium concentration. Figure 19 shows the FRAP analysis of beating control cells and non-beating BDM-treated cells. The comparison of the mobile fractions revealed no difference between control and treated cells indicating that calcium-mediated titin-eGFP dynamics was independent from contraction (Figure 19C and Table 14). Furthermore, beating and non-beating cells displayed similar exchange half-lives of 2.1 h and 2.3 h, respectively (Table 14). Additionally, we examined the influence of calcium on the contraction by treating cardiomyocytes with a combination of high calcium and BDM (Figure 19D). We assumed that the addition of BDM to HCa would rescue the decrease of titin-eGFP mobility to normal levels, only when mobility depends on contraction. Combination of HCa and BDM resulted in a significant depression of the recovery curve similar to HCa treatment alone. Although the half-fluorescence recovery was unchanged, the mobility of titin-eGFP decreased from 49% in control cells to 24% in BDM + HCa treated cells (Figure 19C and Table 14). Our results demonstrated that calcium affected titin's mobile fraction, but not the half-fluorescence recovery, an effect independent from contraction.

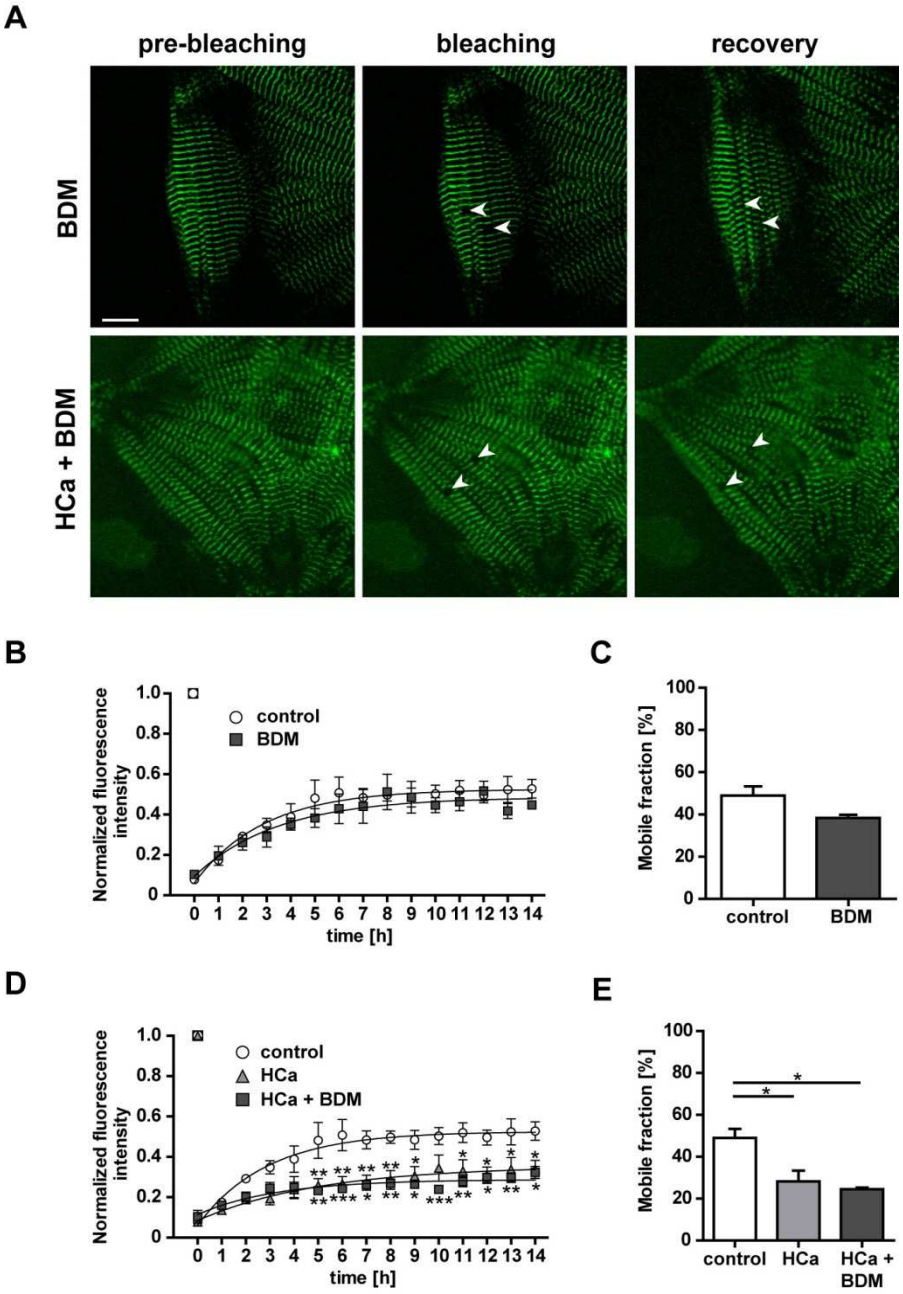

Figure 19. Inhibition of cell contraction did not affect titin-eGFP dynamics. (A) Contraction of embryonic cardiomyocytes was inhibited by the myosin inhibitor 2,3-butanedione monoxime (BDM). Cells were treated with BDM, high calcium concentration (HCa; 2.8 mM), or a combination of BDM and HCa. White arrows indicate the bleached areas. Scale bar 10 µm. (B, C) The fluorescence recovery was equally efficient in non-beating cells compared with beating control cells (control n=4, BDM n=3). Two-way ANOVA, T-test. (D, E) The reduced fluorescence recovery and mobile fraction in FRAP experiments with HCa could not be restored by inhibition of contraction. The fluorescence intensity before bleaching was set as 1 (control n=4, BDM + HCa n=3). Two- and one-way ANOVA *P<0.05, **P<0.01, ***P<0.001. Error bars indicate SEM.

Calcium plays an important role in contraction of cardiac cells and many sarcomeric proteins are calcium-dependent. In this study we analyzed the effect of calcium on the mobility of titin-eGFP by varying the medium calcium concentration. With increasing calcium level the dynamics of titin-eGFP decreased. Inhibition of contraction did not restore the depressed fluorescence recovery.

5.2.6 Mobility of titin-eGFP in embryonic and neonatal cardiomyocytes

Titin undergoes developmental changes in isoform expression (Greaser et al., 2005). After birth, the cardiac titin N2BA isoform is replaced by the shorter N2B isoform in order to adapt to cardiac functions (Lahmers et al., 2004; Opitz et al., 2004; Warren et al., 2004). Using qRT-PCR, we confirmed the expression of different isoforms in embryonic and neonatal cardiomyocytes (NCM). We found a significant increase in the titin N2B level after birth (Figure 20B). In embryonic and neonatal cardiomyocytes, the expression of eGFP and of titin at both the Z-disc (ZEx1-2) and the M-band (MEx3-4) were unchanged (Figure 20A).

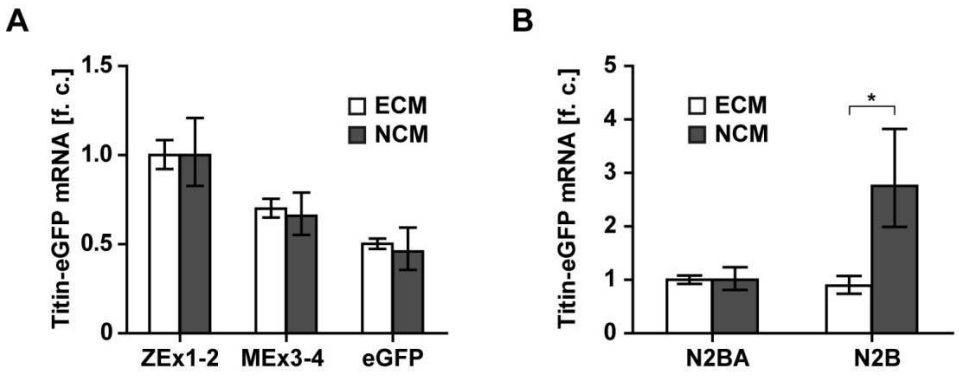

Figure 20. Titin isoform switch in cultured embryonic and neonatal cardiomyocytes. Quantitative real-time PCR analysis of titin isoform expression in cardiomyocytes obtained from embryonic (ECM, E13.5) and neonatal (NCM, P2) homozygous TiMEx6-eGFP mice. (A) Comparison of the expression of titin's N-terminus (ZEx1-2), C-terminus (MEx3-4), and eGFP revealed no differences between embryonic and neonatal cardiomyocytes. (B) The main embryonic titin isoform N2BA is replaced by the smaller N2B isoform after birth. The N2B isoform expression in NCM significantly increased compared with ECM. Data was normalized to 18S RNA and ZEx1-2 or N2BA levels were set as 1 (n=3 per group). F. c. fold change. Two-way ANOVA *P<0.05. Error bars indicate SEM.

Since titin isoform expression was changed after birth, we investigated if differences in the domain composition could influence the properties of titin dynamics. We compared the

mobility of titin-eGFP at two developmental stages: NCM isolated at postnatal day 2 (P2) and ECM isolated at E13.5 (Figure 21). FRAP analysis revealed that fluorescence recovery after photobleaching was equally efficient for NCM compared to ECM (Figure 21B). For NCM, the mobile fraction was 56 ± 3% and the half-fluorescence recovery was 3.7 ± 0.4 h (Figure 21B and C). The kinetic parameters of NCM and ECM were similar (Table 11).

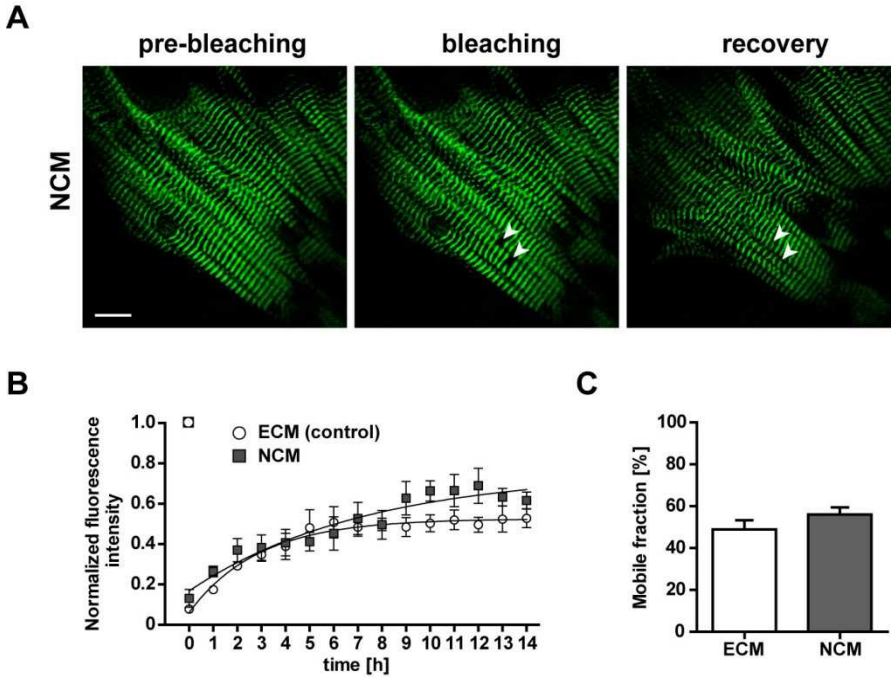

Figure 21. Titin-eGFP mobility in embryonic and neonatal cardiomyocytes. (A) Photobleaching analysis of titin-eGFP in neonatal cardiomyocytes (NCM, P2). Images were obtained before, immediately after bleaching, and after the fluorescence was significantly recovered (white arrows indicate the bleached area). Scale bar 10 µm. (B) Plot of the fluorescence recovery in embryonic (ECM, E13.5) vs. neonatal cardiomyocytes shows no difference over the 14 h of measurement. The fluorescence intensity before bleaching was set as 1 (ECM n=4, NCM n=3). Two-way ANOVA. (C) Mobile fractions measured at the end of the FRAP experiment revealed an equally efficient dynamics of titin-eGFP in embryonic and neonatal cardiomyocytes (ECM n=4, NCM n=3). T-test. Error bars indicate SEM.

In summary, we examined the isoform expression of titin in cultured embryonic and neonatal cardiomyocytes and observed higher expression levels of N2B titin in NCM compared with ECM. FRAP analysis revealed no differences in the mobile fraction and exchange half-life between ECM and NCM, suggesting that mobility of titin is independent of developmental stage and domain composition of the protein.

5.3 The TiEx28-dsRed knockin mouse

5.3.1 Titin's mobility at the Z-disc of the sarcomere

We used the established TiEx28-dsRed knockin mouse to investigate the mobility of titin at the Z-disc region of the sarcomere. The discosoma red fluorescent protein (dsRed) was integrated into titin's exon 28 near the N-terminus of the protein. We used the knockin mouse model to include shorter titin isoforms that do not extend to the M-band region of the sarcomere in the analysis. We performed FRAP experiments of homozygous embryonic cardiomyocytes using a small ROI (1 x 1 sarcomere length) and followed the recovery for 14 h (Figure 22).

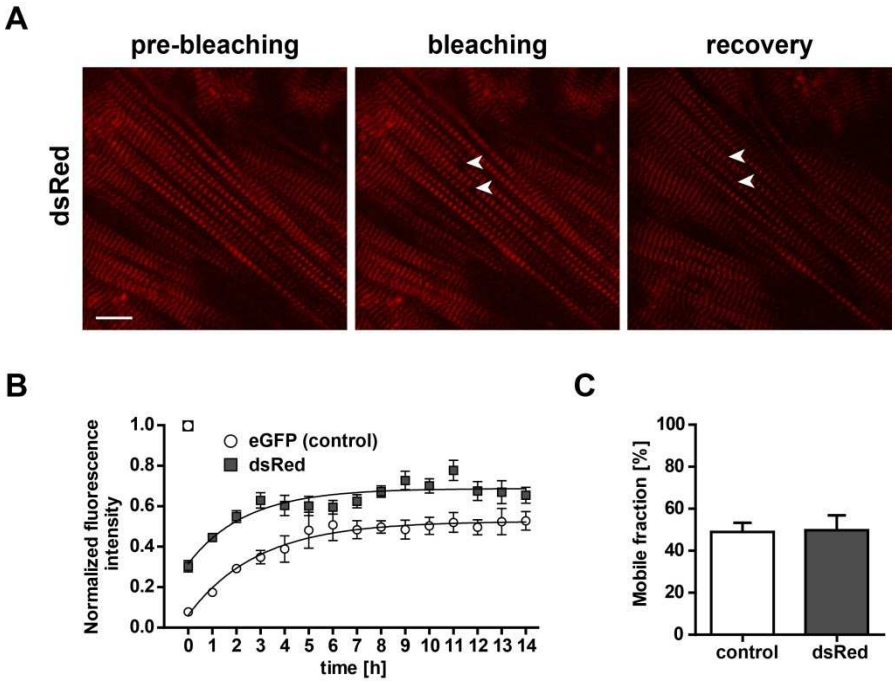

Figure 22. The dynamics of dsRed-titin in embryonic cardiomyocytes. To compare titin mobility at the Z-disc and M-band region of the sarcomere, FRAP analysis were performed in embryonic cardiomyocytes expressing dsRed-titin. (A) Confocal images were obtained before, immediately after photobleaching, and every hour until the fluorescence recovery reached steady state (white arrows indicate ROI). Scale bar 10 µm. (B) Plot of the fluorescence intensity vs. time after photobleaching shows that dsRed-titin displayed similar dynamics compared to titin-eGFP. The fluorescence intensity before bleaching was set as 1 (control n=4, dsRed n=4). Two-way ANOVA. (C) The exchange of titin at the Z-disc and M-band region of the sarcomere occurred with a mobile fraction of about 50% in both dsRed-titin and titin-eGFP cells (control n=4, dsRed n=4). T-test. Error bars indicate SEM.

As indicated in Figure 22B the bleaching of the red fluorophore was not as efficient as the bleaching of eGFP, but curve progression for dsRed-titin was similar to titin-eGFP. The percentage of mobile dsRed-titin was 50% and therefore not different from the mobile fraction obtained for titin-eGFP (Figure 22C and Table 15). The recovery of dsRed occurred with an exchange half-life of 1.8 h, similar to the recovery of eGFP (Table 15).

Investigations of the dynamics of titin-eGFP and dsRed-titin displayed similar mobility at the Z-disc and M-band region of the protein with unchanged mobile fractions and exchange half-lives.

5.3.2 Titin dynamics at the Z-disc and M-band region of the sarcomere

Embryonic cardiomyocytes heterozygous for dsRed-titin and titin-eGFP (TiEx28-dsRed/TiMEx6-eGFP) were isolated at E13.5 and used for FRAP experiments (Figure 23). Since homozygous animals did not show obvious phenotypic defects also heterozygous embryos developed normally. Resulting primary cardiomyocytes showed the expected striated pattern of the sarcomeres. The integration of the fluorophores dsRed at the N-terminus and eGFP at the C-terminus of titin and the protein length of more than 1 μm led to a distinctly alternating pattern of red and green fluorescence. We found that the overall signal intensity was decreased in double heterozygous embryonic cardiomyocytes, but strong enough for detection and FRAP analysis. For simultaneous visualization of titin's mobility at the Z-disc and M-band, we bleached an area of 3 x 3 sarcomere lengths (Figure 23 and Figure 24) and the recovery of dsRed and eGFP were analyzed independently. Comparison of the FRAP curves indicated no difference in the recovery of dsRed-titin versus titin-eGFP in double heterozygous cells (Figure 23B and C). This was also reflected in the mobile fractions and exchange half-lives (Table 15). In comparison to the determined kinetics of homozygous titin-eGFP, we obtained similar mobility and recovery of titin-eGFP in heterozygous cardiomyocytes (Table 12 and Table 15). We also found that the increase in the size of the bleached area from 1 x 1 to 3 x 3 sarcomere lengths led to an increase of the half-fluorescence recovery in heterozygous cells (Table 15), consistent with the data obtained for the dynamics of titin-eGFP in homozygous cardiomyocytes (Table 12).

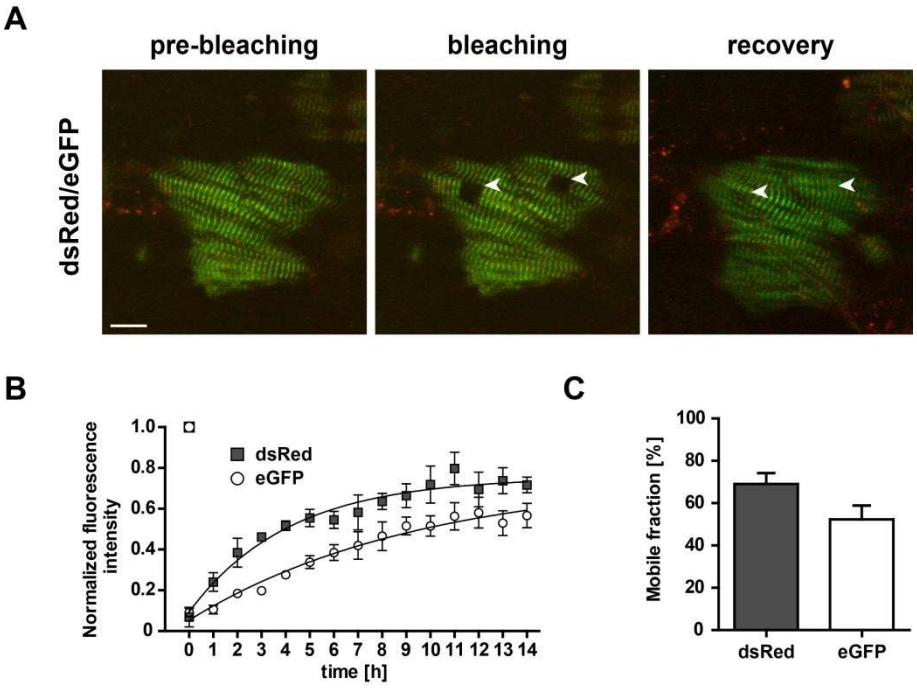

Figure 23. FRAP analysis of double heterozygous dsRed-titin-eGFP. Photobleaching experiments were performed to follow the recovery of titin at the Z-disc and M-band region of the sarcomere at the same time in embryonic cardiomyocytes from double heterozygous TiEx28-dsRed/TiMEx6-eGFP knockin mice. The fluorophore dsRed is located near the Z-disc region and eGFP at the M-band region of titin. (A) Area of 3 x 3 sarcomere lengths (white arrows) were photobleached and images were taken before, after bleaching, and every hour for a 14 h time period. Scale bar 10 µm. (B) Kinetic analysis revealed no difference in the fluorescence recovery for dsRed-titin compared with titin-eGFP. The fluorescence intensity before bleaching was set as 1 (n=3). Two-way ANOVA. (C) The fraction of dsRed-titin participating in the exchange of bleached by unbleached molecules was unchanged compared to titin-eGFP (n=3). T-test. Error bars indicate SEM.

Table 15. Mobile fractions (M_f) and exchange half-lives ($t_{1/2}$) of fluorescent-labeled titin.

Mouse model	Bleached fluorophore	Sarcomere length [s. l.]	M_f [%]	$t_{1/2}$ [h]
TiMEx6-eGFP	eGFP	1 x 1	49 ± 4	2.1 ± 0.4
TiEx28-dsRed	dsRed	1 x 1	50 ± 7	1.8 ± 0.2
TiEx28-dsRed/TiMEx6-eGFP	eGFP	3 x 3	52 ± 7	6.6 ± 1.2
TiEx28-dsRed/TiMEx6-eGFP	dsRed	3 x 3	69 ± 5	4.4 ± 1.0

T-test comparing titin-eGFP vs. dsRed-titin and in double heterozygous cell bleached eGFP vs. dsRed (n=11). Data is indicated as mean ± SEM.

In addition to photobleaching experiments and investigating the kinetic properties of dsRed- and eGFP-tagged titin, we analyzed titin's mobility at the Z-disc and M-band region of the sarcomere by time-lapse imaging (Figure 24). The size and the shape of the bleached area (white arrows) were conserved over the investigation period. Furthermore, the cell shape was

unchanged and we saw only minor myofibril rearrangements. Recovery occurred slightly faster at the boundary of the ROI indicating that neighboring unbleached fluorophores moved into the bleached area and needed more time to reach the center of the ROI. Over time unbleached dsRed-titin and titin-eGFP exchanged with bleached molecules and fluorescence recovered to a steady state.

To get more insight into the mobility of titin, we used simultaneous FRAP of dsRed and eGFP. We found that titin recovery was equally efficient at the Z-disc and at the M-band region of the sarcomere. This indicated that full length titin and shorter isoforms may have similar dynamics. There was no difference between dsRed-titin and titin-eGFP recovery and the exchange half-lives.

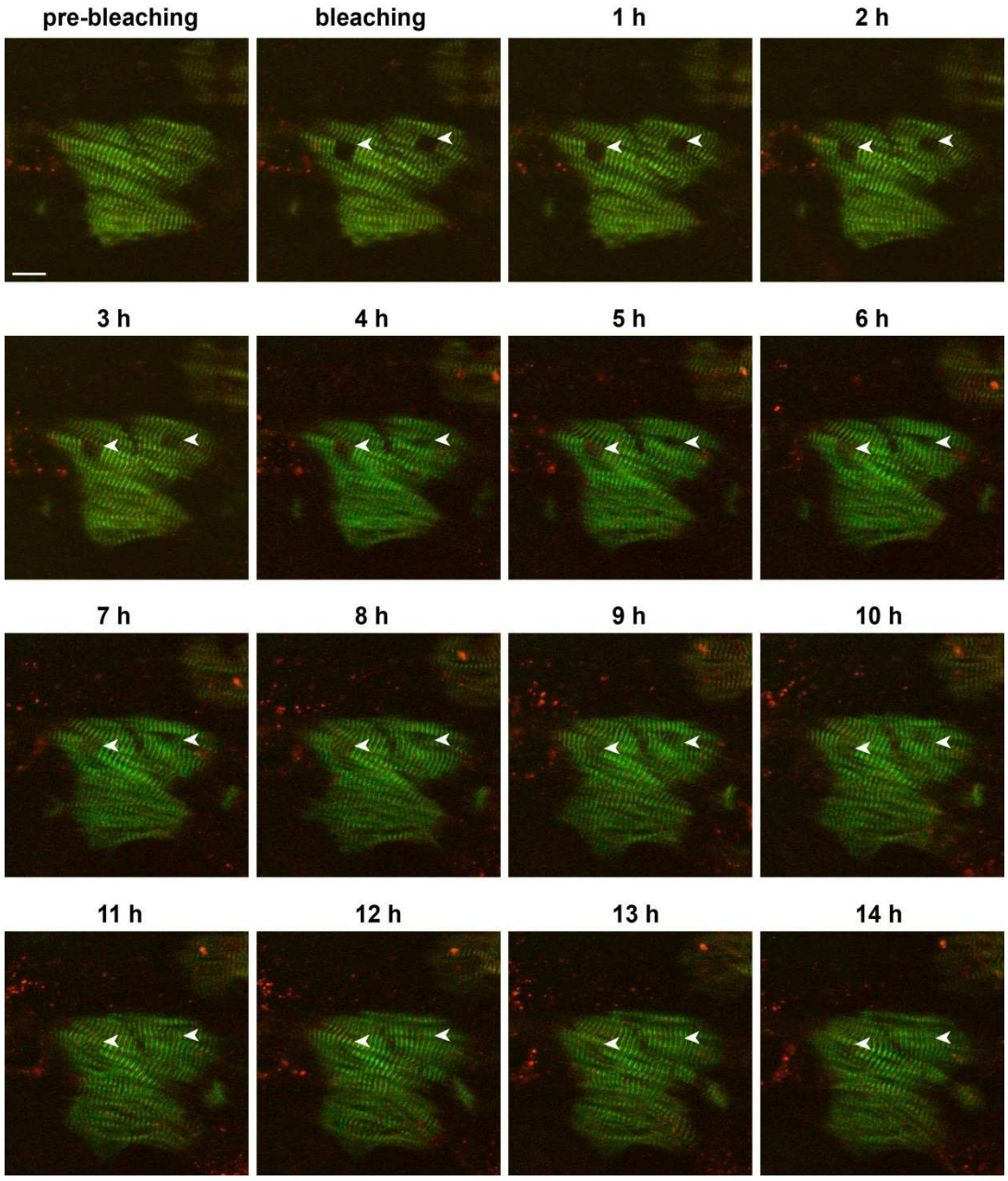

Figure 24. Time-lapse images of fluorescence recovery of double heterozygous dsRed-titin-eGFP. Confocal fluorescence microscopy images acquired at the indicated times after photobleaching of double heterozygous TiEx28-dsRed/TiMEx6-eGFP embryonic cardiomyocytes. The bleached areas of 3 x 3 sarcomere lengths are indicated by white arrows. Fluorescence recovery was slightly faster at the edges of the ROI. dsRed-titin and titin-eGFP were exchanged by unbleached molecules at similar time points and velocity. No major rearrangements were observed during the 14 h time period. Scale bar 10 µm.

5.4 Sarcomere disassembly and reassembly

The TiMEx6-eGFP knockin mouse model was used to investigate the mobility of titin and to evaluate sarcomere disassembly and reassembly after myoseverin treatment. Myoseverin has been identified in a purine library screen with murine muscle cells (Rosania et al., 2000). It binds to microtubules and induces its depolymerization, which leads to the disruption of sarcomeric organization (Ng et al., 2008). Our knockin mice were an appropriate model to visualize the sarcomere disassembly and reassembly in real time, since titin-eGFP was uniformly expressed at physiological levels. We treated homozygous TiMEx6-eGFP cardiomyocytes with myoseverin (dissolved in DMSO) for up to 48 h to induce sarcomere disruption (Figure 25). Control and DMSO-treated cells had a normal sarcomere structure with equal spacing. Immunofluorescence staining showed proper localization of α-actinin at the Z-disc and eGFP at the M-band (Figure 25A). During the first 6 h of myoseverin-treatment, cardiomyocytes displayed an intact myofilament structure. After 12 h of treatment the normal periodic organization of titin abolished and spacing between Z-disc and M-band increased. Proper localization of α-actinin and titin was disrupted in myocytes incubated with myoseverin for 18 h or longer. The proteins appeared in random punctuate patches and striation was only present in a few spots within the cells (Figure 25A).

Live-cell imaging of titin-eGFP in cardiomyocytes incubated with myoseverin revealed that disassembly of mature sarcomeres started after 6 h of treatment, indicated by the disruption of the striation (Figure 25B). The cell shape was unchanged throughout the experiment. Lastly, we observed that titin-eGFP developed a diffuse distribution throughout the cell, with only a few striations after 10 h of treatment (Figure 25B).

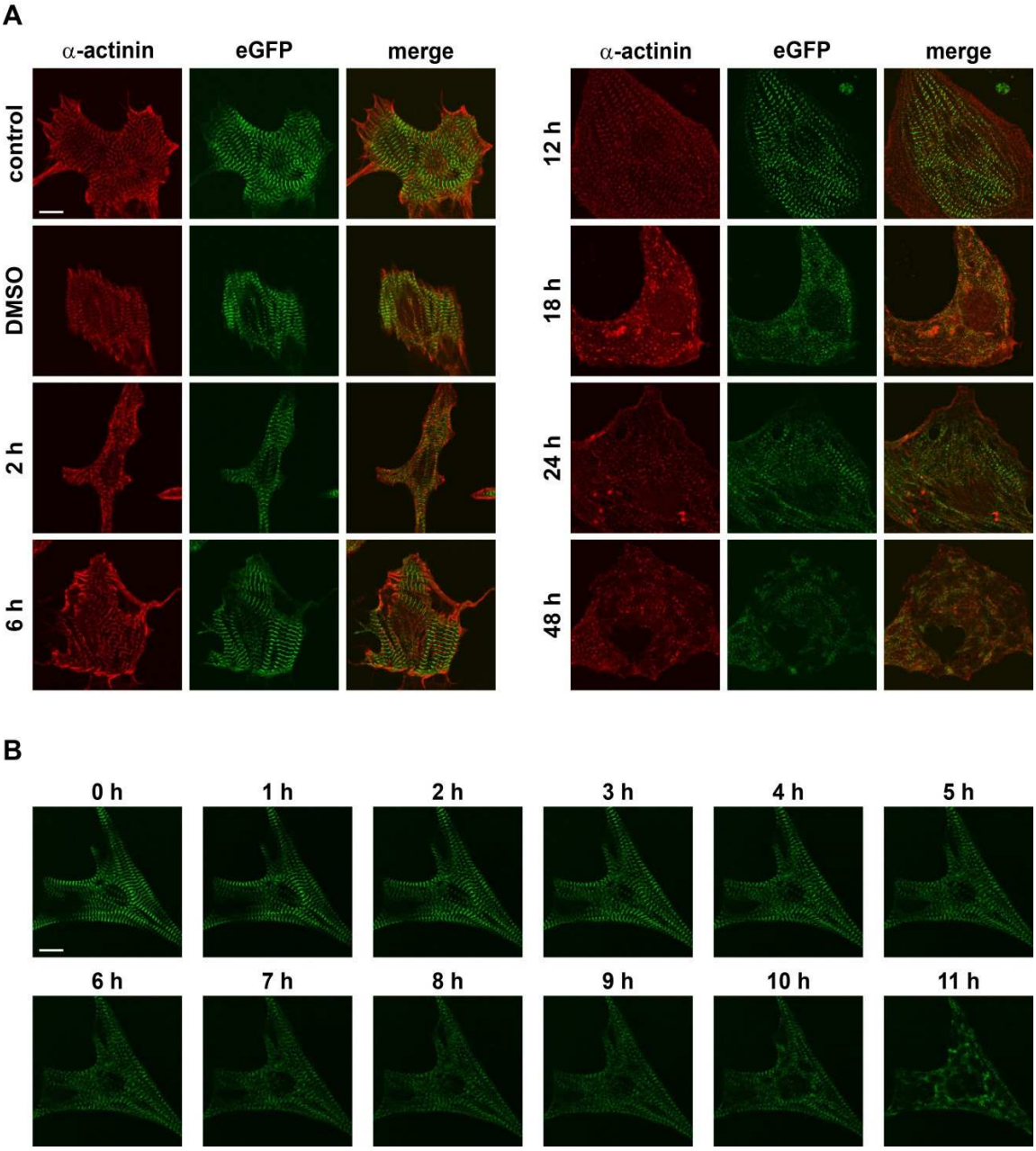

Figure 25. Myoseverin-induced sarcomere disassembly in cardiomyocytes. Embryonic cardiomyocytes from homozygous TiMEx6-eGFP mice were treated with 20 µM myoseverin (dissolved in DMSO) to induce sarcomere disassembly. (A) A striated pattern was visible in control and DMSO-treated cells and in myoseverin-treated cells up to 6 h. Immunofluorescence staining with an antibody against the Z-disc protein α-actinin showed the disruption of the sarcomeric structure between 6 and 12 h after treatment. After 12 h, titin-eGFP and α-actinin became diffuse. (B) Time-lapse images to follow the myoseverin-induced disruption of titin-eGFP localization. Almost no striations were observed after 10 h of treatment. Scale bar 10 µm.

In addition to the sarcomere disassembly, we also investigated its reassembly. Myoseverin-induced microtubule depolymerization was reported to be reversible after myoseverin washout (Rosania et al., 2000; Perez et al., 2002; Ng et al., 2008). Therefore cardiomyocytes were exposed to myoseverin for 12 h and sarcomere reassembly was followed for 6 h after

substance removal (Figure 26). Control cells (either without treatment or treated with the vehicle DMSO), displayed a regular sarcomere structure. The disruption of the striation towards a punctuated pattern by myoseverin was reversible. Starting 2 h after washout and incubation in normal culture medium sarcomeres began to form. Staining with α-actinin (red) revealed that the Z-disc and the M-band appeared point-shaped after 2 h and returned to the striated pattern 6 h after washout (open arrows).

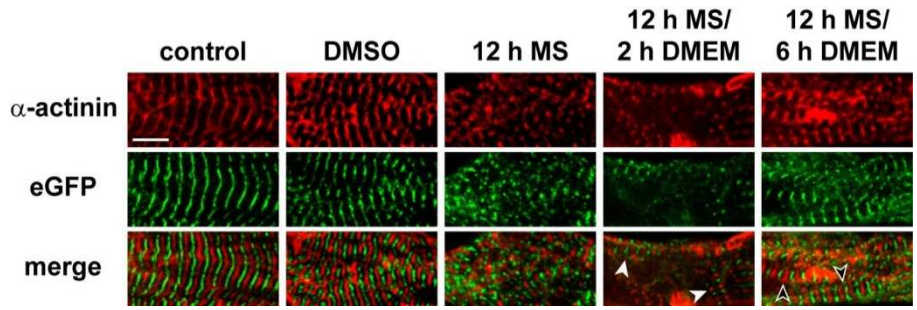

Figure 26. Sarcomere reassembly after removal of myoseverin. Cardiac myocytes derived from TiMEx6-eGFP embryos expressing eGFP (green) at the M-band were stained with α-actinin (red) to visualize the Z-disc of the sarcomere. Cells were treated with myoseverin (MS) for 12 h to disrupt the sarcomeric organization. Recovery of the myofilament structure was investigated 2-6 h after myoseverin removal and incubation in culture medium (white arrows: starting sarcomere reassembly; open arrows: mature sarcomeres). Scale bar 5 µm.

Using the TiMEx6-eGFP knockin mice we were able to visualize myoseverin-induced disassembly of the myofilament in real-time. Immunofluorescence staining revealed that sarcomeres were perturbed after 12 h of treatment. In washout experiments, sarcomeres reassembled and formed a periodic striation after removal of myoseverin.

5.5 Non-muscle titin in the brush border of the small intestine

Titin is an elastic component of the sarcomere and several studies indicated that titin may also be important in non-muscle cells. However, the function of non-muscle titin remains poorly understood. It has been suggested that titin is a structural component in the brush border of the small intestine (Eilertsen and Keller, 1992). To address if non-muscle titin is expressed in the small intestine, we used wild-type, heterozygous, and homozygous TiMEx6-eGFP knockin mice and analyzed the duodenum, jejunum, and ileum of adult males (Figure 27).

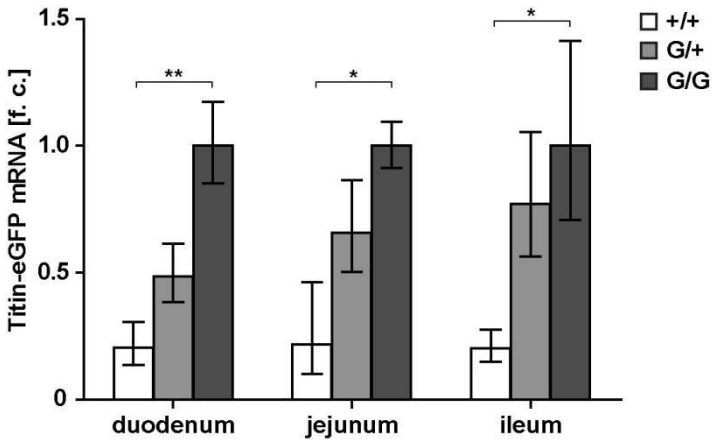

Figure 27. Titin-eGFP expression in the small intestine. Quantitative real-time PCR was used to determine titin-eGFP expression levels in duodenum, jejunum, and ileum of wild-type (+/+), heterozygous (G/+), and homozygous (G/G) knockin mice. The expression of titin-eGFP was significantly increased in G/G compared with wild-type controls (background signal). An intermediate titin-eGFP level could be detected in heterozygous animals. Data was normalized to 18S RNA and the titin-eGFP expression in homozygous knockin mice was set as 1 (n=5 per genotype). F. c. fold change. One-way ANOVA *P<0.05, **P<0.01. Error bars indicate SEM.

We observed that the expression of titin-eGFP in hetero- and homozygous mice was significantly above the background signal of wild-type controls. In addition, all tissues investigated had an intermediate titin-eGFP expression in heterozygous mice (Figure 27). Our data provided evidence that titin is expressed in the small intestine and we generated a tissue specific knockout to assess the role of non-muscle titin in the small intestinal brush border.

5.5.1 Generation of a titin knockout in the small intestine

To analyze the function of non-muscle titin in the intestinal brush border, we generated a conditional knockout (KO) of titin in the small intestine. Homozygous titin exon 2 animals (TiEx2), in which titin's exon 2 containing the translation start is flanked by loxP-sites (RECf), were bred with mice expressing the site-specific DNA recombinase villin-Cre (El Marjou et al., 2004) (Figure 28A). The villin-Cre recombinase is under the control of the murine villin promoter and expressed in the mouse intestinal epithelium (El Marjou et al., 2004). Mating of TiEx2 mice and villin-Cre mice led to offspring (TiEx2-villin Cre), in which titin's exon 2 was excised between the loxP-sites, resulting in a KO of full titin in the mouse digestive epithelium (REC; Figure 28).

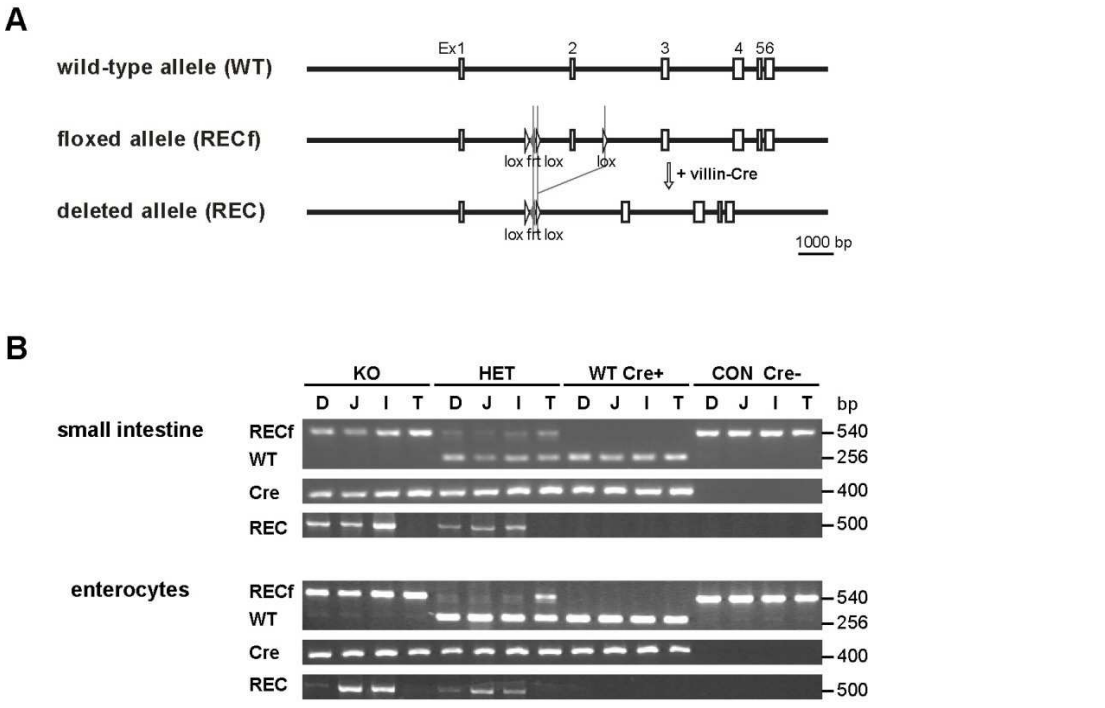

Figure 28. Generation and genotyping of the gut specific titin knockout. (A) Titin's exon 2 is flanked by loxP-sites (RECf). Homozygous animals (RECf/RECf) were bred with heterozygous villin-Cre animals to generate a gut specific titin knockout. The Cre-mediated recombination led to the deletion of the exon 2 containing the translation start site (REC). (B) Genotyping PCRs to confirm the recombination in the small intestine and in the enterocytes of knockout (KO; RECf/RECf) and heterozygous (HET; RECf/WT) animals expressing the villin-Cre recombinase (Cre). Recombination (REC) occurred only in duodenum (D), jejunum (J), and ileum (I), but not in the tail (T) of KO and HET animals. Wild-type (WT/WT Cre+) and control mice (CON; RECf/RECf Cre-) did not show recombination in the small intestine. Bp base pair.

For genotyping, we isolated genomic DNA from small intestine and enterocytes (Figure 28B). The expression of the wild-type allele (WT), the loxP-sites flanked exon 2 allele (RECf), and the villin-Cre were confirmed by PCR. The Cre-mediated recombination of the target exon 2 was verified in duodenum (D), jejunum (J), ileum (I) of RECf/RECf (knockout, KO) and RECf/WT (heterozygotes, HET) animals expressing villin-Cre. We observed that recombination only occurred in the small intestine and in enterocytes, but not in the tail (T), indicating that villin-Cre was expressed and active in the intestinal epithelium (Figure 28B). Analysis on mRNA level in enterocytes revealed that titin expression was below the detection limit. Non-muscle titin is expressed at lower levels than muscle titin and its low abundance complicates investigations (Cavnar et al., 2007). We could not verify titin expression on mRNA and protein level in enterocytes. Only a loss of function approach may provide insights into the role of titin in the small intestinal brush border.

Knockout (RECf/RECf Cre+), heterozygous (RECf/WT Cre-), and control (RECf/RECf Cre-) animals were viable, fertile, and developed normally (Figure 28 and Figure 29). The body weight, heart weight, and heart weight to body weight ratio were unchanged between KO and controls (Figure 29A) and for further analysis we used RECf/RECf Cre- mice as controls.

Eilertsen and Keller suggested that a cellular isoform of titin plays a structural role in the brush border of the small intestine (Eilertsen and Keller, 1992). The deletion of titin could lead to structural changes in the small intestine and consequently affect the absorption of nutrients. Therefore we measured the body composition of 2 month old control and KO animals (Figure 29B) and observed no differences in body fat, free water, and lean mass in KO compared to control animals. To exclude a late onset phenotype, we repeated the body composition analysis after 6 month investigating the same animals and also found no differences (Figure 29B).

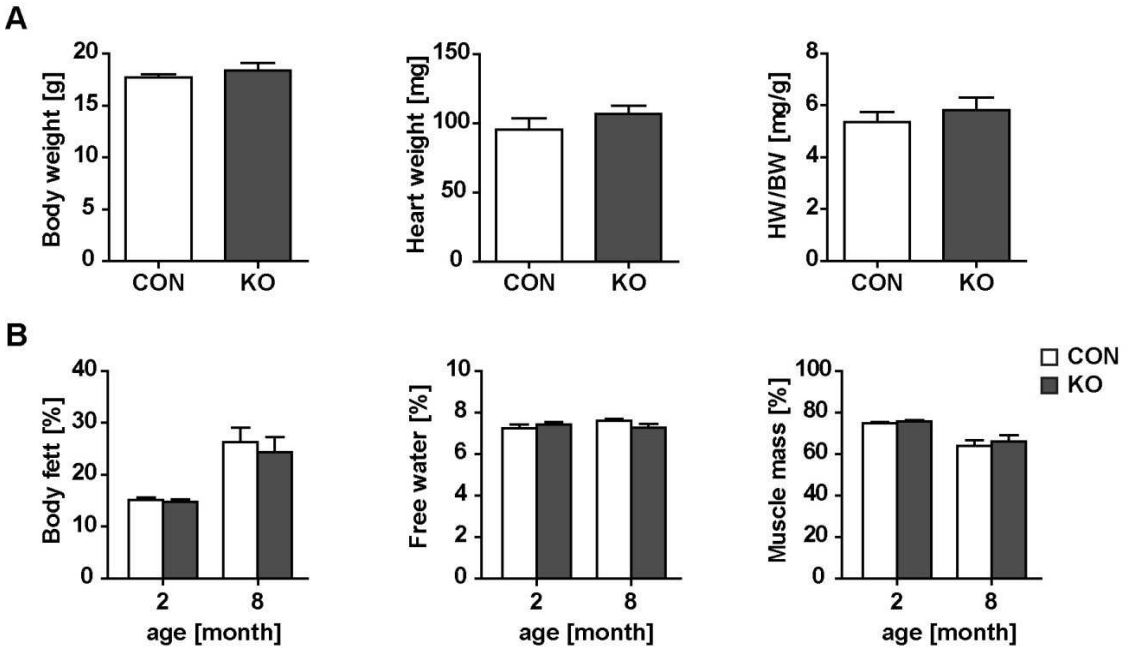

Figure 29. Heart to body weight ratio and body composition analysis of TiEx2-villin Cre mice. (A) Body weight, heart weight, and heart to body weight ratio of female knockout (KO) mice was unchanged compared to controls (CON) (n=3 per group). T-test. (B) Body composition analysis of 2 and 8 month old females revealed no differences in body fat, free water, and lean mass between CON and KO (n=6 per genotype). Two-way ANOVA. Error bars indicate SEM.

We analyzed the expression of non-muscle titin in the small intestine using the TiMEx6-eGFP knockin mice and found evidence for the presence of non-muscle titin. The fluorescent signal was not strong enough for detection in enterocytes and functional analysis. We generated a tissue specific titin knockout mouse to address the function of non-muscle titin in the brush border and confirmed Cre-mediated recombination in the small intestine and enterocytes of KO and HET. KO animals did not develop any obvious phenotypic defects or showed abnormalities in behavior.

5.5.2 Normal small intestinal morphology in TiEx2-villin Cre knockout mice

To investigate the morphology of KO small intestine, we stained paraffin sections of duodenum, jejunum, and ileum with Masson's Trichrome (Figure 30) and observed no differences in the histological appearance of adult TiEx2-villin Cre KO compared with control animals. Organization of villi and crypts was normal without obvious signs of disruption. Villi length as well as villi morphology was unchanged in KO samples. Furthermore, we did not see a difference of mucosa or submucosa between genotypes.

Overall, the enterocyte structure appeared normal at the light microscopy level and KO animals exhibited no obvious phenotypic defects in the structure of duodenum, jejunum, and ileum compared to controls (Figure 30).

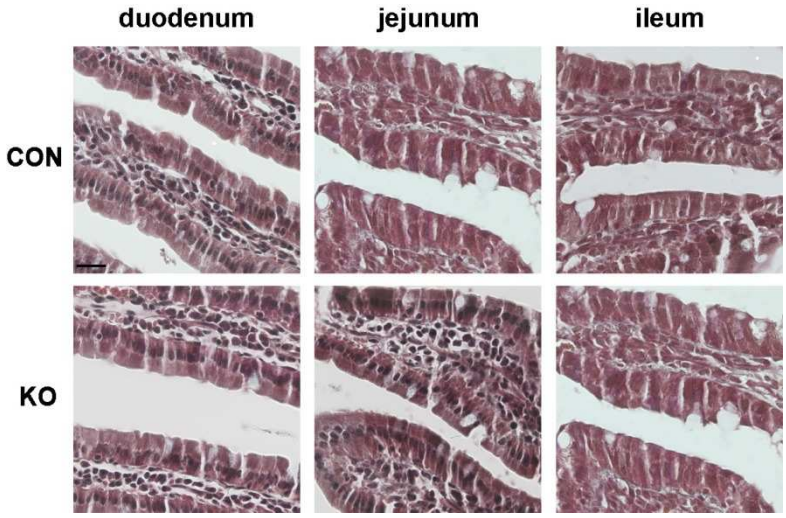

Figure 30. Histological comparison of small intestine from control and TiEx2-villin Cre knockout mice. Paraffin sections of duodenum, jejunum, and ileum from control (CON) and titin knockout (KO) animals were stained with Masson's trichrome. Compared to control animals no structural changes in the small intestine of KO animals were observed. Scale bar 20 µm.

We also assessed structural changes in the small intestine of adult TiEx2-villin Cre KO and control mice by co-immunofluorescence staining (Figure 31). An antibody directed against the brush border marker villin (red) and co-staining of F-actin (green) showed no differences in the localization and expression of villin between genotypes or between the investigated sections of the small intestine (Figure 31). Furthermore, villi displayed normal morphology and we did not observe any structural abnormalities or changes in the overall appearance of the small intestine.

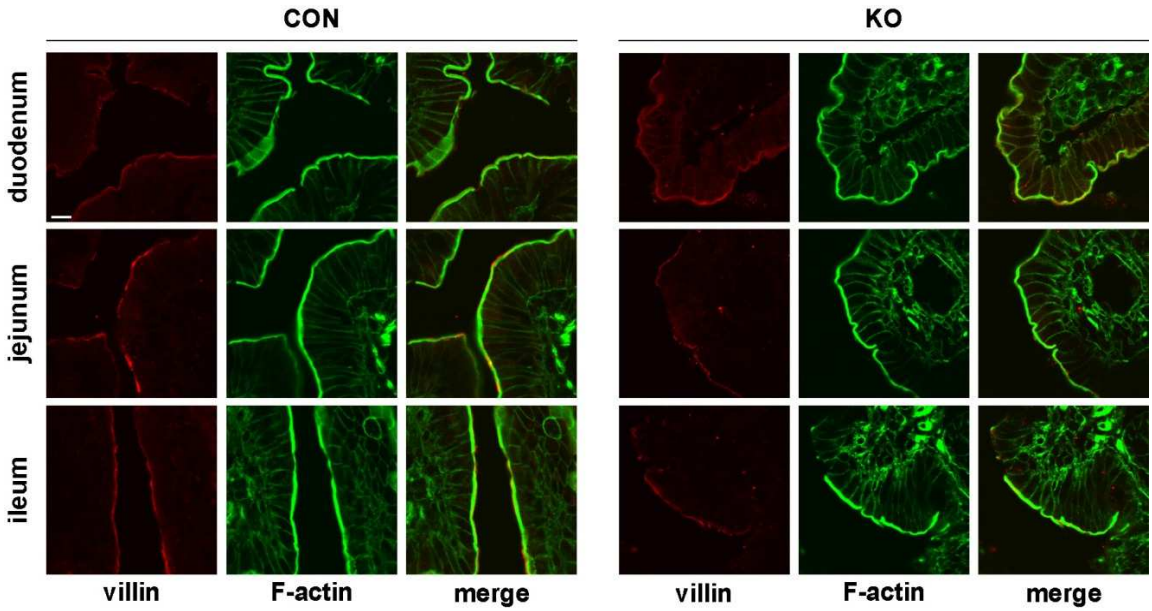

Figure 31. Brush border of control and TiEx2-villin Cre knockout animals. Cryostat sections of the small intestine of control (CON) and titin knockout (KO) animals were co-stained with F-actin (green; phalloidin labeling) and the brush border marker villin (red). Localization and expression were unchanged between control and knockout animals (n=3). Scale bar 10 µm.

5.5.3 Microvillus ultrastructure is unaffected in TiEx2-villin Cre knockouts

The microvillus ultrastructure of TiEx2-villin Cre mice was investigated by electron microscopy of duodenum, jejunum, and ileum from adult control and knockout mice (Figure 32). We focused on the assessment of the apical membrane (brush border) of enterocytes and found that the structural integrity of the brush border was maintained in the KO compared to control. In addition, microvilli (Mv) density appeared unchanged. The parallel oriented actin filaments (A), which extended through the entire length of the microvillus, were visible in all small intestine sections from controls and KO (Figure 32A). Actin bundles reached into the terminal web (TW), which is located at the apical cytoplasm of the cell and we did not observe abnormal organization and thickness of the terminal web in the KO (Figure 32A). Furthermore, we investigated whether the loss of titin alters the microvillus length (Figure 32B). We observed no changes between control and knockout animals.

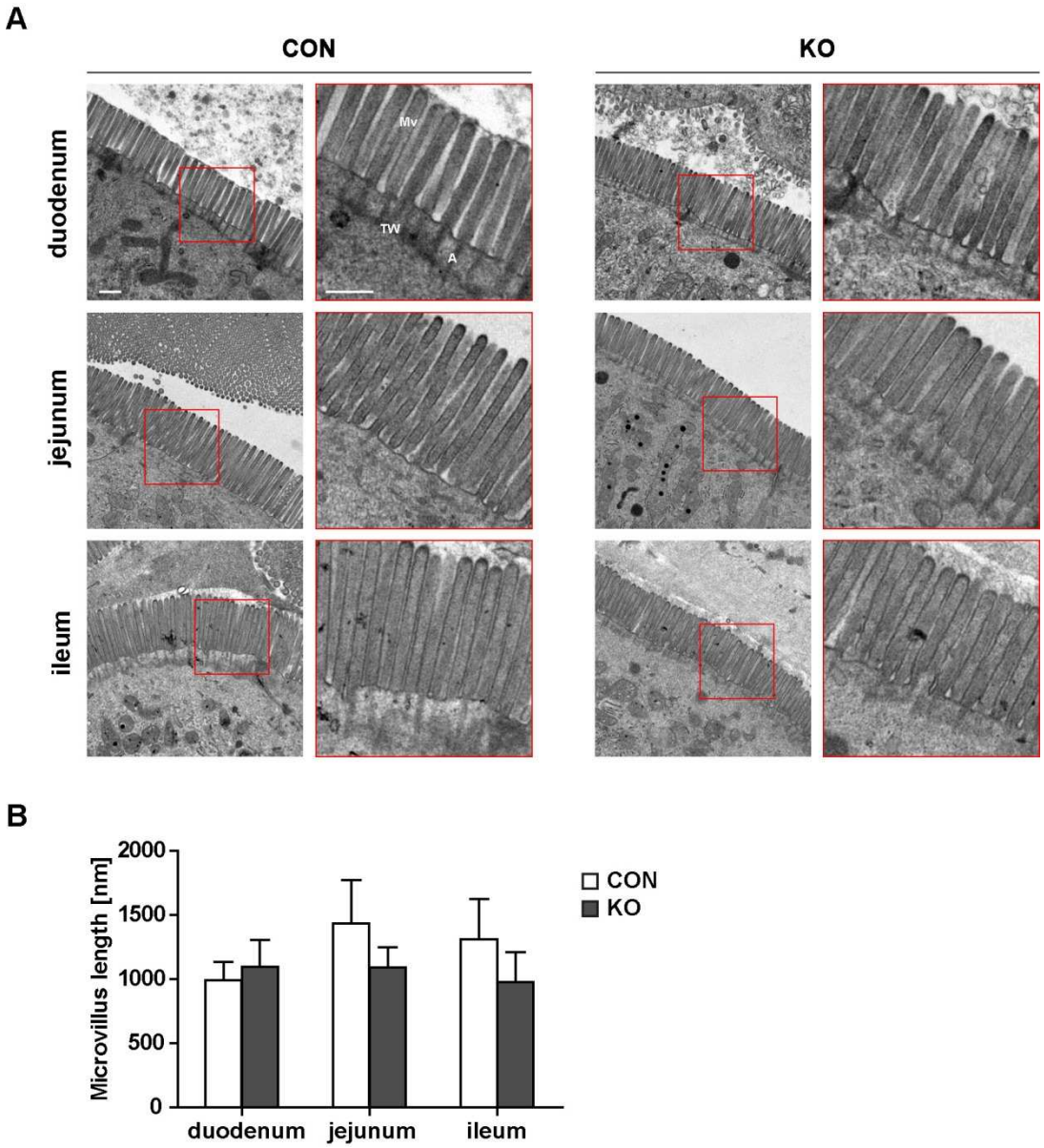

Figure 32. Ultrastructure of intestinal microvilli in control and TiEx2-villin Cre knockout mice. (A) Electron microscopy of microvilli on the apical surface of cells of the small intestine from control (CON) and knockout mice (KO). The longitudinal sections of the microvilli demonstrated normal morphology in KO and control animals (Mv: microvilli; TW: terminal web; A: actin filaments). Scale bar 0.5 µm. (B) Quantification of the microvillus length in duodenum, jejunum, and ileum of CON and KO mice showed no difference (n=40 microvilli per genotype per small intestine section). Two-way ANOVA. Error bars indicate SEM.

Apical surface defects were not observed in KO small intestine. Additionally, the length of the microvillus was unchanged in KO compared to control animals. Our results indicate that the deletion of titin has no effect on the ultrastructure of microvilli of the small intestinal brush border.

6 Discussion

Aim of this study was the investigation of titin's mobility in the sarcomere using the TiMEx6-eGFP knockin mouse, in which titin's C-terminus is tagged with eGFP. Functional studies of titin have been very difficult and several groups described that the transfection and overexpression of titin fragments promoted negative effects on the formation of myofilaments and induced sarcomere disassembly (Peckham et al., 1997; Turnacioglu et al., 1997). Turnacioglu et al. showed that transfection of muscle cells with a fusion construct of titin's Z-disc region with GFP led to an accumulation of the construct and disruption of myofibrils (Turnacioglu et al., 1997). Overexpression of titin's Z-disc region in cultured myocytes has been reported to result in sarcomere disassembly (Peckham et al., 1997). Other studies emphasized that overexpression of single titin Z-repeats, 45-amino acid multiple motifs in the N-terminal region of titin, induced disruption of myofibrils in cultured cardiomyocytes (Gautel et al., 1996; Gregorio et al., 1998; Ayoob et al., 2000). In addition, researchers generated titin knockout models to investigate its functions in the sarcomere and loss of function approaches have been used to analyze titin in cardiac and skeletal muscle during development and disease (Weinert et al., 2006; Radke et al., 2007; Gramlich et al., 2009; Granzier et al., 2009). We used the titin-eGFP knockin mouse, in which the fluorescent-labeled protein is expressed throughout cardiac and skeletal muscle cells by the endogenous promoter, to circumvent toxic effects by transfection and overexpression. The TiMEx6-eGFP knockin mouse model allowed us to study the full length protein at physiological levels and to investigate the dynamics of titin-eGFP within the sarcomere after photobleaching in real-time. We followed the exchange of bleached by unbleached molecules in living cardiomyocytes. Not only the mobility of titin at the M-band of the sarcomere was measured, but also its kinetics at the Z-disc using the TiEx28-dsRed knockin mouse. Furthermore, we used the TiMEx6-eGFP knockin mouse as a model to investigate the expression of non-muscle titin, i.e. the small intestinal brush border. We generated a conditional gut-specific titin knockout mouse to assess the proposed structural function of non-muscle titin in the small intestine by investigating the morphology and ultrastructure of the brush border

6.1 Normal development of TiMEx6-eGFP knockin mice

The fluorescent-labeled titin protein is expressed throughout cardiac and skeletal muscle cells at physiological levels. The enhanced green fluorescent protein eGFP was integrated into titin's C-terminus. The 250 kDa C-terminus of titin lies within the M-band region of the sarcomere. M-band titin is encoded by 6 exons, which referred to as MEx1 to MEx6 (exon 358-363) (Kolmerer et al., 1996). MEx1 encodes for a serine/threonine kinase domain, which has been suggested to be involved in stress-dependent signaling pathways (Labeit et al., 1992; Willis et al., 2007). Deletion of titin's kinase domain in mouse caused disruption of the myofilament and early death (Gotthardt et al., 2003). MEx5 offers a binding site for the protease calpain-3 and is the only titin M-band exon known to be alternatively spliced depending on the muscle (Kolmerer et al., 1996, 1999; Kinbara et al., 1997). No titin-protein interaction has been described for titin's MEx6, which made it suitable for the integration of eGFP (Figure 6). Although no protein binding sites are present in the MEx6 and eGFP did not significantly increase the size of titin, we had to investigate the development of unexpected obvious phenotypic defects or alterations in the sarcomeric structure. Our knockin mice are viable and fertile and their expectancy of life is normal, suggesting that the integration of eGFP into MEx6 did not disrupt the structure of the M-band and cause embryonic lethality, since homozygous knockin mice survive to adult hood. In contrast, the deletion of MEx1 and MEx2 led to early embryonic lethality in a conventional knockout and caused death at 5 weeks of age in a conditional titin knockout (Gotthardt et al., 2003; Weinert et al., 2006). Heterozygous breeding of titin-eGFP resulted in offspring with normal Mendelian ratio and gender distribution. It has been shown that animals expressing a genetically modified titin could develop cardiac atrophy or hypertrophy. For example, the deletion of titin's N2B region resulted in cardiac atrophy with decreased heart to body weight ratio in mouse (Radke et al., 2007). On the other hand, mice expressing a truncated PEVK titin region developed cardiac hypertrophy with an increased HW/BW ratio (Granzier et al., 2009). Heterozygous and homozygous titin-eGFP mice developed normally with unchanged HW/BW ratio compared to wild-type controls (Figure 7).

Analysis of titin-eGFP mRNA expression revealed no differences in the expression of titin's Z-disc, N2A, and M-band region between the investigated genotypes and eGFP was only detected in hetero- and homozygous titin-eGFP mice (Figure 8). This indicates that full length titin is properly expressed from N- to C-terminus. In addition, we confirmed eGFP expression on protein level and observed no differences in the expression of full length titin in hetero- or

homozygous mice compared to wild-types (Figure 9). We detected no alterations in protein size, since eGFP does not significantly increase the molecular weight of titin (>1%). Peng and colleagues showed in Western blot analysis that the deletion of the titin kinase domain in adult mouse heart led to a high mobility titin band in knockout mice (Peng et al., 2007). The mobility of titin-eGFP was not impaired in gel electrophoresis and no shift in the titin band was visible in knockin muscle samples. We showed normal transcription of titin-eGFP and translation into protein by expression analysis on mRNA and protein levels. However, to show that titin-eGFP does not change the sarcomeric structure, we visualized the correct integration of titin into the Z-disc and the M-band of the myofilament by immunofluorescence. Staining with an antibody directed against α-actinin and the N-terminal Z1-Z2 Ig repeats (Z1/Z2) of titin led to a periodic striated pattern and illustrated proper alignment of the sarcomeres (Figure 11). An antibody against titin's M-band region (Ig domains M8 and M9) co-localized with eGFP in all investigated tissues and cells. This emphasized that the targeting vector properly integrated into the titin locus and eGFP localized in the M-band of the sarcomere. We were able to use the knockin mouse to visualize full length titin and investigate the mobility of titin-eGFP using FRAP analysis.

6.2 Titin dynamics is largely independent form *de novo* synthesis

Various sarcomeric proteins assemble to form the highly ordered structure of the sarcomere. The organization of the contractile unit remains stable in order to perform its functions and convert molecular interactions of actin and myosin into contraction. Based on its structure, the sarcomere appears to be a passive and stable framework. However, investigations of sarcomeric proteins showed the direct opposite and revealed that their synthetic half-lives range from ~3 to 10 days (Zak et al., 1977; Isaacs et al., 1989). Thus, components of the sarcomere are dynamic and adapt to certain conditions by changing protein synthesis and degradation or sarcomere assembly and maintenance (Fridén, 1984; Caiozzo et al., 1995; Butterfield et al., 2005; Russell et al., 2010). Researchers have shown that human skeletal muscle cells add new sarcomeres in response to unaccustomed activity (Yu et al., 2003). These findings demonstrate that assembly and organization of myofilaments occur constantly and allow muscle cells to adapt to increased or decreased activity. The architecture of the sarcomere makes it difficult to detect how sarcomeric components might be added, subtracted, and exchanged. Here we use our knockin mouse to visualize the dynamics of titin in living cardiomyocytes. We benefit from the stable titin-eGFP expression at normal levels.

Just because titin is a giant protein and an essential element of the sarcomere that is tightly integrated into the myofilament does not mean titin is a static protein. Using live-cell imaging we were able to study the dynamics of titin-eGFP over a period of 14 h. Primary cardiomyocytes isolated at embryonic day 13.5 were beating and stable throughout the experiments and therefore an ideal model system for the investigation of titin dynamics in real-time. FRAP analysis revealed that bleached titin-eGFP was replaced by unbleached titin-eGFP after photobleaching and fluorescence recovered to a steady state (Figure 12). Issacs and colleges found that the half-life for new synthesized titin protein (synthetic half-life) is 2.9 days (Isaacs et al., 1989). Surprisingly, we observed a much faster recovery of titin-eGFP after photobleaching and conclude that *de novo* synthesis does not make major contributions to the fluorescence recovery within the time of measurement. We confirmed our hypothesis by addition of the protein synthesis inhibitor cycloheximide to the culture medium. CX inhibits the elongation of translation and has been used for FRAP analysis with neonatal and embryonic cardiomyocytes (Zaal et al., 1999; Stahlhut et al., 2006; Wang et al., 2005a). We performed our FRAP experiments in the presence of CX to prevent eGFP recovery due to *de novo* synthesis of titin-eGFP. Inhibition of protein synthesis did not lead to changes in the fluorescence recovery. A depressed recovery curve and a reduction of the mobile fraction would be expected if new synthesized titin-eGFP is required for recovery. We observed that titin is mobile to the same extent in untreated and CX-treated cells, which supports our hypothesis that recovery is largely independent from protein synthesis and occurs either by exchange of bleached and unbleached neighboring molecules or by an unbound, already existing titin pool in the cytosol.

6.3 Titin's mobility depends on protein degradation

Sarcomeric proteins are in a dynamic equilibrium of *de novo* synthesis and degradation. The proteasome system plays an important role in normal muscle homeostasis and alterations in the rate of protein degradation disturb the dynamic state (Powell, 2006; Zolk et al., 2006; Doll et al., 2007). A combination of FRAP and MG132 treatment was used to study the impact of proteasome inhibition on titin-eGFP mobility (Figure 13). Our results show that pharmacological inhibition of the proteasome resulted in a depressed fluorescence recovery curve and a significant decrease of the mobile fraction with increased exchange half-life. Inhibition of protein degradation may lead to an impairment of the sarcomeric protein clearance, including titin, and consequently proteins accumulate within the cell. An impaired

proteasome function has been described in cardiomyopathy to cause protein accumulation, hypertrophy, and subsequently heart failure (Powell, 2006). Decreased mobility of myofilament components could be the result of immobile molecules, which are not degraded to free up binding sites for new titin-eGFP molecules from other regions of the cell or accumulated proteins interfere with the trafficking of proteins from the cytosol to the sarcomere. Under MG123 conditions, we observed low cytotoxicity, which indicates that other mechanisms, such as changes in the protein-protein interaction, could additionally be involved in decreased titin-eGFP mobility. Earlier studies reported that proteasome inhibition induced efficiently the expression of small heat shock proteins (Hsp) (Stangl et al., 2002; Verschuure et al., 2002; Doll et al., 2007). The molecular chaperone αB-crystallin was observed to interact with actin (Verschuure et al., 2002). During proteasome inhibition the αB-crystallin-actin interaction is enhanced, where the Hsp may increase the stability of the actin filament (Iwaki et al., 1994; Verschuure et al., 2002). The more stable thin filament system could reinforce the interaction of actin and titin and consequently cause retention of titin within the sarcomere. Furthermore, it has been reported that αB-crystallin binds to titin's N2B region and that Hsp decreases titin's denaturation by stabilizing the protein during cardiac ischemia, in order to delay ischemic damage (Golenhofen et al., 2002; Bullard et al., 2004). Another small Hsp, Hsp27, is associated with titin in heat-shocked cardiomyocytes from zebrafish, supporting a mechanism where the titin-Hsp27 interaction protects myofibril degradation under stress (Tucker and Shelden, 2009). In summary, these observations suggest that in response to proteasome inhibition the expression of Hsp increases and the interaction of Hsp-titin prevents the degradation of the sarcomere. This is in agreement with our FRAP data, where titin-GFP only slightly recovers in MG132 treated cells indicating that the protein stability is increased and degradation is reduced. We speculate that titin stays bound in the sarcomere, and the exchange with the cytosolic pool is restricted in order to maintain the sarcomeric structure under stress conditions.

6.4 Dynamics of titin in the sarcomere

To determine the underlying mechanism of fluorescence recovery, we increased the size of the bleached area and compared small, intermediate, and large regions (Figure 15). Two types of dynamics are possible: (1) mobility of individual titin molecules and (2) micron-scale dynamic rearrangements of myofibrils. Over the investigated time we did not observe

changes in the shape or diameter of the cultured cells. For example, alterations in cell shape of myocytes and myofibril rearrangement have been reported in isolated cardiomyocytes from infarcted tissue (Weisman et al., 1988; Kozlovskis et al., 1991; Kramer et al., 1998; Zimmerman et al., 2004). We observed only minor rearrangements of myofibrils, due to contraction of the cell and minimal passive movement of the cardiomyocytes in the cell cultured dish during the long period of measurement. Fluorescence recovery by rearrangement would indicate shifting of the position of the bleached area within the cell. Investigation of intermediate and large bleached regions did not show any drifting inside the cell. Quite the contrary has been observed because the shape, border, and location of the area of interest were significantly stable (Figure 15 and Figure 16). We conclude that myofibril rearrangement only adds insignificantly to the fluorescence recovery and movement of titin molecules is the major mechanism. Titin is dynamic within the cell and individual titin-eGFP, either bound or from a free pool of unbleached titin-eGFP, exchange with bleached molecules. Cytosolic proteins are always available as shown for actin and the myosin light chain suggesting that proteins can be rapidly exchanged between the sarcomere and the cytoplasm (Horváth and Gaetjens, 1972; Shimizu and Obinata, 1986). With an increase in size of the bleached area the exchange half-life increased indicating that more time is needed to reach the center of the area, because bleached titin-eGFP is not directly surrounded by unbleached titin molecules.

To examine the direction of titin movement, we measured the longitudinal and lateral titin-eGFP mobility (Figure 17). Longitudinal movement reflects mainly exchange of titin within one myofibril, whereas lateral movement shows primarily exchange between adjacent myofibrils. Our observations showed that longitudinal and lateral movement of titin-eGFP occurs at similar rates. One possibility for longitudinal movement would be that titin detaches from the sarcomere, moves towards the bleached area, and reintegrates by attaching to the Z-disc and M-band. For lateral movement we hypothesize that titin molecules do not require disconnection from the sarcomere, but molecules stay bound and move from neighboring myofibrils into the field of interest. We show that fluorescence recovery results from isotropic titin-eGFP movement. Titin dynamics is unrestricted along and between myofibrils, suggesting a model in which titin freely moves in either direction before it reintegrates.

6.5 Calcium affects titin's mobility

It has been reported that variation of the calcium concentration in the medium influences the cell proliferation of cardiomyocytes and the expression of sarcomeric proteins (Harayama et al., 1998). We performed FRAP experiments on embryonic cardiomyocytes treated with three different calcium concentrations and investigated if calcium affects the dynamics of titin-eGFP.

Calcium is ubiquitous in cells and has an essential role as a second messenger. In myocytes its functions include the regulation of ion currents via channels and exchangers, energy balance (mitochondria), apoptosis or necrosis, the regulation of contraction, and transcription (Denton and McCormack, 1990; Territo et al., 2000; Crabtree, 2001; Orrenius et al., 2003; Hinken and Solaro, 2007; Bers, 2008). Furthermore, calcium regulates the excitation-contraction coupling in muscle cells, which includes calcium mobilization, binding to troponin C, and calcium-dependent cross-bridge cycling by the thin filament complex (Blinks and Endoh, 1986; Endoh, 2008). The interaction of actin and myosin is calcium-dependent and the binding is blocked in the absence of calcium and the rate slowed for strong interaction (Lehrer and Morris, 1982; Vibert et al., 1997; Lehman and Craig, 2008; Sich et al., 2010). In addition, calcium also regulates the interaction between actin and titin (Granzier and Labeit, 2006). The binding of titin's elastic PEVK domain to actin contributes to the passive tension (Yamasaki et al., 2001). It has been shown that calcium directly binds to titin's PEVK region and consequently decreases the elastic properties of the PEVK segment (Tatsumi et al., 2001; Labeit et al., 2003; Fujita et al., 2004). Since calcium is an essential component for normal muscle cell function, we tested the influence of calcium on the mobility of titin-eGFP (Figure 18). Indeed, we found that titin mobility was significantly increased at low calcium levels, but the exchange half-life was unchanged compared to control cells under normal calcium conditions. In contrast, high calcium significantly reduced titin dynamics, but had no influence on the half-fluorescence recovery. The unaltered exchange half-life and mobile fraction indicate that calcium is not required for the movement of titin molecules within the sarcomere, but influences the pool of available unbleached titin-eGFP able to exchange with bleached molecules. Studying the binding properties of titin to actin, Kellermayer and Granzier saw an enhanced association of titin and thin filaments and suppressed *in vitro* the motility under increased calcium levels (Kellermayer and Granzier, 1996). Subsequent investigations of Linke and colleagues demonstrated that the interaction of titin's PEVK domain and actin is relatively weak (Linke et al., 2002). Thus, retention of titin-eGFP within

the sarcomere cannot be explained by enhanced titin-actin association only. We tested the hypothesis if calcium-induced variations of titin dynamics were due to alterations in contraction. Recent studies showed that in cardiomyocytes actin dynamics is contractility-dependent (Skwarek-Maruszewska et al., 2009). The addition of the myosin II inhibitor BDM revealed that titin-eGFP mobility is independent from myosin and myocyte contraction, since treatment did not lead to a rescue of the reduced titin mobility under high calcium conditions (Figure 19). Calcium-mediated signaling or transcriptional regulation may also be responsible for alterations in titin dynamics. For example, cardiomyocytes cultured in low calcium showed a suppressed expression of sarcomeric proteins and an enhanced cell proliferation (Harayama et al., 1998). Calcium in the culture medium may have the ability to alter the transcription of key proteins in signaling and calcium transport, but future studies may elucidate the role of extracellular calcium on the regulation of protein mobility.

Calcium determines the mobility of titin, but does not affect the protein transport itself. Under high calcium conditions titin remains within the myofilament, a mechanism which is likely due to the modulation of protein-protein interactions, but independent from contraction.

6.6 Titin dynamics in development

During development, the expression pattern of sarcomeric proteins changes and isoform transition occurs after birth. Not only titin, but also proteins of the thin and thick filament are expressed in diverse isoforms in order to adapt to the functional properties of the developing muscle. The myocardium expresses two myosin heavy chain isoforms, α- and β-MHC (Nadal-Ginard and Mahdavi, 1989; Metzger et al., 1999). In the ventricle of small mammals, the MHC isoform expression switches from the predominantly embryonic/neonatal β-MHC to the predominantly α-MHC isoform in adults (Nadal-Ginard and Mahdavi, 1989). Changes in MHC isoform expression are correlated with different functions of the myocardium during development (Schwartz et al., 1981; Swynghedauw, 1986; Nadal-Ginard and Mahdavi, 1989). Likewise, in the developing heart the α-cardiac actin and the α-skeletal actin are co-expressed (Sassoon et al., 1988). In mouse hearts α-skeletal actin declines after birth and is hardly detectable in adult ventricle (Sassoon et al., 1988; Carrier et al., 1992; Tondeleir et al., 2009). In addition, other components of the thin filament system change isoform expression during cardiac development. The ratio of α- and β-tropomyosin is altered during embryonic stage and α-tropomyosin increases in the adult myocardium (L'Ecuyer et al., 1991). Similar,

isoform switch of troponin I and troponin T starts already during embryonic heart development (Saggin et al., 1988, 1989; L'Ecuyer et al., 1991; Metzger et al., 2003). The M-band protein myomesin is expressed as a 195 kDa isoform and throughout development a transition occurs from this isoform to the slightly smaller 190 kDa isoform (Grove et al., 1985; Agarkova et al., 2000). The isoform distribution of sarcomeric proteins correlates with the contractile properties of the heart. For cardiac titin three classes of isoforms exist, the N2B, the N2BA, and the fetal N2BA titin isoform (Trombitas et al., 2001). At embryonic stage, the larger N2BA titin isoform (~3.7 MDa) is replaced by a smaller N2BA and the N2B titin isoform (Opitz et al., 2004; Warren et al., 2004). Neonatal hearts express both N2BA and N2B titin. In the adult myocardium the stiffer N2B titin is the main isoform (Lahmers et al., 2004; Opitz et al., 2004; Warren et al., 2004). Co-expression of titin isoforms is used for fine adjustment of titin-based passive tension during development and in adult muscle (Neagoe et al., 2002; Makarenko et al., 2004). In this study we evaluated if changes in titin's isoform expression lead to differences in titin-eGFP mobility. We confirmed the switch of titin isoforms using qRT-PCR (Figure 20). The comparison of titin dynamics at different developmental stages of the heart showed similar mobility of embryonic and neonatal titin-eGFP (Figure 21). We also investigated titin-eGFP in cardiomyocytes isolated from adult heart, but cells were very sensitive and did not endure the long scanning periods during FRAP experiments. Since the major isoform switch of titin's expression occurs right after birth, we did not expect alterations in the mobility of titin-eGFP from adult cardiomyocytes (Lahmers et al., 2004; Opitz et al., 2004; Warren et al., 2004). The amount of molecules available for exchange with bleached molecules as well as the half-fluorescence recovery was unchanged between embryonic and neonatal titin-eGFP. This indicates that the ability of titin-eGFP to move freely within and between the sarcomere is independent from the domain composition of the molecule. Previous investigations of the expression and dynamics of two cardiac specific and developmentally regulated tropomyosin isoforms, TPM1κ and TPM1α, revealed similar dynamic exchange rates and half-fluorescence recoveries for both isoforms (Wang et al., 2007). Also we observed that different isoforms displayed similar dynamics.

6.7 Full length titin and shorter isoforms show similar mobility

Human titin is encoded by a single gene, which contains 363 exons and undergoes extensive alternative splicing (Labeit and Kolmerer, 1995). Isoforms of various lengths are expressed in different muscle and protein sizes reach from 625 kDa (novex-3) up to 3700 kDa for titin in

the soleus muscle (Freiburg et al., 2000; Bang et al., 2001). The three unique I-band titin isoforms novex 1-3 are expressed in skeletal muscle and heart, where novex-1/N2B and novex-2/N2B are co-expressed with the major cardiac isoforms N2B and N2BA (Cazorla et al., 2000; Freiburg et al., 2000; Bang et al., 2001). The smallest isoform novex-3 integrates into the Z-disc, but is too short to reach the A-band region of the sarcomere (Bang et al., 2001). Investigations of titin's mobility using the TiMEx6-eGFP knockin mouse focused on full length titin, which extends from the Z-disc to the M-band of the myofilament. To include the shorter titin isoforms we performed FRAP experiments using the TiEx28-dsRed knockin mouse, in which the fluorophore dsRed is integrated close to titin's N-terminus at the Z-disc region. FRAP analysis of homozygous dsRed-titin included full length and shorter titin isoforms and showed similar recovery rates compared to homozygous titin-eGFP (Figure 22). Our results suggest similar dynamic properties for full length titin and shorter titin isoforms. Various titin isoforms facilitate different functions in the sarcomere. Titin molecules that span from the Z-disc to the M-band and interact with thin and thick filaments, play an important role in sarcomere assembly and maintenance as well as muscle elasticity (Trinick, 1994; Wang, 1996; Helmes et al., 1999). The functions for novex-3 titin are still not completely understood. Bang and colleagues showed the interaction of novex-3 and obscurin, another giant sarcomeric protein (~800 kDa) (Bang et al., 2001; Young et al., 2001). Obscurin also binds to peripheral Z-disc domains of full length titin (Young et al., 2001). The obscurin-titin interaction may play a distinct role in the organization and stabilization of the sarcomere as well as the mobility of titin itself (Bang et al., 2001; Bowman et al., 2007). Moreover, titin isoforms span the entire Z-disc and interact with other myofibrillar proteins, including α-actinin and T-cap (Ohtsuka et al., 1997a; Sorimachi et al., 1997; Ohtsuka et al., 1997b; Gregorio et al., 1998; Mues et al., 1998; Young et al., 1998). Through functional studies it has been shown that Z-disc titin is crucial for the stability of the sarcomere (Peckham et al., 1997; Turnacioglu et al., 1997; Gregorio et al., 1998; Ayoob et al., 2000). We investigated if dsRed-titin dynamics occurred at a different level compared with titin-eGFP. We speculated that the mobility of dsRed-titin could be increased to ensure rapid exchange of titin molecules in case of need, since the integration of Z-disc titin is essential for maintenance of the sarcomeric structure. In addition, there are more fluorescently labeled titin proteins at the Z-disc, since the TiEx28-dsRed encloses all isoforms. The novex titin isoforms may be able to move faster within the myofilament, because of their smaller sizes. However, the novex isoforms are much less abundant than titin spanning the half-sarcomere (Bang et al., 2001). Thus, shorter isoforms may only have minor contributions to the fluorescent recovery.

DsRed-titin and titin-eGFP showed similar dynamics with unaltered mobile fraction and half-fluorescence recovery suggesting that titin has similar kinetics at the Z-disc and M-band. We studied the dynamics of titin in double heterozygous cardiac cells to compare the mobility of dsRed-titin and titin-eGFP (Figure 23 and Figure 24). This allowed us to follow the recovery of fluorescently labeled titin molecules at the Z-disc and M-band of the sarcomere simultaneously. Also here we found that dsRed-titin (full length and novex titins) and titin-eGFP (full length titin only) moved within the sarcomere at similar rates. Mobile fractions and exchange half-lives were unchanged indicating that titin molecules detach from the Z-disc and M-band at the same time after photobleaching, move along and within the myofibril in the same speed, and reintegrate into the sarcomere with the N- and C-terminus.

6.8 Dynamics of sarcomeric proteins

Even though the sarcomere is a highly organized structure and appears as very stable, proteins of the myofilament exchange constantly. The mobility of fluorescent-tagged sarcomeric proteins was assessed by researchers using FRAP, but data about the dynamics of titin have been missing (Wang et al., 2005a; Sanger et al., 2009; Skwarek-Maruszewska et al., 2009; Pappas et al., 2010). Individual components of the sarcomere exchange and replace at different rates and surprisingly, recovery occurred much faster than new proteins can be synthesized (Zak et al., 1977; Isaacs et al., 1989; Wang et al., 2005a). Proteins of the thin, thick, and titin filament system of the sarcomere have a synthetic half-life of several days, e.g. myosin heavy chain 5.9 days, actin 7.7 days, and titin 2.9 days (Zak et al., 1977; Isaacs et al., 1989). The exchange rates of bleached by non-bleached fluorescent molecules obtained from FRAP analysis indicated that movement occurs within the myofilament and that there are proteins, either from a free pool or molecules which are able to detach from the sarcomere, that diffuse into the bleached area. Experiments *in vivo* predicted that actin is exchanged in the order of minutes in myofibrils (Martonosi et al., 1960). Subsequent studies showed that actin is highly mobile, but FRAP analysis provided variable exchange half-lives reaching from minutes to hours (Suzuki et al., 1998; Hasebe-Kishi and Shimada, 2000; Wang et al., 2005a; Sanger et al., 2009; Skwarek-Maruszewska et al., 2009). Injection of skeletal actin labeled with rhodamine or fluorescein into embryonic chicken cardiomyocytes revealed a recovery rate of 50-60% after 2 h of photobleaching (Suzuki et al., 1998; Hasebe-Kishi and Shimada, 2000). A recent study by Skwarek-Maruszewska et al. reported a mobile fraction of ~50% for GFP-fused β–actin transfected into neonatal rat cardiomyocytes, in which saturated

recovery was accomplished within 7 min and actin dynamics appeared contractile-dependent (Skwarek-Maruszewska et al., 2009). A similar mobile fraction was observed for actin in quail myotubes, where recovery was measured over a 20-minute period (Wang et al., 2005a). These results demonstrate that actin dynamics occur rapidly and distinctly suggesting that the exchange of actin plays an important role in the assembly and maintenance of thin filament arrays (Skwarek-Maruszewska et al., 2009). Furthermore, the actin binding protein α-actinin showed mobility, but observations vary from almost no recovery of skeletal α-actinin injected into chicken cardiomyocytes to ~30-50% in quail myotubes and zebrafish, and almost complete recovery in fibroblasts (Hasebe-Kishi and Shimada, 2000; Wang et al., 2005a; Sanger et al., 2009). The variation in mobility rate and half-fluorescence recovery of the same sarcomeric protein may result from differences in the investigated species, developmental stage and cell type, source and amount of injected protein as well as other experimental procedures. The dynamics of myosin have been studied in mammalian cells and *Caenorhabditis elegans* (Johnson et al., 1988; Ghosh and Hope, 2010). Microinjection of fluorescein-coupled skeletal muscle myosin into chicken skeletal myotubes showed a recovery of 22% within the first 4 h after photobleaching and ~70% recovery by 18 h suggesting that once myosin was incorporated into myofibrils the binding was relatively stable (Johnson et al., 1988). Stable integration of myosin was confirmed by FRAP analysis in *Caenorhabditis elegans in vivo*, were MYO-3::GFP (myosin heavy chain A labeled with GFP) displayed a very slow fluorescence recovery rate over the 15 min time-scale of the experiment (Ghosh and Hope, 2010). Also the giant protein titin is in a dynamic equilibration. With a half-fluorescence recovery of approximately 2 h and a mobile fraction of 50% titin is far from being a static and immobile protein in the myofilament (Figure 12 and Table 11). The integration of titin in the Z-disc is mediated by T-cap, which has been shown to be dynamic, but exchange occurred much slower compared with other Z-disc proteins indicating that T-cap may be exchanged when titin is replaced in the sarcomere (Gregorio et al., 1998; Wang et al., 2005a).

FRAP analysis of sarcomeric proteins showed that recovery rates are much shorter than the synthetic half-lives for newly synthesized proteins. Photobleaching of fluorescently labeled proteins, injected into muscle cells or stable expressed dsRed-titin and titin-eGFP, demonstrated that bleached molecules are replaced by non-bleached molecules and recovery occurs at specific rates, which may reflect the degree of stable incorporation of the protein into the sarcomere. Furthermore, the replacement takes place without disassembly of the sarcomere and other studies including our investigations observed no changes in the

myofilament structure (Figure 12). Thus, the exchange of sarcomeric proteins has to be rapid to maintain the structure and stability of the myofilament. Sarcomeres are more dynamic than suggested and there is a rapid exchange between bound and unbound proteins.

6.9 Titin is required for sarcomeric organization

One of the main focus in muscle research is the investigation of processes involved in sarcomere assembly. We visualized sarcomere disassembly and subsequent reassembly using the TiMEx6-eGFP knockin mouse (Figure 25 and Figure 26). Myofibrillogenesis has been studied using antibody staining, FRAP techniques, and fluorescence resonance energy transfer (Rhee et al., 1994; Du et al., 2003; Wang et al., 2005a; Stout et al., 2008). The integration of actin and myosin into the sarcomere requires a structure that interacts with both filaments and coordinates their proper assembly. This function is carried out by titin, which contains binding domains for actin and myosin (Isaacs et al., 1992; Linke et al., 1997; Trombitás et al., 1997; Trombitas and Granzier, 1997). Based on that titin has been proposed to act as a blueprint in myofibrillogenesis. The important role of titin's Z-disc region in sarcomere assembly, stabilization, and preservation has been shown by overexpression experiments of its Z-disc part, which resulted in disorganization of the sarcomere and disruption of myofibrils (Peckham et al., 1997; Turnacioglu et al., 1997; Gregorio et al., 1998; Ayoob et al., 2000). The effects were not only apparent at the Z-disc and associated structures, but also thick filaments were affected indicating that there is a "cross-talk" between both ends of titin (Kontrogianni-Konstantopoulos et al., 2009). This is consistent with findings from Miller et al., where the deletion of titin's C-terminus led to impaired myofibril organization both at the Z-disc and M-band (Miller et al., 2003a). Titin's M-band region contains a kinase domain, which has been shown to phosphorylate the Z-disc protein T-cap during muscle development *in vitro* (Mayans et al., 1998). The deletion of the titin kinase domain led to disruption of the sarcomeric structure, suggesting an important role of M-band titin in sarcomere integrity and maintenance during development and postnatally (Gotthardt et al., 2003; Weinert et al., 2006). Subsequent studies emphasized the significance of titin's M-band region, showing that deletion of the titin kinase resulted in sarcomeric disassembly with loss of striation in skeletal muscle (Peng et al., 2006). These results indicate that titin is essential for sarcomere assembly and maintenance, based on its tight integration into the myofilament and multiple binding sites for sarcomeric proteins. We studied titin's organization and localization during sarcomere disassembly and reassembly and incubated

embryonic cardiomyocytes with myoseverin. It has been reported that myoseverin leads to disorganization of the sarcomeric structure in myocytes (Ng et al., 2008). We found that application of myoseverin disrupted the myofilament after 12 h, but was reversible on removing the substance and impaired sarcomeres reassembled within 6 h. We hypothesized that myoseverin treatment results in an impaired interactions between sarcomeric proteins and induces disassembly of the myofibrils. Sarcomeres reassembled or newly assembled from premyofibrils forming first nascent and then mature myofibrils. Thereby, sarcomeric proteins reattach to their substrate and form a continuous filament system. Premyofibrils and nascent Z-bodies, which contain α-actinin and actin, transform and develop into Z-discs in mature myofibrils (Du et al., 2003; Sanger et al., 2006). Titin and myosin are expressed when premyofibrils begin to align and nascent myofibrils are formed (Rhee et al., 1994). Following removal of myoseverin, we observed myofibrillogenesis in nascent myofibrils, which contain α-actinin and titin (Figure 26). We concluded that the punctuated pattern of α-actinin are nascent Z-bodies that align within 6 h, fuse, and form the Z-disc. This is consistent with earlier findings, when fluorescent-labeled α-actinin was detected in muscle cells and Z-bodies assembled and fused to form Z-discs (McKenna et al., 1985; Sanger et al., 1986; Dabiri et al., 1997; Wang et al., 2005a). We found that α-actinin and titin organize in mature myofibrils as seen by the periodic striation after 6 h of myoseverin removal (Figure 26). Our observations are in agreement with the premyofibril model. Formation of minisarcomeres starts at the edge of the cardiomyocytes and at the level of Z-bodies they fuse to form mature myofibrils.

6.10 Non-muscle titin is not essential for the brush border structure

The structure and function of titin have been well characterized in striated muscle. Beyond that, titin has been found in non-muscle contractile systems, which also use actin-myosin filaments to perform important cell functions such as movement, cleavage, or transport (Eilertsen and Keller, 1992; Eilertsen et al., 1994; Machado et al., 1998; Machado and Andrew, 2000; Zastrow et al., 2006; Fabian et al., 2007). It has been suggested that cellular titin plays a role in organizing, stabilizing, and maintaining cytoskeletal structures, since it co-assembles with non-muscle myosin, but functional studies are missing (Eilertsen and Keller, 1992; Eilertsen et al., 1994, 1997; Keller et al., 2000). Eilertsen and Keller identified a cellular isoform of titin in the small intestine, which is similar in molecular weight to full length muscle titin and may facilitate structural functions in the intestinal brush border of the

epithelial cell (Eilertsen and Keller, 1992). The structure of the intestinal brush border has been elucidated already decades ago. It is clear from EM examinations of chicken and human epithelium that parallel oriented actin bundles extend from the microvillus core into the terminal web (Drenckhahn and Dermietzel, 1988). Within the terminal web, myosin II binds actin and cross-links the actin bundles from two neighboring microvilli (Bretscher and Weber, 1978; Mooseker et al., 1978; Drenckhahn and Gröschel-Stewart, 1980; Hirokawa et al., 1982). The interaction of myosin II and actin has been implicated in the contraction of the terminal web, which was first observed in isolated brush border from neonatal rats (Rodewald et al., 1976). The cellular cytoskeleton, which includes the microvillus core and the terminal web, contributes to the stability of the cell, and contraction of the terminal web may increase absorption efficiency (Keller et al., 1985). Non-muscle titin was absent from the microvillus core of the intestinal brush border, but expressed in the terminal web, were it co-localized with myosin II (Eilertsen and Keller, 1992; Eilertsen et al., 1994). Within the terminal web cellular titin may interact with myosin filaments and take part in the structural organization of the brush border (Eilertsen and Keller, 1992). Co-localization and interaction of non-muscle titin with myosin II has been also shown in fibroblast stress fibers, in which isolated myosin formed highly ordered arrays in a cellular titin-dependent manner (Eilertsen et al., 1994). Association of cellular titin with non-muscle myosin has only been verified in isolated brush border and co-localization *in vivo* has not been shown (Eilertsen and Keller, 1992; Eilertsen et al., 1994). In this study we used the TiMEx6-eGFP knockin mouse to investigate non-muscle titin and found evidence that titin is expressed in the small intestine (Figure 27). We investigated the structural function of cellular titin in the brush border and generated a gut-specific titin knockout by crossing villin-Cre mice with TiEx2 mice, in which titin's exon 2 (contains the translation start) is flanked by loxP-sites (Figure 28). Villin-Cre is under the control of the villin promoter (El Marjou et al., 2004). Mice carrying the villin-Cre gene have been successfully used to generate tissue specific KO mice and animals developed distinct phenotypic defects depending on the gene of interest (Jones et al., 2006; Galy et al., 2008). Tissue specificity as well as efficient recombination has been demonstrated in intestinal epithelial cells and kidney (El Marjou et al., 2004; Valentin-Vega et al., 2008). The genetic recombination was initiated at embryonic day 9 leading to a gut-specific titin KO. Recombination efficiency was confirmed in small intestines and enterocytes of adult KO mice (Figure 28). TiEx2-villin Cre animals were viable and fertile indicating that deletion of titin in the intestine was not essential for early development, since embryos developed normally and animals reached adulthood (Figure 29). Mice did not develop an obvious

phenotype and heart weight to body weight ratio was unchanged between control and KO as well as the body composition (Figure 29). These results indicated that loss of titin in the brush border did not negatively influence the nutrient uptake. Analysis of the myosin-1a knockout mouse showed similar results (Tyska et al., 2005). Myosin-1a is expressed in the microvillus core and interacts with the actin bundle indicating that the actin-based motor protein is important for brush border structure and function (Tyska and Nambiar, 2010). Knockout mice developed normally with respect to growth, weight, and behavior, but displayed significant impairments at the cellular level (Tyska et al., 2005). In contrast, the deletion of the actin remodeler Eps8, which is localized to intestinal microvilli, resulted in a decreased body weight due to reduced fat and lean mass in young and more pronounced in old knockout mice (Tocchetti et al., 2010). The negative energy balance in Eps8 knockout mice correlated with impaired absorption and reduced microvilli lengths (Tocchetti et al., 2010). We characterized the morphology of the brush border, but histological analysis of the small intestine did not reveal differences between control and KO, including villi number and lengths (Figure 30 and Figure 31). Furthermore, ultrastructure showed normal appearance of microvilli and terminal web. Microvilli number, lengths, and spacing were unchanged in KO animals compared to control (Figure 32) and we did not observe disruption of the brush border structure. Interestingly, in villin KO mice the microvillar actin-binding protein villin also showed no alterations in the ultrastructural organization of microvilli suggesting that villin may only play a redundant role for the brush border structure (Pinson et al., 1998; Ferrary et al., 1999). However, in response to elevated intracellular calcium levels brush border from villin KO mice were unaffected, whereas WT mice showed disrupted microvilli indicating that villin controls the calcium-dependent actin fractionation (Ferrary et al., 1999). Similar to villin, titin may not be essential for maintaining the structure, but could be involved in reorganization in response to various signals, e.g. cell motility or wound healing of the brush border. The low expression level of non-muscle titin and the regular organization of the brush border in TiEx2-villin Cre KO mice support our hypothesis, but further studies are necessary to address titin's function in non-muscle cells. Since muscle titin is calcium-sensitive, non-muscle titin may be regulated by calcium. Calcium treatment of isolated brush border from control and TiEx2-villin Cre KO mice and subsequent analysis of structure and functions are possible experiments to address whether non-muscle titin is important for reorganization of impaired small intestinal brush border.

6.11 Conclusion and perspective

Sarcomeric proteins are not permanently fixed in position, but there is a constant exchange of proteins between a sarcomeric (bound) and non-sarcomeric (free) pool (Sanger and Sanger, 2008). In this study we showed that even the giant muscle protein titin readily moves within the sarcomere. We used the TiMEx6-eGFP knockin mouse to visualize the full length protein in cultured cardiomyocytes and investigated its mobility (Figure 33). We found that titin's mobility is largely independent from protein synthesis, supported by the relatively short half-fluorescence recovery of ~2 h compared with the synthetic half-life of ~3 days for newly synthesized protein (Isaacs et al., 1989). Surprisingly, protein degradation influenced the dynamics of titin and inhibition of the proteasome led to a decreased mobile fraction with increased exchange half-life. Follow-up studies, e.g. analysis of protein expression and localization, will show if the accumulation of proteins in the cell caused the decrease in titin mobility. In addition, Hsp protein levels and subsequent titin-Hsp interaction could be investigated by qRT-PCR, Western blotting, and immunofluorescence staining in TiMEx6-eGFP cardiomyocytes treated with a proteasome inhibitor. Furthermore, calcium affected the dynamics of titin. Exposing cells to high calcium levels reduced the exchange of titin-eGFP molecules, an effect independent of contraction. We presume that calcium influences the interaction of sarcomeric proteins, such as titin and actin. It remains to be determined if extracellular calcium alters protein expression. Analysis of calcium-dependent myofilament proteins on mRNA and protein level will help to answer this question. In addition, specific knockdown experiments on calcium signaling pathways in cultured cardiomyocytes may contribute to the understanding of calcium-dependent mobility of titin. Changing the size of the bleached region as well as bleaching longitudinal and lateral areas were used to experimentally test the mechanism we proposed for titin-eGFP movement. Rearrangement of myofibrils only added minimally to the fluorescence recovery. We postulate that titin moves in either direction, within and between myofibrils, and dynamics are independent from titin's domain composition.

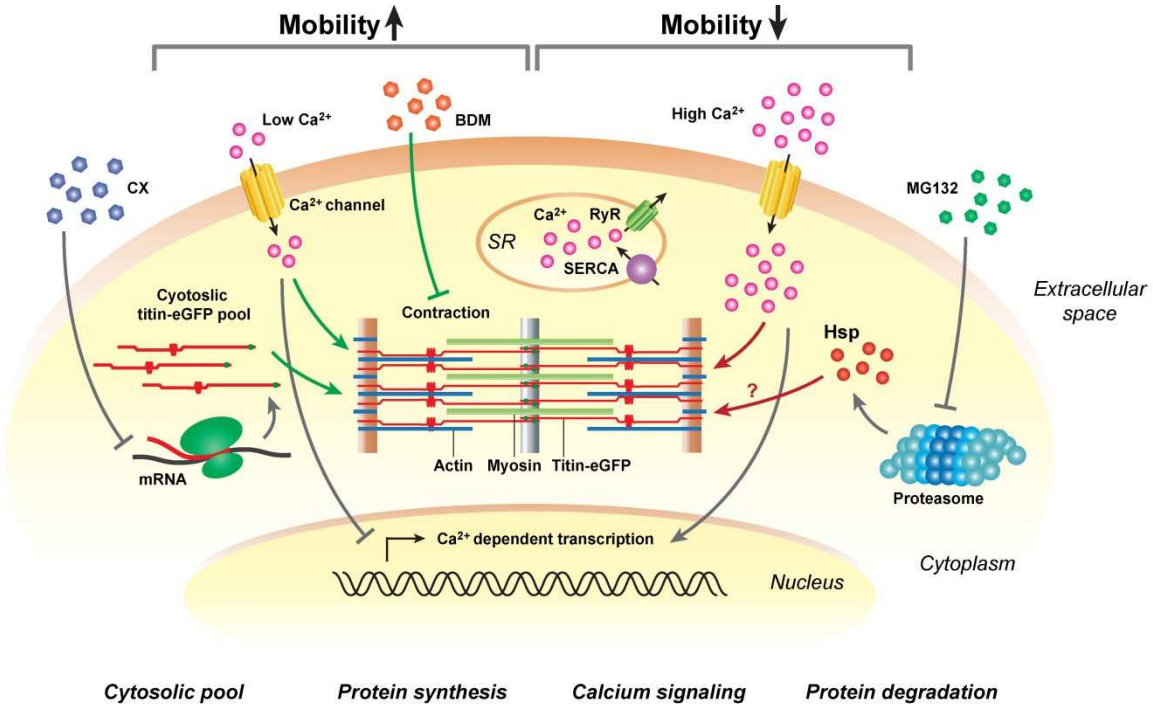

Figure 33. Pathways that control titin mobility. Sarcomeric titin is in a dynamic exchange with unbound protein. This equilibration is independent from protein synthesis, since the inhibition of translation by cycloheximide (CX) does not change the mobility. Addition of MG132 inhibits the proteasome, which may induce heat shock protein (Hsp) expression. Hsp interact with actin and titin thereby decreasing titin's degradation. Consequently, titin remains bound in the sarcomere and its mobility is reduced. Low calcium concentration suppresses sarcomeric protein expression and enhances titin mobility. In contrast, high calcium levels lead to the binding of calcium to sarcomeric proteins, which may result in stronger protein-protein interaction and decreased titin mobility. Titin's mobility is independent from contraction, since inhibition by 2,3-butanedione monoxime (BDM) did not change the dynamics of titin. Intracellular calcium is stored in the sarcoplasmic reticulum (SR), taken up from the cytosol by the ATPase SERCA and released by the ryanodine receptor (RyR). Green arrow: titin mobility; red arrow: reduced mobility; gray arrow: regulation of transcription, translation, and degradation.

Titin is dynamically exchanged in the myofilament, which raises the possibility that other giant muscle proteins, e.g. nebulin (600-900 kDa) or obscurin (~720-900 kDa), are more dynamic in the cell. Using the knockin technology can help to investigate the full length proteins *in vivo*, evaluate their mobility, and determine the kinetics for their exchange within the sarcomere. Understanding how titin and other sarcomeric proteins move between the myofilament and the cytosol or a pool of bound and free proteins is important in order to understand sarcomere assembly during normal development and in disease. Cardiac myopathies and skeletal muscle dystrophies have been intensively studied and the role of titin in these diseases has been investigated, but information about titin's stability and mobility in the sarcomere is lacking. Investigating the structure and the function of titin in detail will help

to follow titin's mobility in the impaired muscle. Advances in genetic, molecular, and imaging technology made it possible to generate a fluorescently labeled titin knockin mouse, which enabled us to elucidate the mobility of titin in real-time and its regulation. The powerful FRAP technique has provided novel insights on how titin moves within the sarcomere, between myofilaments, and in the cytosolic pool. The analysis of titin mobility under physiological conditions is the basis to understand titin dynamics in the diseased muscle and heart. Towards a therapeutic approach, sarcomeres could be fortified by increasing the time titin remains attached in the Z-disc and M-band. Conversely remodeling could be facilitated by increasing the mobility of titin through interfering with its binding proteins. Thus, it is important to determine the factors that influence the stability of proteins within the myofilament in future studies.

7 Bibliography

Agarkova, I., D. Auerbach, E. Ehler, and J.C. Perriard. 2000. A novel marker for vertebrate embryonic heart, the EH-myomesin isoform. *J. Biol. Chem*. 275:10256-10264.

Agarkova, I., and J.C. Perriard. 2005. The M-band: an elastic web that crosslinks thick filaments in the center of the sarcomere. *Trends Cell Biol*.

Al Tanoury, Z., E. Schaffner-Reckinger, A. Halavatyi, C. Hoffmann, M. Moes, E. Hadzic, M. Catillon, M. Yatskou, and E. Friederich. 2010. Quantitative kinetic study of the actin-bundling protein L-plastin and of its impact on actin turn-over. *PLoS ONE*. 5:e9210.

Ayoob, J.C., K.K. Turnacioglu, B. Mittal, J.M. Sanger, and J.W. Sanger. 2000. Targeting of cardiac muscle titin fragments to the Z-bands and dense bodies of living muscle and non-muscle cells. *Cell Motil Cytoskeleton*. 45:67-82.

Bang, M.L., T. Centner, F. Fornoff, A.J. Geach, M. Gotthardt, M. McNabb, C.C. Witt, D. Labeit, C.C. Gregorio, H. Granzier, et al. 2001. The complete gene sequence of titin, expression of an unusual approximately 700-kDa titin isoform, and its interaction with obscurin identify a novel Z-line to I-band linking system. *Circ Res*. 89:1065-1072.

Bartles, J.R., L. Zheng, A. Li, A. Wierda, and B. Chen. 1998. Small espin: a third actin-bundling protein and potential forked protein ortholog in brush border microvilli. *J. Cell Biol*. 143:107-119.

Bennett, P., R. Craig, R. Starr, and G. Offer. 1986. The ultrastructural location of C-protein, X-protein and H-protein in rabbit muscle. *J. Muscle Res. Cell. Motil*. 7:550-567.

Van den Bergh, P.Y.K., O. Bouquiaux, C. Verellen, S. Marchand, I. Richard, P. Hackman, and B. Udd. 2003. Tibial muscular dystrophy in a Belgian family. *Ann. Neurol*. 54:248-251.

Bers, D.M. 2008. Calcium cycling and signaling in cardiac myocytes. *Annu. Rev. Physiol*. 70:23-49.

Blinks, J.R., and M. Endoh. 1986. Modification of myofibrillar responsiveness to Ca++ as an inotropic mechanism. *Circulation*. 73:III85-98.

Bowman, A.L., A. Kontrogianni-Konstantopoulos, S.S. Hirsch, S.B. Geisler, H. Gonzalez-Serratos, M.W. Russell, and R.J. Bloch. 2007. Different obscurin isoforms localize to distinct sites at sarcomeres. *FEBS Lett*. 581:1549-1554.

Bretscher, A., and K. Weber. 1978. Localization of actin and microfilament-associated proteins in the microvilli and terminal web of the intestinal brush border by immunofluorescence microscopy. *J. Cell Biol*. 79:839-845.

Bretscher, A., and K. Weber. 1979. Villin: the major microfilament-associated protein of the intestinal microvillus. *Proc. Natl. Acad. Sci. U.S.A*. 76:2321-2325.

Bretscher, A., and K. Weber. 1980. Fimbrin, a new microfilament-associated protein present in microvilli and other cell surface structures. *J. Cell Biol*. 86:335-340.

Brown, D.D., A.C. Davis, and F.L. Conlon. 2006. Xtn3 is a developmentally expressed cardiac and skeletal muscle-specific novex-3 titin isoform. *Gene Expr. Patterns*. 6:913-918.

Bullard, B., C. Ferguson, A. Minajeva, M.C. Leake, M. Gautel, D. Labeit, L. Ding, S. Labeit, J. Horwitz, K.R. Leonard, et al. 2004. Association of the chaperone alphaB-crystallin with titin in heart muscle. *J Biol Chem*. 279:7917-7924.

Butterfield, T.A., T.R. Leonard, and W. Herzog. 2005. Differential serial sarcomere number adaptations in knee extensor muscles of rats is contraction type dependent. *J. Appl. Physiol*. 99:1352-1358.

Caiozzo, V.J., F. Haddad, M.J. Baker, and K.M. Baldwin. 1995. Functional and cellular adaptations of rodent skeletal muscle to weightlessness. *J Gravit Physiol*. 2:P39-42.

Carmignac, V., M.A. Salih, S. Quijano-Roy, S. Marchand, M.M. Al Rayess, M.M. Mukhtar, J.A. Urtizberea, S. Labeit, P. Guicheney, F. Leturcq, et al. 2007. C-terminal titin deletions cause a novel early-onset myopathy with fatal cardiomyopathy. *Ann Neurol*. 61:340-351.

Carrier, L., K.R. Boheler, C. Chassagne, D. de la Bastie, C. Wisnewsky, E.G. Lakatta, and K. Schwartz. 1992. Expression of the sarcomeric actin isogenes in the rat heart with development and senescence. *Circ. Res*. 70:999-1005.

Cavnar, P.J., S.G. Olenych, and T.C.S. Keller 3rd. 2007. Molecular identification and localization of cellular titin, a novel titin isoform in the fibroblast stress fiber. *Cell Motil. Cytoskeleton*. 64:418-433.

Cazorla, O., A. Freiburg, M. Helmes, T. Centner, M. McNabb, Y. Wu, K. Trombitas, S. Labeit, and H.L. Granzier. 2000. Differential expression of cardiac titin isoforms and modulation of cellular stiffness. *Circ Res*. 86:59-67.

Centner, T., J. Yano, E. Kimura, A.S. McElhinny, K. Pelin, C.C. Witt, M.L. Bang, K. Trombitas, H. Granzier, C.C. Gregorio, et al. 2001. Identification of Muscle Specific Ring Finger Proteins as Potential Regulators of the Titin Kinase Domain. *J Mol Biol*. 306:717-726.

Collins, K., J. Sellers, and P. Matsudaira. 1991. Myosin I: a new insight into the mechanism and cellular significance of actin-based motility. *Adv. Biophys*. 27:221-226.

Crabtree, G.R. 2001. Calcium, calcineurin, and the control of transcription. *J. Biol. Chem*. 276:2313-2316.

Dabiri, G.A., K.K. Turnacioglu, J.M. Sanger, and J.W. Sanger. 1997. Myofibrillogenesis visualized in living embryonic cardiomyocytes. *Proc Natl Acad Sci U S A*. 94:9493-9498.

Denton, R.M., and J.G. McCormack. 1990. Ca2+ as a second messenger within mitochondria of the heart and other tissues. *Annu. Rev. Physiol*. 52:451-466.

Dlugosz, A.A., P.B. Antin, V.T. Nachmias, and H. Holtzer. 1984. The relationship between stress fiber-like structures and nascent myofibrils in cultured cardiac myocytes. *J. Cell Biol*. 99:2268-2278.

Doll, D., A. Sarikas, R. Krajcik, and O. Zolk. 2007. Proteomic expression analysis of cardiomyocytes subjected to proteasome inhibition. *Biochem. Biophys. Res. Commun*. 353:436-442.

Drabikowski, W., and E. Nowak. 1973. Interaction of F-actin with troponin constituents. *Biochim. Biophys. Acta*. 328:470-480.

Drenckhahn, D., and R. Dermietzel. 1988. Organization of the actin filament cytoskeleton in the intestinal brush border: a quantitative and qualitative immunoelectron microscope study. *J. Cell Biol*. 107:1037-1048.

Drenckhahn, D., and U. Gröschel-Stewart. 1980. Localization of myosin, actin, and tropomyosin in rat intestinal epithelium: immunohistochemical studies at the light and electron microscope levels. *J. Cell Biol*. 86:475-482.

Du, A., J.M. Sanger, K.K. Linask, and J.W. Sanger. 2003. Myofibrillogenesis in the first cardiomyocytes formed from isolated quail precardiac mesoderm. *Dev. Biol*. 257:382-394.

Eilertsen, K.J., S.T. Kazmierski, and T.C. Keller. 1994. Cellular titin localization in stress fibers and interaction with myosin II filaments in vitro. *J Cell Biol*. 126:1201-10.

Eilertsen, K.J., and T.C. Keller. 1992. Identification and characterization of two huge protein components of the brush border cytoskeleton: evidence for a cellular isoform of titin. *J Cell Biol*. 119:549-557.

Eilertsen, K.J., S.T. Kazmierski, and T.C. Keller. 1997. Interaction of alpha-actinin with cellular titin. *Eur J Cell Biol*. 74:361-364.

El Marjou, F., K.P. Janssen, C.B. Hung-Junn, M. Li, V. Hindie, L. Chan, D. Louvard, P. Chambon, D. Metzger, and S. Robine. 2004. Tissue-specific and inducible Cre-mediated recombination in the gut epithelium. *Genesis*. 39:186-193.

Endoh, M. 2008. Cardiac Ca2+ signaling and Ca2+ sensitizers. *Circ. J*. 72:1915-1925.

Fabian, L., X. Xia, D.V. Venkitaramani, K.M. Johansen, J. Johansen, D.J. Andrew, and A. Forer. 2007. Titin in insect spermatocyte spindle fibers associates with microtubules, actin, myosin and the matrix proteins skeletor, megator and chromator. *J Cell Sci*. 120:2190-2204.

Fernando, P., J.S. Sandoz, W. Ding, Y. de Repentigny, S. Brunette, J.F. Kelly, R. Kothary, and L.A. Megeney. 2009. Bin1 SRC homology 3 domain acts as a scaffold for myofiber sarcomere assembly. *J. Biol. Chem*. 284:27674-27686.

Ferrary, E., M. Cohen-Tannoudji, G. Pehau-Arnaudet, A. Lapillonne, R. Athman, T. Ruiz, L. Boulouha, F. El Marjou, A. Doye, J.J. Fontaine, et al. 1999. In vivo, villin is required for Ca(2+)-dependent F-actin disruption in intestinal brush borders. *J. Cell Biol*. 146:819-830.

Franke, W.W., S. Winter, C. Grund, E. Schmid, D.L. Schiller, and E.D. Jarasch. 1981. Isolation and characterization of desmosome-associated tonofilaments from rat intestinal brush border. *J. Cell Biol*. 90:116-127.

Freiburg, A., and M. Gautel. 1996. A molecular map of the interactions between titin and myosin-binding protein C. Implications for sarcomeric assembly in familial hypertrophic cardiomyopathy. *Eur J Biochem*. 235:317-323.

Freiburg, A., K. Trombitas, W. Hell, O. Cazorla, F. Fougerousse, T. Centner, B. Kolmerer, C. Witt, J.S. Beckmann, C.C. Gregorio, et al. 2000. Series of exon-skipping events in the elastic spring region of titin as the structural basis for myofibrillar elastic diversity. *Circ Res*. 86:1114-1121.

Fridén, J. 1984. Changes in human skeletal muscle induced by long-term eccentric exercise. *Cell Tissue Res*. 236:365-372.

Fujita, H., D. Labeit, B. Gerull, S. Labeit, and H.L. Granzier. 2004. Titin isoform-dependent effect of calcium on passive myocardial tension. *Am J Physiol Heart Circ Physiol*. 287:H2528-H2534.

Fukuzawa, A., S. Lange, M. Holt, A. Vihola, V. Carmignac, A. Ferreiro, B. Udd, and M. Gautel. 2008. Interactions with titin and myomesin target obscurin and obscurin-like 1 to the M-band: implications for hereditary myopathies. *J Cell Sci*. 121:1841-1851.

Furst, D.O., M. Osborn, R. Nave, and K. Weber. 1988. The organization of titin filaments in the half-sarcomere revealed by monoclonal antibodies in immunoelectron microscopy: a map of ten nonrepetitive epitopes starting at the Z line extends close to the M line. *J Cell Biol*. 106:1563-1572.

Furst, D.O., U. Vinkemeier, and K. Weber. 1992. Mammalian skeletal muscle C-protein: purification from bovine muscle, binding to titin and the characterization of a full-length human cDNA. *J Cell Sci*. 102 (Pt 4):769-778.

Galy, B., D. Ferring-Appel, S. Kaden, H.-J. Gröne, and M.W. Hentze. 2008. Iron regulatory proteins are essential for intestinal function and control key iron absorption molecules in the duodenum. *Cell Metab*. 7:79-85.

Gautel, M., D. Goulding, B. Bullard, K. Weber, and D.O. Fürst. 1996. The central Z-disk region of titin is assembled from a novel repeat in variable copy numbers. *J. Cell. Sci*. 109 (Pt 11):2747-2754.

Gautel, M., M. Castiglione, M. Pfuhl, A. Motta, and A. Pastore. 1995. A calmodulin-binding sequence in the C-terminus of human cardiac titin kinase. *Eur J Biochem*. 230:752-759.

Gautel, M., K. Leonard, and S. Labeit. 1993. Phosphorylation of KSP motifs in the C-terminal region of titin in differentiating myoblasts. *EMBO J*. 12:3827-3834.

Geetha, T., and M.W. Wooten. 2002. Structure and functional properties of the ubiquitin binding protein p62. *FEBS Lett*. 512:19-24.

Gerull, B., M. Gramlich, J. Atherton, M. McNabb, K. Trombitas, S. Sasse-Klaassen, J.G. Seidman, C. Seidman, H. Granzier, S. Labeit, et al. 2002. Mutations of TTN, encoding the giant muscle filament titin, cause familial dilated cardiomyopathy. *Nat Genet*. 30:201-204.

Gerull, B., J. Atherton, A. Geupel, S. Sasse-Klaassen, A. Heuser, M. Frenneaux, M. McNabb, H. Granzier, S. Labeit, and L. Thierfelder. 2006. Identification of a novel frameshift mutation in the giant muscle filament titin in a large Australian family with dilated cardiomyopathy. *J. Mol. Med*. 84:478-483.

Ghosh, S.R., and I.A. Hope. 2010. Determination of the mobility of novel and established Caenorhabditis elegans sarcomeric proteins in vivo. *Eur. J. Cell Biol*. 89:437-448.

Goldman, R.D., Y. Gruenbaum, R.D. Moir, D.K. Shumaker, and T.P. Spann. 2002. Nuclear lamins: building blocks of nuclear architecture. *Genes Dev*. 16:533-547.

Golenhofen, N., A. Arbeiter, R. Koob, and D. Drenckhahn. 2002. Ischemia-induced association of the stress protein alpha B-crystallin with I-band portion of cardiac titin. *J Mol Cell Cardiol*. 34:309-319.

Gomez, L.A., A.E. Alekseev, L.A. Aleksandrova, P.A. Brady, and A. Terzic. 1997. Use of the MTT assay in adult ventricular cardiomyocytes to assess viability: effects of adenosine and potassium on cellular survival. *J. Mol. Cell. Cardiol*. 29:1255-1266.

Gotthardt, M., R.E. Hammer, N. Hubner, J. Monti, C.C. Witt, M. McNabb, J.A. Richardson, H. Granzier, S. Labeit, and J. Herz. 2003. Conditional expression of mutant M-line titins results in cardiomyopathy with altered sarcomere structure. *J Biol Chem*. 278:6059-6065.

Gramlich, M., B. Michely, C. Krohne, A. Heuser, B. Erdmann, S. Klaassen, B. Hudson, M. Magarin, F. Kirchner, M. Todiras, et al. 2009. Stress-induced dilated cardiomyopathy in a knock-in mouse model mimicking human titin-based disease. *J. Mol. Cell. Cardiol*. 47:352-358.

Granzier, H.L., and S. Labeit. 2006. The giant muscle protein titin is an adjustable molecular spring. *Exerc Sport Sci Rev*. 34:50-53.

Granzier, H.L., M.H. Radke, J. Peng, D. Westermann, O.L. Nelson, K. Rost, N.M.P. King, Q. Yu, C. Tschöpe, M. McNabb, et al. 2009. Truncation of titin's elastic PEVK region leads to cardiomyopathy with diastolic dysfunction. *Circ. Res*. 105:557-564.

Gräsbeck, R. 1997. Selective cobalamin malabsorption and the cobalamin-intrinsic factor receptor. *Acta Biochim. Pol*. 44:725-733.

Greaser, M.L., S.M. Wang, M. Berri, P. Mozdziak, and Y. Kumazawa. 2000. Sequence and mechanical implications of titin's PEVK region. *Adv. Exp. Med. Biol*. 481:53-63; discussion 64-66, 107-110.

Greaser, M.L., P.R. Krzesinski, C.M. Warren, B. Kirkpatrick, K.S. Campbell, and R.L. Moss. 2005. Developmental changes in rat cardiac titin/connectin: transitions in normal animals and in mutants with a delayed pattern of isoform transition. *J Muscle Res Cell Motil*. 26:325-332.

Gregorio, C.C., H. Granzier, H. Sorimachi, and S. Labeit. 1999. Muscle assembly: a titanic achievement? *Curr Opin Cell Biol*. 11:18-25.

Gregorio, C.C., K. Trombitás, T. Centner, B. Kolmerer, G. Stier, K. Kunke, K. Suzuki, F. Obermayr, B. Herrmann, H. Granzier, et al. 1998. The NH2 terminus of titin spans the

Z-disc: its interaction with a novel 19-kD ligand (T-cap) is required for sarcomeric integrity. *J Cell Biol*. 143:1013-27.

Gregorio, C.C., C.N. Perry, and A.S. McElhinny. 2005. Functional properties of the titin/connectin-associated proteins, the muscle-specific RING finger proteins (MURFs), in striated muscle. *J. Muscle Res. Cell. Motil*. 26:389-400.

Grove, B.K., L. Cerny, J.C. Perriard, and H.M. Eppenberger. 1985. Myomesin and M-protein: expression of two M-band proteins in pectoral muscle and heart during development. *J Cell Biol*. 101:1413-1421.

Hackman, P., A. Vihola, H. Haravuori, S. Marchand, J. Sarparanta, J. De Seze, S. Labeit, C. Witt, L. Peltonen, I. Richard, et al. 2002. Tibial muscular dystrophy is a titinopathy caused by mutations in TTN, the gene encoding the giant skeletal-muscle protein titin. *Am J Hum Genet*. 71:492-500.

Hackman, P., S. Marchand, J. Sarparanta, A. Vihola, I. Pénisson-Besnier, B. Eymard, J.M. Pardal-Fernández, E.-H. Hammouda, I. Richard, I. Illa, et al. 2008. Truncating mutations in C-terminal titin may cause more severe tibial muscular dystrophy (TMD). *Neuromuscul. Disord*. 18:922-928.

Harayama, H., M. Koide, K. Obata, A. Iio, M. Iida, N. Matsuda, R.E. Akins, M. Yokota, R.S. Tuan, and H. Saito. 1998. Influence of calcium on proliferation and phenotype alteration of cardiomyocyte in vitro. *J. Cell. Physiol*. 177:289-298.

Hasebe-Kishi, F., and Y. Shimada. 2000. Dynamics of actin and alpha-actinin in nascent myofibrils and stress fibers. *J. Muscle Res. Cell. Motil*. 21:717-724.

Helmes, M., K. Trombitas, T. Centner, M. Kellermayer, S. Labeit, W.A. Linke, and H. Granzier. 1999. Mechanically driven contour-length adjustment in rat cardiac titin's unique N2B sequence: titin is an adjustable spring. *Circ Res*. 84:1339-1352.

Hinken, A.C., and R.J. Solaro. 2007. A dominant role of cardiac molecular motors in the intrinsic regulation of ventricular ejection and relaxation. *Physiology (Bethesda)*. 22:73-80.

Hirokawa, N., R.E. Cheney, and M. Willard. 1983. Location of a protein of the fodrin-spectrin-TW260/240 family in the mouse intestinal brush border. *Cell*. 32:953-965.

Hirokawa, N., L.G. Tilney, K. Fujiwara, and J.E. Heuser. 1982. Organization of actin, myosin, and intermediate filaments in the brush border of intestinal epithelial cells. *J. Cell Biol*. 94:425-443.

Horváth, B.Z., and E. Gaetjens. 1972. Immunochemical studies on the light chains from skeletal muscle myosin. *Biochim. Biophys. Acta*. 263:779-793.

Houmeida, A., J. Holt, L. Tskhovrebova, and J. Trinick. 1995. Studies of the interaction between titin and myosin. *J Cell Biol*. 131:1471-1481.

Huang, J., and N.E. Forsberg. 1998. Role of calpain in skeletal-muscle protein degradation. *Proc. Natl. Acad. Sci. U.S.A*. 95:12100-12105.

Huxley, A.F. 2000. Cross-bridge action: present views, prospects, and unknowns. *J Biomech*. 33:1189-1195.

Huxley, A.F., and R. Niedergerke. 1954. Structural changes in muscle during contraction; interference microscopy of living muscle fibres. *Nature*. 173:971-973.

Huxley, H., and J. Hanson. 1954. Changes in the cross-striations of muscle during contraction and stretch and their structural interpretation. *Nature*. 173:973-6.

Hynes, T.R., S.M. Block, B.T. White, and J.A. Spudich. 1987. Movement of myosin fragments in vitro: domains involved in force production. *Cell*. 48:953-963.

Isaacs, W.B., I.S. Kim, A. Struve, and A.B. Fulton. 1989. Biosynthesis of titin in cultured skeletal muscle cells. *J Cell Biol*. 109:2189-2195.

Isaacs, W.B., I.S. Kim, A. Struve, and A.B. Fulton. 1992. Association of titin and myosin heavy chain in developing skeletal muscle. *Proc Natl Acad Sci U S A*. 89:7496-7500.

Itoh-Satoh, M., T. Hayashi, H. Nishi, Y. Koga, T. Arimura, T. Koyanagi, M. Takahashi, S. Hohda, K. Ueda, T. Nouchi, et al. 2002. Titin Mutations as the Molecular Basis for Dilated Cardiomyopathy. *Biochem Biophys Res Commun*. 291:385-393.

Iwaki, T., A. Iwaki, J. Tateishi, and J.E. Goldman. 1994. Sense and antisense modification of glial alpha B-crystallin production results in alterations of stress fiber formation and thermoresistance. *J. Cell Biol*. 125:1385-1393.

Johnson, C.S., N.M. McKenna, and Y. Wang. 1988. Association of microinjected myosin and its subfragments with myofibrils in living muscle cells. *J. Cell Biol*. 107:2213-2221.

Jones, R.G., X. Li, P.D. Gray, J. Kuang, F. Clayton, W.S. Samowitz, B.B. Madison, D.L. Gumucio, and S.K. Kuwada. 2006. Conditional deletion of beta1 integrins in the intestinal epithelium causes a loss of Hedgehog expression, intestinal hyperplasia, and early postnatal lethality. *J. Cell Biol*. 175:505-514.

Karlson, P., D. Doenecke, and J. Koolman. 1994. Kurzes Lehrbuch der Biochemie für Mediziner und Naturwissenschaftler. Thieme, Stuttgart.

Kaul, A., M. Koster, H. Neuhaus, and T. Braun. 2000. Myf-5 revisited: loss of early myotome formation does not lead to a rib phenotype in homozygous Myf-5 mutant mice. *Cell*. 102:17-19.

Keller, T.C., K.A. Conzelman, R. Chasan, and M.S. Mooseker. 1985. Role of myosin in terminal web contraction in isolated intestinal epithelial brush borders. *J Cell Biol*. 100:1647-55.

Keller, T.C., K. Eilertsen, M. Higginbotham, S. Kazmierski, K.T. Kim, and M. Velichkova. 2000. Role of titin in nonmuscle and smooth muscle cells. *Adv. Exp. Med. Biol*. 481:265-277; discussion 278-281.

Kellermayer, M.S., and H.L. Granzier. 1996. Calcium-dependent inhibition of in vitro thin-filament motility by native titin. *FEBS Lett*. 380:281-286.

Kelly, D.E. 1969. Myofibrillogenesis and Z-band differentiation. *Anat. Rec*. 163:403-425.

Kinbara, K., H. Sorimachi, S. Ishiura, and K. Suzuki. 1997. Muscle-specific calpain, p94, interacts with the extreme C-terminal region of connectin, a unique region flanked by two immunoglobulin C2 motifs. *Arch Biochem Biophys*. 342:99-107.

Kolega, J. 2004. Phototoxicity and photoinactivation of blebbistatin in UV and visible light. *Biochem. Biophys. Res. Commun*. 320:1020-1025.

Kolmerer, B., C.C. Witt, A. Freiburg, S. Millevoi, G. Stier, H. Sorimachi, K. Pelin, L. Carrier, K. Schwartz, D. Labeit, et al. 1999. The titin cDNA sequence and partial genomic sequences: insights into the molecular genetics, cell biology and physiology of the titin filament system. *Rev. Physiol. Biochem. Pharmacol*. 138:19-55.

Kolmerer, B., N. Olivieri, C.C. Witt, B.G. Herrmann, and S. Labeit. 1996. Genomic organization of M line titin and its tissue-specific expression in two distinct isoforms. *J Mol Biol*. 256:556-563.

Kontrogianni-Konstantopoulos, A., M.A. Ackermann, A.L. Bowman, S.V. Yap, and R.J. Bloch. 2009. Muscle giants: molecular scaffolds in sarcomerogenesis. *Physiol. Rev*. 89:1217-1267.

Kontrogianni-Konstantopoulos, A., and R.J. Bloch. 2003. The hydrophilic domain of small ankyrin-1 interacts with the two N-terminal immunoglobulin domains of titin. *J. Biol. Chem*. 278:3985-3991.

Kozlovskis, P.L., A.M. Gerdes, M. Smets, J.A. Moore, A.L. Bassett, and R.J. Myerburg. 1991. Regional increase in isolated myocyte volume in chronic myocardial infarction in cats. *J. Mol. Cell. Cardiol*. 23:1459-1466.

Kramer, C.M., W.J. Rogers, C.S. Park, P.S. Seibel, A. Shaffer, T.M. Theobald, N. Reichek, T. Onodera, and A.M. Gerdes. 1998. Regional myocyte hypertrophy parallels regional myocardial dysfunction during post-infarct remodeling. *J. Mol. Cell. Cardiol*. 30:1773-1778.

L'Ecuyer, T.J., D. Schulte, and J.J. Lin. 1991. Thin filament changes during in vivo rat heart development. *Pediatr. Res*. 30:232-238.

Labeit, D., K. Watanabe, C. Witt, H. Fujita, Y. Wu, S. Lahmers, T. Funck, S. Labeit, and H. Granzier. 2003. Calcium-dependent molecular spring elements in the giant protein titin. *Proc. Natl. Acad. Sci. U.S.A*. 100:13716-13721.

Labeit, S., and B. Kolmerer. 1995. Titins: giant proteins in charge of muscle ultrastructure and elasticity. *Science*. 270:293-296.

Labeit, S., D.P. Barlow, M. Gautel, T. Gibson, J. Holt, C.L. Hsieh, U. Francke, K. Leonard, J. Wardale, A. Whiting, et al. 1990. A regular pattern of two types of 100-residue motif in the sequence of titin. *Nature*. 345:273-276.

Labeit, S., M. Gautel, A. Lakey, and J. Trinick. 1992. Towards a molecular understanding of titin. *EMBO J*. 11:1711-1716.

Labeit, S., B. Kolmerer, and W.A. Linke. 1997. The giant protein titin. Emerging roles in physiology and pathophysiology. *Circ Res*. 80:290-294.

Labeit, S., S. Lahmers, C. Burkart, C. Fong, M. McNabb, S. Witt, C. Witt, D. Labeit, and H. Granzier. 2006. Expression of distinct classes of titin isoforms in striated and smooth muscles by alternative splicing, and their conserved interaction with filamins. *J Mol Biol*. 362:664-681.

Lahmers, S., Y. Wu, D.R. Call, S. Labeit, and H. Granzier. 2004. Developmental control of titin isoform expression and passive stiffness in fetal and neonatal myocardium. *Circ. Res*. 94:505-513.

Lange, S., D. Auerbach, P. McLoughlin, E. Perriard, B.W. Schafer, J.C. Perriard, and E. Ehler. 2002. Subcellular targeting of metabolic enzymes to titin in heart muscle may be mediated by DRAL/FHL-2. *J Cell Sci*. 115:4925-4936.

Lange, S., F. Xiang, A. Yakovenko, A. Vihola, P. Hackman, E. Rostkova, J. Kristensen, B. Brandmeier, G. Franzen, B. Hedberg, et al. 2005. The Kinase Domain of Titin Controls Muscle Gene Expression and Protein Turnover. *Science*. 308:1599-1603.

Latunde-Dada, G.O., J. Van der Westhuizen, C.D. Vulpe, G.J. Anderson, R.J. Simpson, and A.T. McKie. 2002. Molecular and functional roles of duodenal cytochrome B (Dcytb) in iron metabolism. *Blood Cells Mol. Dis*. 29:356-360.

Lehman, W., and R. Craig. 2008. Tropomyosin and the steric mechanism of muscle regulation. *Adv. Exp. Med. Biol*. 644:95-109.

Lehrer, S.S., and E.P. Morris. 1982. Dual effects of tropomyosin and troponin-tropomyosin on actomyosin subfragment 1 ATPase. *J. Biol. Chem*. 257:8073-8080.

Li, S., M.P. Czubryt, J. McAnally, R. Bassel-Duby, J.A. Richardson, F.F. Wiebel, A. Nordheim, and E.N. Olson. 2005. Requirement for serum response factor for skeletal muscle growth and maturation revealed by tissue-specific gene deletion in mice. *Proc. Natl. Acad. Sci. U.S.A*. 102:1082-1087.

Linke, W.A., M. Ivemeyer, S. Labeit, H. Hinssen, J.C. Ruegg, and M. Gautel. 1997. Actin-titin interaction in cardiac myofibrils: probing a physiological role. *Biophys J*. 73:905-919.

Linke, W.A., M. Ivemeyer, P. Mundel, M.R. Stockmeier, and B. Kolmerer. 1998. Nature of PEVK-titin elasticity in skeletal muscle. *Proc Natl Acad Sci U S A*. 95:8052-8057.

Linke, W.A., M. Ivemeyer, N. Olivieri, B. Kolmerer, J.C. Ruegg, and S. Labeit. 1996. Towards a molecular understanding of the elasticity of titin. *J Mol Biol*. 261:62-71.

Linke, W.A., D.E. Rudy, T. Centner, M. Gautel, C. Witt, S. Labeit, and C.C. Gregorio. 1999. I-band titin in cardiac muscle is a three-element molecular spring and is critical for maintaining thin filament structure. *J Cell Biol*. 146:631-644.

Linke, W.A. 2008. Sense and stretchability: the role of titin and titin-associated proteins in myocardial stress-sensing and mechanical dysfunction. *Cardiovasc. Res*. 77:637-648.

Linke, W.A., M. Kulke, H. Li, S. Fujita-Becker, C. Neagoe, D.J. Manstein, M. Gautel, and J.M. Fernandez. 2002. PEVK domain of titin: an entropic spring with actin-binding properties. *J. Struct. Biol*. 137:194-205.

van der Loop, F.T., D. van, D.O. Furst, M. Gautel, G.J. van Eys, and F.C. Ramaekers. 1996. Integration of titin into the sarcomeres of cultured differentiating human skeletal muscle cells. *Eur J Cell Biol*. 69:301-307.

Ma, K., and K. Wang. 2002. Interaction of nebulin SH3 domain with titin PEVK and myopalladin: implications for the signaling and assembly role of titin and nebulin. *FEBS Lett*. 532:273-8.

Machado, C., C.E. Sunkel, and D.J. Andrew. 1998. Human autoantibodies reveal titin as a chromosomal protein. *J Cell Biol*. 141:321-33.

Machado, C., and D.J. Andrew. 2000. D-Titin. A giant protein with dual roles in chromosomes and muscles. *J Cell Biol*. 151:639-652.

Makarenko, I., C.A. Opitz, M.C. Leake, C. Neagoe, M. Kulke, J.K. Gwathmey, M.F. del, R.J. Hajjar, and W.A. Linke. 2004. Passive stiffness changes caused by upregulation of compliant titin isoforms in human dilated cardiomyopathy hearts. *Circ Res*. 95:708-716.

Martonosi, A., M.A. Gouvea, and J. Gergely. 1960. Studies on actin. III. G-F transformation of actin and muscular contraction (experiments in vivo). *J. Biol. Chem*. 235:1707-1710.

Maruyama, K., and S. Ebashi. 1965. Alpha-actinin, a new structural protein from striated muscle. II. Action on actin. *J. Biochem*. 58:13-19.

Maruyama, K., S. Kimura, K. Ohashi, and Y. Kuwano. 1981. Connectin, an elastic protein of muscle. Identification of "titin" with connectin. *J. Biochem*. 89:701-709.

Maruyama, K., F. Murakami, and K. Ohashi. 1977. Connectin, an elastic protein of muscle. Comparative Biochemistry. *J Biochem (Tokyo)*. 82:339-345.

Matsumoto, Y., T. Hayashi, N. Inagaki, M. Takahashi, S. Hiroi, T. Nakamura, T. Arimura, K. Nakamura, N. Ashizawa, M. Yasunami, et al. 2005. Functional analysis of titin/connectin N2-B mutations found in cardiomyopathy. *J Muscle Res Cell Motil*. 26:367-374.

Mayans, O., P.F. van der Ven, M. Wilm, A. Mues, P. Young, D.O. Fürst, M. Wilmanns, and M. Gautel. 1998. Structural basis for activation of the titin kinase domain during myofibrillogenesis. *Nature*. 395:863-9.

McElhinny, A.S., K. Kakinuma, H. Sorimachi, S. Labeit, and C.C. Gregorio. 2002. Muscle-specific RING finger-1 interacts with titin to regulate sarcomeric M-line and thick filament structure and may have nuclear functions via its interaction with glucocorticoid modulatory element binding protein-1. *J Cell Biol*. 157:125-136.

McElhinny, A.S., S.T. Kazmierski, S. Labeit, and C.C. Gregorio. 2003. Nebulin: the nebulous, multifunctional giant of striated muscle. *Trends Cardiovasc Med*. 13:195-201.

McElhinny, A.S., S. Labeit, and C.C. Gregorio. 2000. Probing the functional roles of titin ligands in cardiac myofibril assembly and maintenance. *Adv Exp Med Biol*. 481:67-86.

McElhinny, A.S., C.N. Perry, C.C. Witt, S. Labeit, and C.C. Gregorio. 2004. Muscle-specific RING finger-2 (MURF-2) is important for microtubule, intermediate filament and sarcomeric M-line maintenance in striated muscle development. *J Cell Sci*. Pt.

McKenna, N.M., J.B. Meigs, and Y.L. Wang. 1985. Exchangeability of alpha-actinin in living cardiac fibroblasts and muscle cells. *J. Cell Biol*. 101:2223-2232.

Metzger, J.M., P.A. Wahr, D.E. Michele, F. Albayya, and M.V. Westfall. 1999. Effects of myosin heavy chain isoform switching on Ca2+-activated tension development in single adult cardiac myocytes. *Circ. Res*. 84:1310-1317.

Metzger, J.M., D.E. Michele, E.M. Rust, A.R. Borton, and M.V. Westfall. 2003. Sarcomere thin filament regulatory isoforms. Evidence of a dominant effect of slow skeletal troponin I on cardiac contraction. *J. Biol. Chem*. 278:13118-13123.

Miller, G., H. Musa, M. Gautel, and M. Peckham. 2003a. A targeted deletion of the C-terminal end of titin, including the titin kinase domain, impairs myofibrillogenesis. *J Cell Sci*. 116:4811-4819.

Miller, M.K., M.L. Bang, C.C. Witt, D. Labeit, C. Trombitas, K. Watanabe, H. Granzier, A.S. McElhinny, C.C. Gregorio, and S. Labeit. 2003b. The Muscle Ankyrin Repeat Proteins: CARP, ankrd2/Arpp and DARP as a Family of Titin Filament-based Stress Response Molecules. *J Mol Biol*. 333:951-964.

Mooseker, M.S. 1983. Actin binding proteins of the brush border. *Cell*. 35:11-13.

Mooseker, M.S. 1985. Organization, chemistry, and assembly of the cytoskeletal apparatus of the intestinal brush border. *Annu. Rev. Cell Biol*. 1:209-241.

Mooseker, M.S., and R.E. Cheney. 1995. Unconventional myosins. *Annu. Rev. Cell Dev. Biol*. 11:633-675.

Mooseker, M.S., and L.G. Tilney. 1975. Organization of an actin filament-membrane complex. Filament polarity and membrane attachment in the microvilli of intestinal epithelial cells. *J. Cell Biol*. 67:725-743.

Mooseker, M.S., E.M. Bonder, K.A. Conzelman, D.J. Fishkind, C.L. Howe, and T.C. Keller 3rd. 1984. Brush border cytoskeleton and integration of cellular functions. *J. Cell Biol*. 99:104s-112s.

Mooseker, M.S., T.D. Pollard, and K. Fujiwara. 1978. Characterization and localization of myosin in the brush border of intestinal epithelial cells. *J. Cell Biol*. 79:444-453.

Morano, I., K. Hädicke, S. Grom, A. Koch, R.H. Schwinger, M. Böhm, S. Bartel, E. Erdmann, and E.G. Krause. 1994. Titin, myosin light chains and C-protein in the developing and failing human heart. *J. Mol. Cell. Cardiol*. 26:361-368.

Mues, A., P.F. van der Ven, P. Young, D.O. Fürst, and M. Gautel. 1998. Two immunoglobulin-like domains of the Z-disc portion of titin interact in a conformation-dependent way with telethonin. *FEBS Lett*. 428:111-114.

Muller-Seitz, M., K. Kaupmann, S. Labeit, and H. Jockusch. 1993. Chromosomal localization of the mouse titin gene and its relation to “muscular dystrophy with myositis” and nebulin genes on chromosome 2. *Genomics*. 18:559-561.

Myung, J., K.B. Kim, and C.M. Crews. 2001. The ubiquitin-proteasome pathway and proteasome inhibitors. *Med Res Rev*. 21:245-273.

Nadal-Ginard, B., and V. Mahdavi. 1989. Molecular basis of cardiac performance. Plasticity of the myocardium generated through protein isoform switches. *J. Clin. Invest*. 84:1693-1700.

Nave, R., D.O. Furst, and K. Weber. 1989. Visualization of the polarity of isolated titin molecules: a single globular head on a long thin rod as the M band anchoring domain? *J Cell Biol*. 109:2177-2187.

Neagoe, C., M. Kulke, F. del Monte, J.K. Gwathmey, P.P. de Tombe, R.J. Hajjar, and W.A. Linke. 2002. Titin isoform switch in ischemic human heart disease. *Circulation*. 106:1333-1341.

Ng, D.C.H., B.L. Gebski, M.D. Grounds, and M.A. Bogoyevitch. 2008. Myoseverin disrupts sarcomeric organization in myocytes: an effect independent of microtubule assembly inhibition. *Cell Motil. Cytoskeleton*. 65:40-58.

Oakley, C.E., J. Chamoun, L.J. Brown, and B.D. Hambly. 2007. Myosin binding protein-C: enigmatic regulator of cardiac contraction. *Int. J. Biochem. Cell Biol*. 39:2161-2166.

Obermann, W.M., M. Gautel, F. Steiner, P.F. van der Ven, K. Weber, and D.O. Furst. 1996. The structure of the sarcomeric M band: localization of defined domains of myomesin, M-protein, and the 250-kD carboxy-terminal region of titin by immunoelectron microscopy. *J Cell Biol*. 134:1441-1453.

Obermann, W.M., M. Gautel, K. Weber, and D.O. Furst. 1997. Molecular structure of the sarcomeric M band: mapping of titin and myosin binding domains in myomesin and the identification of a potential regulatory phosphorylation site in myomesin. *EMBO J*. 16:211-220.

Ohtsuka, H., H. Yajima, K. Maruyama, and S. Kimura. 1997a. Binding of the N-terminal 63 kDa portion of connectin/titin to alpha-actinin as revealed by the yeast two-hybrid system. *FEBS Lett*. 401:65-67.

Ohtsuka, H., H. Yajima, K. Maruyama, and S. Kimura. 1997b. The N-terminal Z repeat 5 of connectin/titin binds to the C-terminal region of alpha-actinin. *Biochem Biophys Res Commun*. 235:1-3.

Opitz, C.A., M.C. Leake, I. Makarenko, V. Benes, and W.A. Linke. 2004. Developmentally regulated switching of titin size alters myofibrillar stiffness in the perinatal heart. *Circ Res*. 94:967-975.

Orrenius, S., B. Zhivotovsky, and P. Nicotera. 2003. Regulation of cell death: the calcium-apoptosis link. *Nat. Rev. Mol. Cell Biol*. 4:552-565.

Ottenheijm, C.A.C., A.M. Knottnerus, D. Buck, X. Luo, K. Greer, A. Hoying, S. Labeit, and H. Granzier. 2009. Tuning Passive Mechanics through Differential Splicing of Titin during Skeletal Muscle Development. *Biophys. J*. 97:2277-2286.

Pappas, C.T., P.A. Krieg, and C.C. Gregorio. 2010. Nebulin regulates actin filament lengths by a stabilization mechanism. *J Cell Biol*.

Peckham, M., P. Young, and M. Gautel. 1997. Constitutive and variable regions of Z-disk titin/connectin in myofibril formation: a dominant-negative screen. *Cell Struct Funct*. 22:95-101.

Pelin, K., M. Ridanpää, K. Donner, S. Wilton, J. Krishnarajah, N. Laing, B. Kolmerer, S. Millevoi, S. Labeit, A. de la Chapelle, et al. 1997. Refined localisation of the genes for nebulin and titin on chromosome 2q allows the assignment of nebulin as a candidate gene for autosomal recessive nemaline myopathy. *Eur. J. Hum. Genet*. 5:229-234.

Peng, J., K. Raddatz, S. Labeit, H. Granzier, and M. Gotthardt. 2006. Muscle atrophy in Titin M-line deficient mice. *J Muscle Res Cell Motil*. 1-8.

Peng, J., K. Raddatz, J.D. Molkentin, Y. Wu, S. Labeit, H. Granzier, and M. Gotthardt. 2007. Cardiac hypertrophy and reduced contractility in hearts deficient in the titin kinase region. *Circulation*. 115:743-751.

Perez, O.D., Y.-T. Chang, G. Rosania, D. Sutherlin, and P.G. Schultz. 2002. Inhibition and reversal of myogenic differentiation by purine-based microtubule assembly inhibitors. *Chem. Biol*. 9:475-483.

Peterson, L.J., Z. Rajfur, A.S. Maddox, C.D. Freel, Y. Chen, M. Edlund, C. Otey, and K. Burridge. 2004. Simultaneous stretching and contraction of stress fibers in vivo. *Mol. Biol. Cell*. 15:3497-3508.

Pinson, K.I., L. Dunbar, L. Samuelson, and D.L. Gumucio. 1998. Targeted disruption of the mouse villin gene does not impair the morphogenesis of microvilli. *Dev. Dyn*. 211:109-121.

Powell, S.R. 2006. The ubiquitin-proteasome system in cardiac physiology and pathology. *Am. J. Physiol. Heart Circ. Physiol*. 291:H1-H19.

Prado, L.G., I. Makarenko, C. Andresen, M. Krüger, C.A. Opitz, and W.A. Linke. 2005. Isoform diversity of giant proteins in relation to passive and active contractile properties of rabbit skeletal muscles. *J. Gen. Physiol*. 126:461-480.

Radke, M.H., J. Peng, Y. Wu, M. McNabb, O.L. Nelson, H. Granzier, and M. Gotthardt. 2007. Targeted deletion of titin N2B region leads to diastolic dysfunction and cardiac atrophy. *Proc Natl Acad Sci U S A*. 104:3444-3449.

Rayment, I., H.M. Holden, M. Whittaker, C.B. Yohn, M. Lorenz, K.C. Holmes, and R.A. Milligan. 1993. Structure of the actin-myosin complex and its implications for muscle contraction. *Science*. 261:58-65.

Raynaud, F., C. Astier, and Y. Benyamin. 2004. Evidence for a direct but sequential binding of titin to tropomyosin and actin filaments. *Biochim Biophys Acta*. 1700:171-178.

Rhee, D., J.M. Sanger, and J.W. Sanger. 1994. The premyofibril: evidence for its role in myofibrillogenesis. *Cell Motil Cytoskeleton*. 28:1-24.

Richardson, P., W. McKenna, M. Bristow, B. Maisch, B. Mautner, J. O'Connell, E. Olsen, G. Thiene, J. Goodwin, I. Gyarfas, et al. 1996. Report of the 1995 World Health Organization/International Society and Federation of Cardiology Task Force on the Definition and Classification of cardiomyopathies. *Circulation*. 93:841-842.

Rodewald, R., S.B. Newman, and M.J. Karnovsky. 1976. Contraction of isolated brush borders from the intestinal epithelium. *J. Cell Biol*. 70:541-554.

Rosania, G.R., Y.T. Chang, O. Perez, D. Sutherlin, H. Dong, D.J. Lockhart, and P.G. Schultz. 2000. Myoseverin, a microtubule-binding molecule with novel cellular effects. *Nat Biotechnol*. 18:304-308.

Rossi, E., A. Faiella, M. Zeviani, S. Labeit, G. Floridia, S. Brunelli, M. Cammarata, E. Boncinelli, and O. Zuffardi. 1994. Order of six loci at 2q24-q31 and orientation of the HOXD locus. *Genomics*. 24:34-40.

Russell, B., M.W. Curtis, Y.E. Koshman, and A.M. Samarel. 2010. Mechanical stress-induced sarcomere assembly for cardiac muscle growth in length and width. *J. Mol. Cell. Cardiol*. 48:817-823.

Saggin, L., S. Ausoni, L. Gorza, S. Sartore, and S. Schiaffino. 1988. Troponin T switching in the developing rat heart. *J. Biol. Chem*. 263:18488-18492.

Saggin, L., L. Gorza, S. Ausoni, and S. Schiaffino. 1989. Troponin I switching in the developing heart. *J. Biol. Chem*. 264:16299-16302.

Sanger, J.M., B. Mittal, M.B. Pochapin, and J.W. Sanger. 1986. Myofibrillogenesis in living cells microinjected with fluorescently labeled alpha-actinin. *J. Cell Biol*. 102:2053-2066.

Sanger, J.W., J.M. Sanger, and C. Franzini-Armstrong. 2004. Assembly of the skeletal muscle cell. *In* Myology. McGraw-Hill Professional, New York, NY, USA. 45-65.

Sanger, J.W., J.C. Ayoob, P. Chowrashi, D. Zurawski, and J.M. Sanger. 2000. Assembly of myofibrils in cardiac muscle cells. *Adv Exp Med Biol*. 481:89-102.

Sanger, J.W., S. Kang, C.C. Siebrands, N. Freeman, A. Du, J. Wang, A.L. Stout, and J.M. Sanger. 2006. How to build a myofibril. *J Muscle Res Cell Motil*. 1-12.

Sanger, J.M., and J.W. Sanger. 2008. The dynamic Z bands of striated muscle cells. *Sci Signal*. 1:pe37.

Sanger, J.W., J. Wang, B. Holloway, A. Du, and J.M. Sanger. 2009. Myofibrillogenesis in skeletal muscle cells in zebrafish. *Cell Motil. Cytoskeleton*. 66:556-566.

Sassoon, D.A., I. Garner, and M. Buckingham. 1988. Transcripts of alpha-cardiac and alpha-skeletal actins are early markers for myogenesis in the mouse embryo. *Development*. 104:155-164.

Satoh, M., M. Takahashi, T. Sakamoto, M. Hiroe, F. Marumo, and A. Kimura. 1999. Structural analysis of the titin gene in hypertrophic cardiomyopathy: identification of a novel disease gene. *Biochem Biophys Res Commun*. 262:411-7.

Schaffner, W., and C. Weissmann. 1973. A rapid, sensitive, and specific method for the determination of protein in dilute solution. *Anal Biochem*. 56:502-514.

Schultheiss, T., Z.X. Lin, M.H. Lu, J. Murray, D.A. Fischman, K. Weber, T. Masaki, M. Imamura, and H. Holtzer. 1990. Differential distribution of subsets of myofibrillar proteins in cardiac nonstriated and striated myofibrils. *J Cell Biol*. 110:1159-1172.

Schwartz, K., Y. Lecarpentier, J.L. Martin, A.M. Lompré, J.J. Mercadier, and B. Swynghedauw. 1981. Myosin isoenzymic distribution correlates with speed of myocardial contraction. *J. Mol. Cell. Cardiol*. 13:1071-1075.

Sebestyen, M.G., J.D. Fritz, J.A. Wolff, and M.L. Greaser. 1996. Primary structure of the kinase domain region of rabbit skeletal and cardiac muscle titin. *J Muscle Res Cell Motil*. 17:343-348.

Seetharam, B., and R.R. Yammani. 2003. Cobalamin transport proteins and their cell-surface receptors. *Expert Rev Mol Med*. 5:1-18.

Seibenhener, M.L., J.R. Babu, T. Geetha, H.C. Wong, N.R. Krishna, and M.W. Wooten. 2004. Sequestosome 1/p62 is a polyubiquitin chain binding protein involved in ubiquitin proteasome degradation. *Mol Cell Biol*. 24:8055-8068.

Sheikh, F., A. Raskin, P.-H. Chu, S. Lange, A.A. Domenighetti, M. Zheng, X. Liang, T. Zhang, T. Yajima, Y. Gu, et al. 2008. An FHL1-containing complex within the cardiomyocyte sarcomere mediates hypertrophic biomechanical stress responses in mice. *J Clin Invest*. 118:3870-80.

Shimizu, N., and T. Obinata. 1986. Actin concentration and monomer-polymer ratio in developing chicken skeletal muscle. *J. Biochem*. 99:751-759.

Sich, N.M., T.J. O'Donnell, S.A. Coulter, O.A. John, M.S. Carter, C.R. Cremo, and J.E. Baker. 2010. Effects of actin-myosin kinetics on the calcium sensitivity of regulated thin filaments. *J. Biol. Chem*. 285:39150-39159.

Siebrands, C.C., J.M. Sanger, and J.W. Sanger. 2004. Myofibrillogenesis in skeletal muscle cells in the presence of taxol. *Cell Motil. Cytoskeleton*. 58:39-52.

Skwarek-Maruszewska, A., P. Hotulainen, P.K. Mattila, and P. Lappalainen. 2009. Contractility-dependent actin dynamics in cardiomyocyte sarcomeres. *J. Cell. Sci*. 122:2119-2126.

Sorimachi, H., A. Freiburg, B. Kolmerer, S. Ishiura, G. Stier, C.C. Gregorio, D. Labeit, W.A. Linke, K. Suzuki, and S. Labeit. 1997. Tissue-specific expression and alpha-actinin binding properties of the Z-disc titin: implications for the nature of vertebrate Z-discs. *J. Mol. Biol*. 270:688-695.

Sorimachi, H., S. Kimura, K. Kinbara, J. Kazama, M. Takahashi, H. Yajima, S. Ishiura, N. Sasagawa, I. Nonaka, H. Sugita, et al. 1996. Structure and physiological functions of

ubiquitous and tissue-specific calpain species. Muscle-specific calpain, p94, interacts with connectin/titin. *Adv. Biophys*. 33:101-122.

Sorimachi, H., K. Kinbara, S. Kimura, M. Takahashi, S. Ishiura, N. Sasagawa, N. Sorimachi, H. Shimada, K. Tagawa, and K. Maruyama. 1995. Muscle-specific calpain, p94, responsible for limb girdle muscular dystrophy type 2A, associates with connectin through IS2, a p94-specific sequence. *J Biol Chem*. 270:31158-62.

Stahlhut, M., J.S. Petersen, J.K. Hennan, and M.T. Ramirez. 2006. The antiarrhythmic peptide rotigaptide (ZP123) increases connexin 43 protein expression in neonatal rat ventricular cardiomyocytes. *Cell Commun. Adhes*. 13:21-27.

Stangl, K., C. Günther, T. Frank, M. Lorenz, S. Meiners, T. Röpke, L. Stelter, M. Moobed, G. Baumann, P.-M. Kloetzel, et al. 2002. Inhibition of the ubiquitin-proteasome pathway induces differential heat-shock protein response in cardiomyocytes and renders early cardiac protection. *Biochem. Biophys. Res. Commun*. 291:542-549.

Stout, A.L., J. Wang, J.M. Sanger, and J.W. Sanger. 2008. Tracking changes in Z-band organization during myofibrillogenesis with FRET imaging. *Cell Motil. Cytoskeleton*. 65:353-367.

Suzuki, H., M. Komiyama, A. Konno, and Y. Shimada. 1998. Exchangeability of actin in cardiac myocytes and fibroblasts as determined by fluorescence photobleaching recovery. *Tissue Cell*. 30:274-280.

Swynghedauw, B. 1986. Developmental and functional adaptation of contractile proteins in cardiac and skeletal muscles. *Physiol. Rev*. 66:710-771.

Tatsumi, R., K. Maeda, A. Hattori, and K. Takahashi. 2001. Calcium binding to an elastic portion of connectin/titin filaments. *J Muscle Res Cell Motil*. 22:149-162.

Territo, P.R., V.K. Mootha, S.A. French, and R.S. Balaban. 2000. Ca(2+) activation of heart mitochondrial oxidative phosphorylation: role of the F(0)/F(1)-ATPase. *Am. J. Physiol., Cell Physiol*. 278:C423-435.

Tocchetti, A., C.B.E. Soppo, F. Zani, F. Bianchi, M.C. Gagliani, B. Pozzi, J. Rozman, R. Elvert, N. Ehrhardt, B. Rathkolb, et al. 2010. Loss of the actin remodeler Eps8 causes intestinal defects and improved metabolic status in mice. *PLoS ONE*. 5:e9468.

Tondeleir, D., D. Vandamme, J. Vandekerckhove, C. Ampe, and A. Lambrechts. 2009. Actin isoform expression patterns during mammalian development and in pathology: insights from mouse models. *Cell Motil. Cytoskeleton*. 66:798-815.

Trinick, J. 1994. Titin and nebulin: protein rulers in muscle? *Trends Biochem Sci*. 19:405-409.

Trinick, J. 1996. Titin as a scaffold and spring. Cytoskeleton. *Curr Biol*. 6:258-260.

Trombitás, K., M.L. Greaser, and G.H. Pollack. 1997. Interaction between titin and thin filaments in intact cardiac muscle. *J Muscle Res Cell Motil*. 18:345-51.

Trombitas, K., and H. Granzier. 1997. Actin removal from cardiac myocytes shows that near Z line titin attaches to actin while under tension. *Am J Physiol*. 273:C662-C670.

Trombitas, K., Y. Wu, D. Labeit, S. Labeit, and H. Granzier. 2001. Cardiac titin isoforms are coexpressed in the half-sarcomere and extend independently. *Am J Physiol Heart Circ Physiol*. 281:H1793-H1799.

Truett, G.E., P. Heeger, R.L. Mynatt, A.A. Truett, J.A. Walker, and M.L. Warman. 2000. Preparation of PCR-quality mouse genomic DNA with hot sodium hydroxide and tris (HotSHOT). *BioTechniques*. 29:52, 54.

Tskhovrebova, L., and J. Trinick. 2003. Titin: properties and family relationships. *Nat Rev Mol Cell Biol*. 4:679-689.

Tskhovrebova, L., and J. Trinick. 2004. Properties of titin immunoglobulin and fibronectin-3 domains. *J. Biol. Chem*. 279:46351-46354.

Tucker, N.R., and E.A. Shelden. 2009. Hsp27 associates with the titin filament system in heat-shocked zebrafish cardiomyocytes. *Exp. Cell Res*. 315:3176-3186.

Turnacioglu, K.K., B. Mittal, G.A. Dabiri, J.M. Sanger, and J.W. Sanger. 1997. An N-terminal fragment of titin coupled to green fluorescent protein localizes to the Z-bands in living muscle cells: overexpression leads to myofibril disassembly. *Mol. Biol. Cell*. 8:705-717.

Tyska, M.J., A.T. Mackey, J.D. Huang, N.G. Copeland, N.A. Jenkins, and M.S. Mooseker. 2005. Myosin-1a is critical for normal brush border structure and composition. *Mol Biol Cell*. 16:2443-2457.

Tyska, M.J., and R. Nambiar. 2010. Myosin-1a: A motor for microvillar membrane movement and mechanics. *Commun Integr Biol*. 3:64-66.

Valentin-Vega, Y.A., H. Okano, and G. Lozano. 2008. The intestinal epithelium compensates for p53-mediated cell death and guarantees organismal survival. *Cell Death Differ*. 15:1772-1781.

Valle, G., G. Faulkner, A. De Antoni, B. Pacchioni, A. Pallavicini, D. Pandolfo, N. Tiso, S. Toppo, S. Trevisan, and G. Lanfranchi. 1997. Telethonin, a novel sarcomeric protein of heart and skeletal muscle. *FEBS Lett*. 415:163-168.

van der Ven, P.F., W.M. Obermann, B. Lemke, M. Gautel, K. Weber, and D.O. Fürst. 2000. Characterization of muscle filamin isoforms suggests a possible role of gamma-filamin/ABP-L in sarcomeric Z-disc formation. *Cell Motil. Cytoskeleton*. 45:149-162.

van der Ven, P.F., W.M. Obermann, K. Weber, and D.O. Furst. 1996. Myomesin, M-protein and the structure of the sarcomeric M-band. *Adv Biophys*. 33:91-99.

Verschuure, P., Y. Croes, P.R. van den IJssel, R.A. Quinlan, W.W. de Jong, and W.C. Boelens. 2002. Translocation of small heat shock proteins to the actin cytoskeleton upon proteasomal inhibition. *J Mol Cell Cardiol*. 34:117-128.

Vibert, P., R. Craig, and W. Lehman. 1997. Steric-model for activation of muscle thin filaments. *J. Mol. Biol*. 266:8-14.

Vinkemeier, U., W. Obermann, K. Weber, and D.O. Furst. 1993. The globular head domain of titin extends into the center of the sarcomeric M band. cDNA cloning, epitope

mapping and immunoelectron microscopy of two titin-associated proteins. *J Cell Sci*. 106 (Pt 1):319-330.

Wang, J., N. Shaner, B. Mittal, Q. Zhou, J. Chen, J.M. Sanger, and J.W. Sanger. 2005a. Dynamics of Z-band based proteins in developing skeletal muscle cells. *Cell Motil Cytoskeleton*. 61:34-48.

Wang, J., J.M. Sanger, and J.W. Sanger. 2005b. Differential effects of Latrunculin-A on myofibrils in cultures of skeletal muscle cells: insights into mechanisms of myofibrillogenesis. *Cell Motil. Cytoskeleton*. 62:35-47.

Wang, J., J.M. Sanger, S. Kang, H. Thurston, L.Z. Abbott, D.K. Dube, and J.W. Sanger. 2007. Ectopic expression and dynamics of TPM1alpha and TPM1kappa in myofibrils of avian myotubes. *Cell Motil. Cytoskeleton*. 64:767-776.

Wang, K. 1996. Titin/connectin and nebulin: giant protein rulers of muscle structure and function. *Adv. Biophys*. 33:123-134.

Wang, K., and J. Wright. 1988. Architecture of the sarcomere matrix of skeletal muscle: immunoelectron microscopic evidence that suggests a set of parallel inextensible nebulin filaments anchored at the Z line. *J Cell Biol*. 107:2199-212.

Wang, K., J. McClure, and A. Tu. 1979. Titin: major myofibrillar components of striated muscle. *Proc Natl Acad Sci U S A*. 76:3698-3702.

Wang, S.M., C.J. Jeng, and M.C. Sun. 1992. Studies on the interaction between titin and myosin. *Histol. Histopathol*. 7:333-337.

Wang, S.M., M.C. Sun, and C.J. Jeng. 1991. Location of the C-terminus of titin at the Z-line region in the sarcomere. *Biochem. Biophys. Res. Commun*. 176:189-193.

Warren, C.M., P.R. Krzesinski, and M.L. Greaser. 2003. Vertical agarose gel electrophoresis and electroblotting of high-molecular-weight proteins. *Electrophoresis*. 24:1695-1702.

Warren, C.M., P.R. Krzesinski, K.S. Campbell, R.L. Moss, and M.L. Greaser. 2004. Titin isoform changes in rat myocardium during development. *Mech Dev*. 121:1301-1312.

Watanabe, K., P. Nair, D. Labeit, M. Kellermayer, M. Greaser, S. Labeit, and H. Granzier. 2002. Molecular mechanics of cardiac titin's PEVK and N2B spring elements. *J Biol Chem*.

Weber, A., and J.M. Murray. 1973. Molecular control mechanisms in muscle contraction. *Physiol. Rev*. 53:612-673.

Weber, A., C.R. Pennise, G.G. Babcock, and V.M. Fowler. 1994. Tropomodulin caps the pointed ends of actin filaments. *J. Cell Biol*. 127:1627-1635.

Wegner, A. 1979. Equilibrium of the actin-tropomyosin interaction. *J. Mol. Biol*. 131:839-853.

Weinert, S., N. Bergmann, X. Luo, B. Erdmann, and M. Gotthardt. 2006. M line-deficient titin causes cardiac lethality through impaired maturation of the sarcomere. *J Cell Biol*. 173:559-570.

Weisman, H.F., D.E. Bush, J.A. Mannisi, M.L. Weisfeldt, and B. Healy. 1988. Cellular mechanisms of myocardial infarct expansion. *Circulation*. 78:186-201.

Whiting, A., J. Wardale, and J. Trinick. 1989. Does titin regulate the length of muscle thick filaments? *J. Mol. Biol*. 205:263-268.

Willis, M.S., C. Ike, L. Li, D.Z. Wang, D.J. Glass, and C. Patterson. 2007. Muscle Ring Finger 1, but not Muscle Ring Finger 2, Regulates Cardiac Hypertrophy In Vivo. *Circ Res*.

Witt, C.C., C. Burkart, D. Labeit, M. McNabb, Y. Wu, H. Granzier, and S. Labeit. 2006. Nebulin regulates thin filament length, contractility, and Z-disk structure in vivo. *EMBO J*. 25:3843-3855.

Witt, S.H., H. Granzier, C.C. Witt, and S. Labeit. 2005. MURF-1 and MURF-2 target a specific subset of myofibrillar proteins redundantly: towards understanding MURF-dependent muscle ubiquitination. *J Mol Biol*. 350:713-722.

Yamasaki, R., M. Berri, Y. Wu, K. Trombitas, M. McNabb, M.S. Kellermayer, C. Witt, D. Labeit, S. Labeit, M. Greaser, et al. 2001. Titin-actin interaction in mouse myocardium: passive tension modulation and its regulation by calcium/S100A1. *Biophys J*. 81:2297-2313.

Yamasaki, R., Y. Wu, M. McNabb, M. Greaser, S. Labeit, and H. Granzier. 2002. Protein kinase A phosphorylates titin's cardiac-specific N2B domain and reduces passive tension in rat cardiac myocytes. *Circ Res*. 90:1181-1188.

Young, P., E. Ehler, and M. Gautel. 2001. Obscurin, a giant sarcomeric Rho guanine nucleotide exchange factor protein involved in sarcomere assembly. *J Cell Biol*. 154:123-136.

Young, P., C. Ferguson, S. Banuelos, and M. Gautel. 1998. Molecular structure of the sarcomeric Z-disk: two types of titin interactions lead to an asymmetrical sorting of alpha-actinin. *EMBO J*. 17:1614-1624.

Yu, J.-G., D.O. Fürst, and L.-E. Thornell. 2003. The mode of myofibril remodelling in human skeletal muscle affected by DOMS induced by eccentric contractions. *Histochem. Cell Biol*. 119:383-393.

Zaal, K.J., C.L. Smith, R.S. Polishchuk, N. Altan, N.B. Cole, J. Ellenberg, K. Hirschberg, J.F. Presley, T.H. Roberts, E. Siggia, et al. 1999. Golgi membranes are absorbed into and reemerge from the ER during mitosis. *Cell*. 99:589-601.

Zak, R., A.F. Martin, G. Prior, and M. Rabinowitz. 1977. Comparison of turnover of several myofibrillar proteins and critical evaluation of double isotope method. *J. Biol. Chem*. 252:3430-3435.

Zastrow, M.S., D.B. Flaherty, G.M. Benian, and K.L. Wilson. 2006. Nuclear Titin interacts with A- and B-type lamins in vitro and in vivo. *J Cell Sci*. 119:239-249.

Zhou, D., C.S. Birkenmeier, M.W. Williams, J.J. Sharp, J.E. Barker, and R.J. Bloch. 1997. Small, membrane-bound, alternatively spliced forms of ankyrin 1 associated with the sarcoplasmic reticulum of mammalian skeletal muscle. *J. Cell Biol*. 136:621-631.

Zimmerman, S.D., J. Criscione, and J.W. Covell. 2004. Remodeling in myocardium adjacent to an infarction in the pig left ventricle. *Am. J. Physiol. Heart Circ. Physiol*. 287:H2697-2704.

Zolk, O., C. Schenke, and A. Sarikas. 2006. The ubiquitin-proteasome system: focus on the heart. *Cardiovasc. Res*. 70:410-421.

Zou, P., N. Pinotsis, S. Lange, Y.H. Song, A. Popov, I. Mavridis, O.M. Mayans, M. Gautel, and M. Wilmanns. 2006. Palindromic assembly of the giant muscle protein titin in the sarcomeric Z-disk. *Nature*. 439:229-233.

8 Abbreviations

APS	ammonium persulfate
BDM	2,3-butanedione monoxime
bp	base pair
BSA	bovine serum albumin
BW	body weight
CARP	cardiac ankyrin repeat protein
cDNA	complementary DNA
CON	control
Cre	Cre recombinase (causes recombination)
CX	cycloheximide
Da	Dalton
DARP	diabetes-related ankyrin repeat protein
DCM	dilated cardiomyopathy
dH_2O	distilled water
DEPC	diethylpyrocarbonate
DIC	differential interference contrast
DMEM	Dulbecco's modified Eagle Medium
DMSO	dimethyl sulfoxide
DNA	deoxyribonucleic acid
DNase	deoxyribonuclease
dNTP	deoxynucleoside triphosphate
dsRed	discosoma red fluorescent protein
DTT	dithiothreitol

E	embryonic day post fertilization
ECL	enhanced chemiluminescence
ECM	embryonic cardiomyocytes
EDTA	ethylenediamine tetraacetic acid
eGFP	enhanced green fluorescent protein
EGTA	ethylene glycol-bis(2-aminoethylether)N,N,N′,N′tetraacetic acid
EM	electron microscopy
Ex	exon
FA	formaldehyde
f. c.	fold change
FBS	fetal bovine serum
FHL	four and a half LIM domain protein
Flp	flippase recombination enzyme
FN	fibronectin
FRAP	fluorescence recovery after photobleaching
frt	flippase recognition target
HCa	high calcium
HCM	hypertrophic cardiomyopathy
HET	heterozygous
HRP	horseradish peroxidase
Hsp	heat shock protein
HW	heart weight
IF	immunofluorescence
Ig	immunoglobulin
IVC	individually ventilated cage
KI	knockin

KO	knockout
LCa	low calcium
loxP-site	locus of crossing over-site
MARP	muscle-ankyrin-repeat proteins
MHC	myosin heavy chain
MLC	myosin light chain
MLCK	myosin light-chain kinase
mRNA	messenger RNA
MuRF	muscle-specific RING finger protein
MyBP	myosin binding protein
nbr1	neighbor of Brca1 gene
NCa	normal calcium
NCM	neonatal cardiomyocytes
Neo	neomycin
P	postnatal day
PAGE	polyacrylamide gel electrophoresis
PBS	phosphate buffered saline
PBS-T	PBS-Tween 20
PCR	polymerase chain reaction
PFA	paraformaldehyde
PKA	protein kinase A
PVDF	polyvinylidene difluoride
qRT-PCR	quantitative real-time PCR
RNA	ribonucleic acid
RNase	ribonulease

ROI	region of interest
rpm	revolution per minute
RT-PCR	reverse transcription PCR
RyR	ryanodine receptor
SDS	sodium dodecyl sulfate
SEM	standard error of the mean
SRF	serum response factor
s. l.	sarcomere length
SR	sarcoplasmic reticulum
TAE	Tris-acetate EDTA
Taq	*Thermus aquaticus*
TBS-T	Tris-buffered saline with Tween 20
TE	Tris-EDTA
TEMED	N, N, N′, N′-tetramethylethylendiamin
Tn	troponin
TPM	tropomyosin
Tris	tris(hydroxymethyl)-aminomethane
U	unit
UNG	uracil-N-glycosylase
VAGE	vertical SDS-agarose gel electrophoresis
WB	Western blotting
WT	wild-type

9 List of figures

10 List of tables

11 Curriculum vitae and publications

Der Lebenslauf ist in der Online-Version aus Gründen des Datenschutzes nicht enthalten

Due to data privacy protection there is no curriculum vitae in the online version.

Curriculum Vitae

Der Lebenslauf ist in der Online-Version
aus Gründen des Datenschutzes nicht enthalten